MINI-WORKSHOP:
RELATIVISTIC FLUIDS AT THE INTERSECTION OF MATHEMATICS AND PHYSICS

Mathematisches Forschungsinstitut Oberwolfach (MFO, Oberwolfach Research Institute for Mathematics)

14. 12. 2020

# Properties of hypermassive hybrid stars from binary compact star mergers


MATTHIAS HANAUSKE
FRANKFURT INSTITUTE FOR ADVANCED STUDIES
JOHANN WOLFGANG GOETHE UNIVERSITÄT
INSTITUT FÜR THEORETISCHE PHYSIK
ARBEITSGRUPPE RELATIVISTISCHE ASTROPHYSIK
D-60438 FRANKFURT AM MAIN


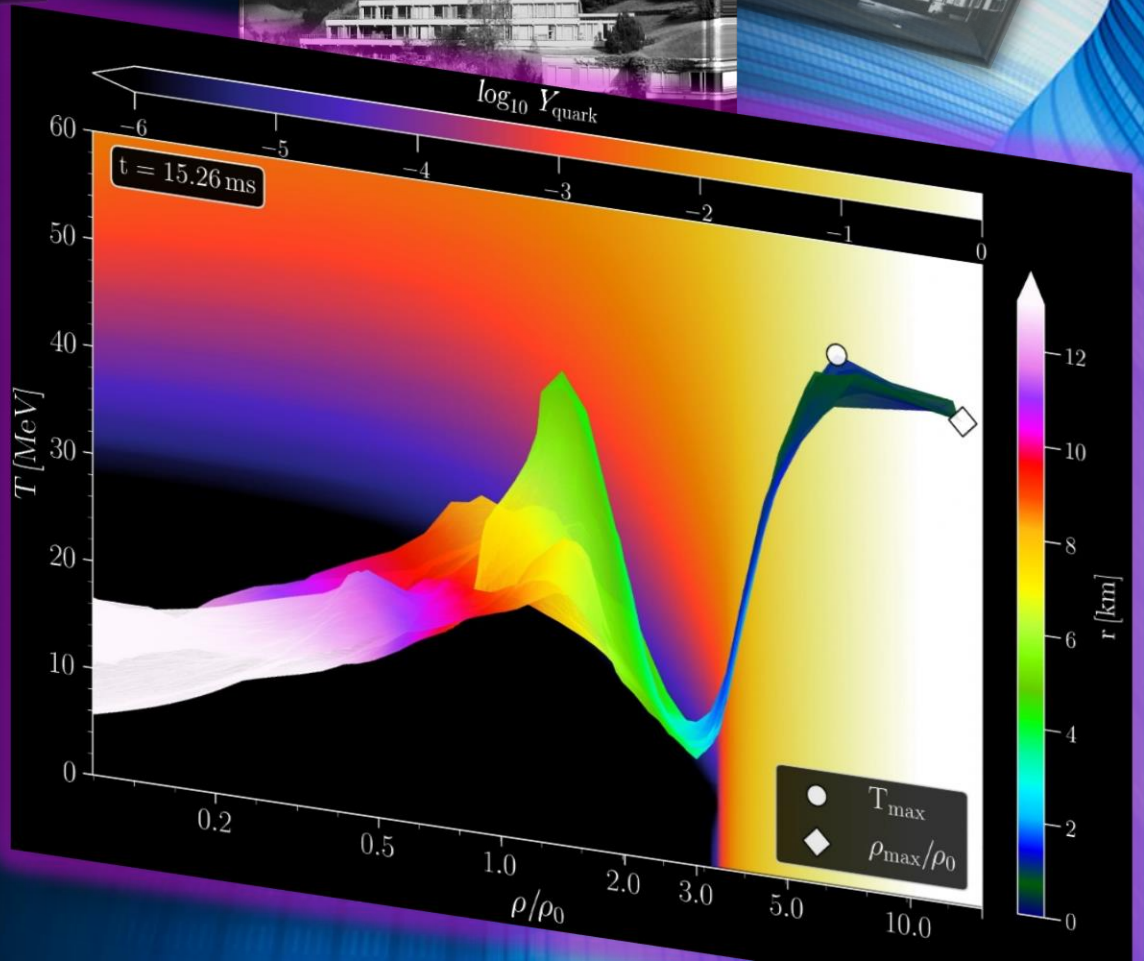


*In collaboration with Lukas Weih, Elias R. Most, Jens Papenfort, Luke Bovard, Gloria Montana, Laura Tolos, Jan Steinheimer, Anton Motornenko, Veronica Dexheimer, Horst Stöcker, and Luciano Rezzolla*

# Numerical Relativity and Relativistic Hydrodynamics of Binary Compact Star Mergers

Einstein's theory of general relativity and the resulting general relativistic conservation laws for energy-momentum in connection with the rest-mass conservation are the theoretical groundings of neutron star binary mergers:

$$R_{\mu\nu} - \frac{1}{2} g_{\mu\nu} R = 8\pi T_{\mu\nu}$$

$$\nabla_\mu (\rho u^\mu) = 0\,, \qquad \nabla_\nu T^{\mu\nu} = 0\,.$$

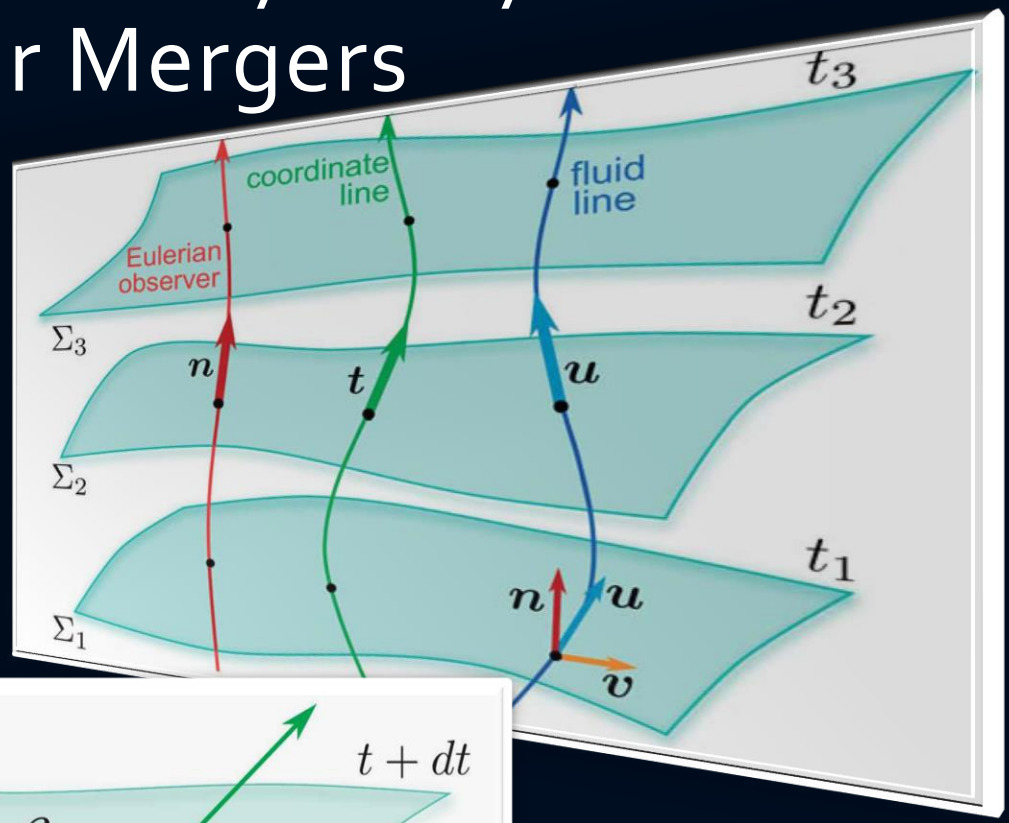


(3+1) decomposition of spacetime

$$g_{\mu\nu} = \begin{pmatrix} -\alpha^2 + \beta_i \beta^i & \beta_i \\ \beta_i & \gamma_{ij} \end{pmatrix}$$

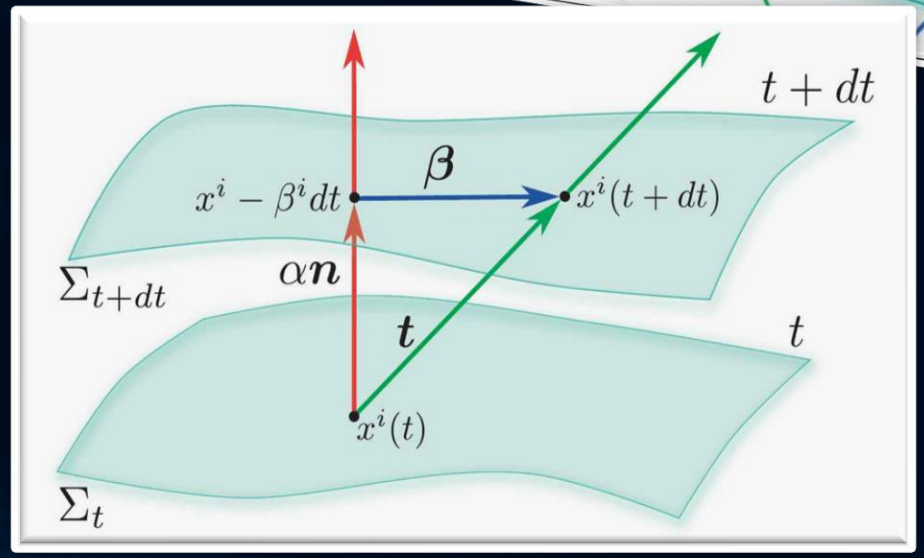


$$d\tau^2 = \alpha^2(t, x^j) dt^2$$

$$x^i_{t+dt} = x^i_t - \beta^i(t, x^j) dt$$

*Talk yesterday by L. Rezzolla*

All figures and equations from: Luciano Rezzolla, Olindo Zanotti: Relativistic Hydrodynamics, Oxford Univ. Press, Oxford (2013)

# The Einstein Equation and the EOS of Compact Stars

| ART | Yang-Mills-Theories |
|---|---|
| $D_\beta v^\alpha = \partial_\beta v^\alpha + \Gamma^\alpha_{\sigma\beta} v^\sigma$ | $D_{\beta a}{}^b = \partial_\beta 1_a{}^b + ig A_{\beta a}{}^b$ |
| $R^\delta{}_{\mu\alpha\beta} v^\mu = [D_\alpha, D_\beta] v^\delta$ | $F_{\alpha\beta a}{}^b = \frac{1}{ig} [D_{\alpha a}{}^c, D_{\beta c}{}^b]$ |
| $R^\delta{}_{\mu\alpha\beta} = \Gamma^\delta_{\mu\alpha\|\beta} - \Gamma^\delta_{\mu\beta\|\alpha}$ | $= A_{\beta a}{}^b{}_{\|\alpha} - A_{\alpha a}{}^b{}_{\|\beta}$ |

QuantumCromoDynamic:

($SU(3)_{(c)}$- Color Yang-Mills-Gauge Theory)

$D_{\beta A}{}^B = \partial_\beta 1_A{}^B + ig G_{\beta A}{}^B$

${}_A{}^B$ =red, green, blue

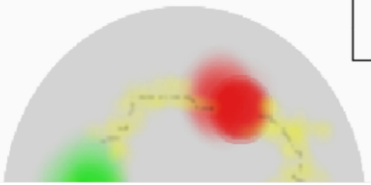

$$\psi^f_A = \begin{pmatrix} \psi^f_r \\ \psi^f_g \end{pmatrix}$$

GR: Covariant derivative: $D_\nu v^\mu := v^\mu{}_{\|\nu} = v^\mu{}_{|\nu} + \Gamma^\mu_{\beta\nu} v^\beta$

Field strength: $R^\alpha{}_{\sigma\nu\mu} v^\sigma = -[D_\mu, D_\nu] v^\alpha = \left(\Gamma^\alpha_{\sigma\nu|\mu} - \Gamma^\alpha_{\sigma\mu|\nu} + \Gamma^\alpha_{\beta\mu}\Gamma^\beta_{\sigma\nu} - \Gamma^\alpha_{\beta\nu}\Gamma^\beta_{\sigma\mu}\right) v^\sigma$

Lagrangian: $\mathcal{L}_{GR} = R$

QCD: Covariant derivative: $D_{\mu a}{}^b \psi_b = \left(\partial_\mu 1_a{}^b + ig_3 G_{\mu i} \tau^i{}_a{}^b\right) \psi_b = \psi_{a|\mu} + ig_3 G_{\mu a}{}^b \psi_b$

Field strength: $\mathcal{F}_{\mu\nu} = F_{\mu\nu a}{}^b = \frac{i}{g_3} \left[D_{\mu a}{}^c, D_{\nu c}{}^b\right] = F_{\mu\nu i} \tau^i{}_a{}^b$

Field strength: $F_{\mu\nu i} = G_{\nu i|\mu} G_{\nu i|\mu} - g_3 f^{jk}{}_i G_{\mu j} G_{\nu k}$

Lagrangian: $\mathcal{L}_{QCD} = \frac{1}{16\pi} F_{\mu\nu i} F^{\mu\nu i}$ ,

# The QCD Phase Diagram

*Talk on Monday by M. Strickland*

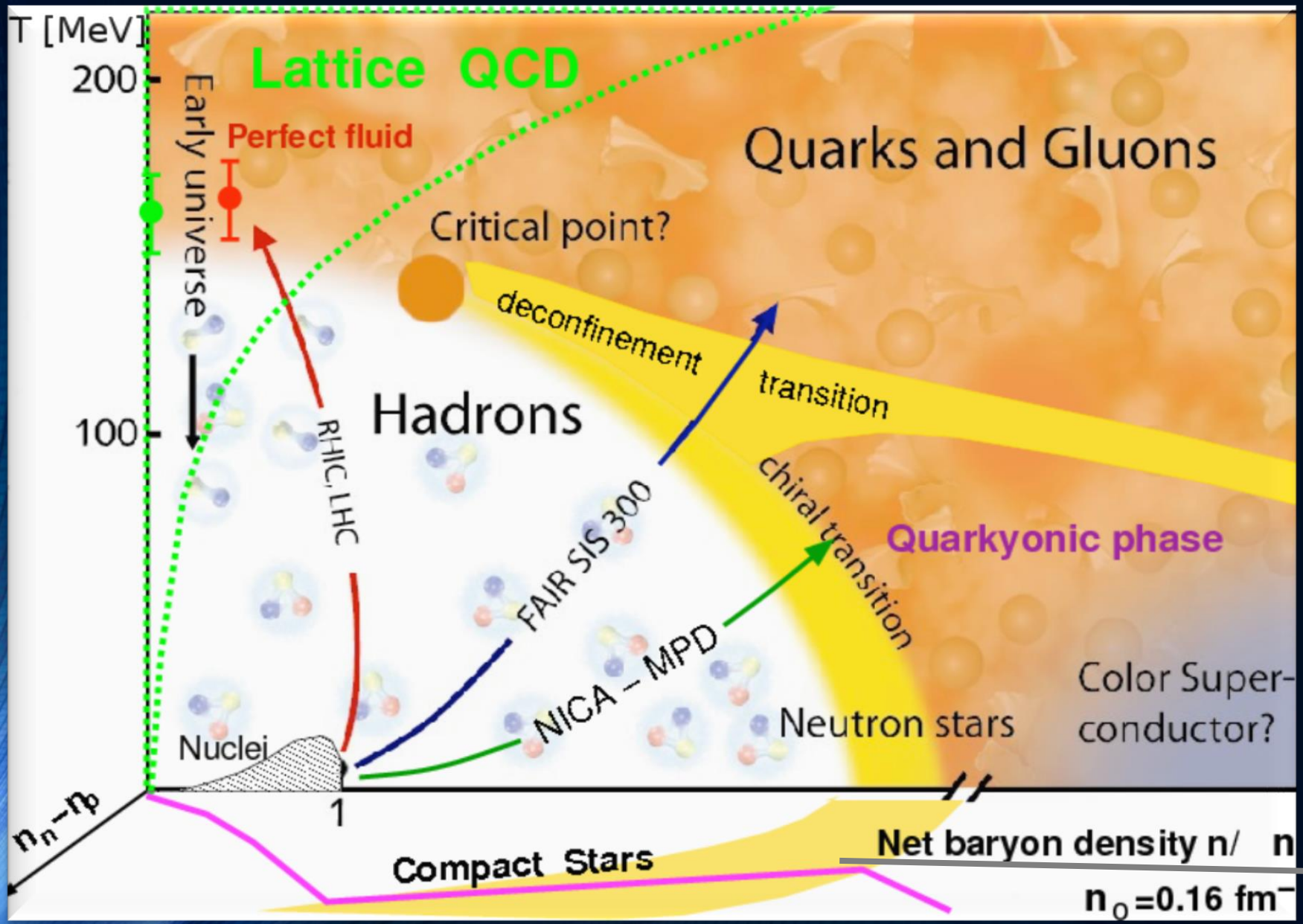


The Gibbs Construction

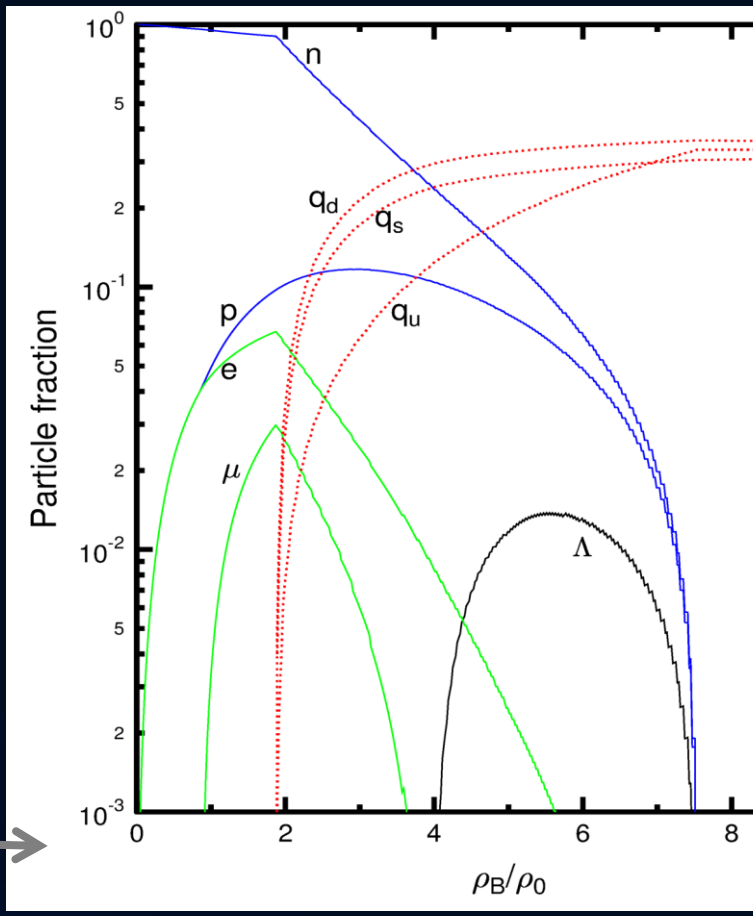

# The QCD – Phase Transition and the Interior of a Hybrid Star

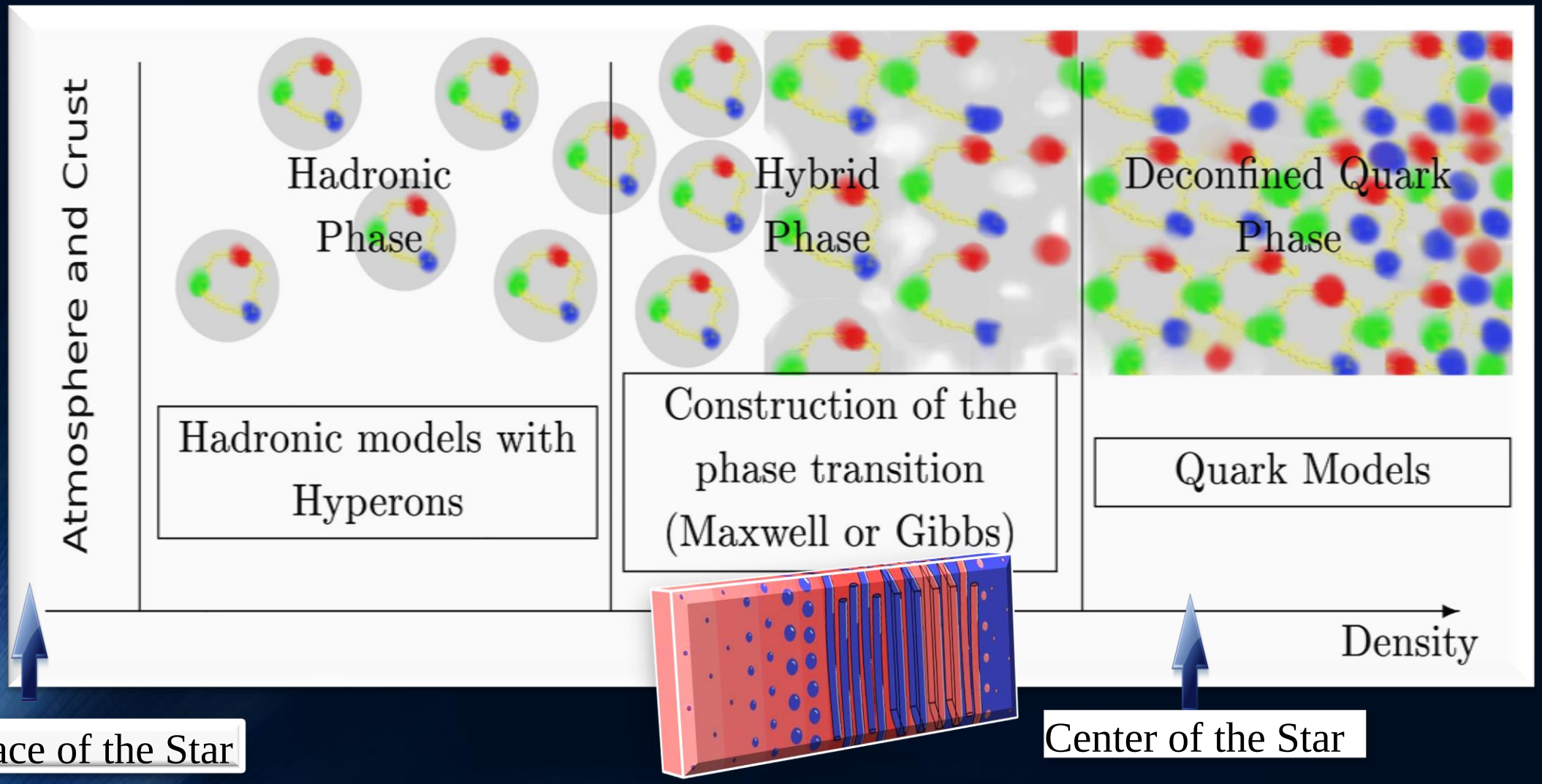


*Matthias Hanauske; Doctoral Thesis:*
*Properties of Compact Stars within QCD-motivated Models; University Library Publication Frankfurt (2004)*

# Broadbrush picture

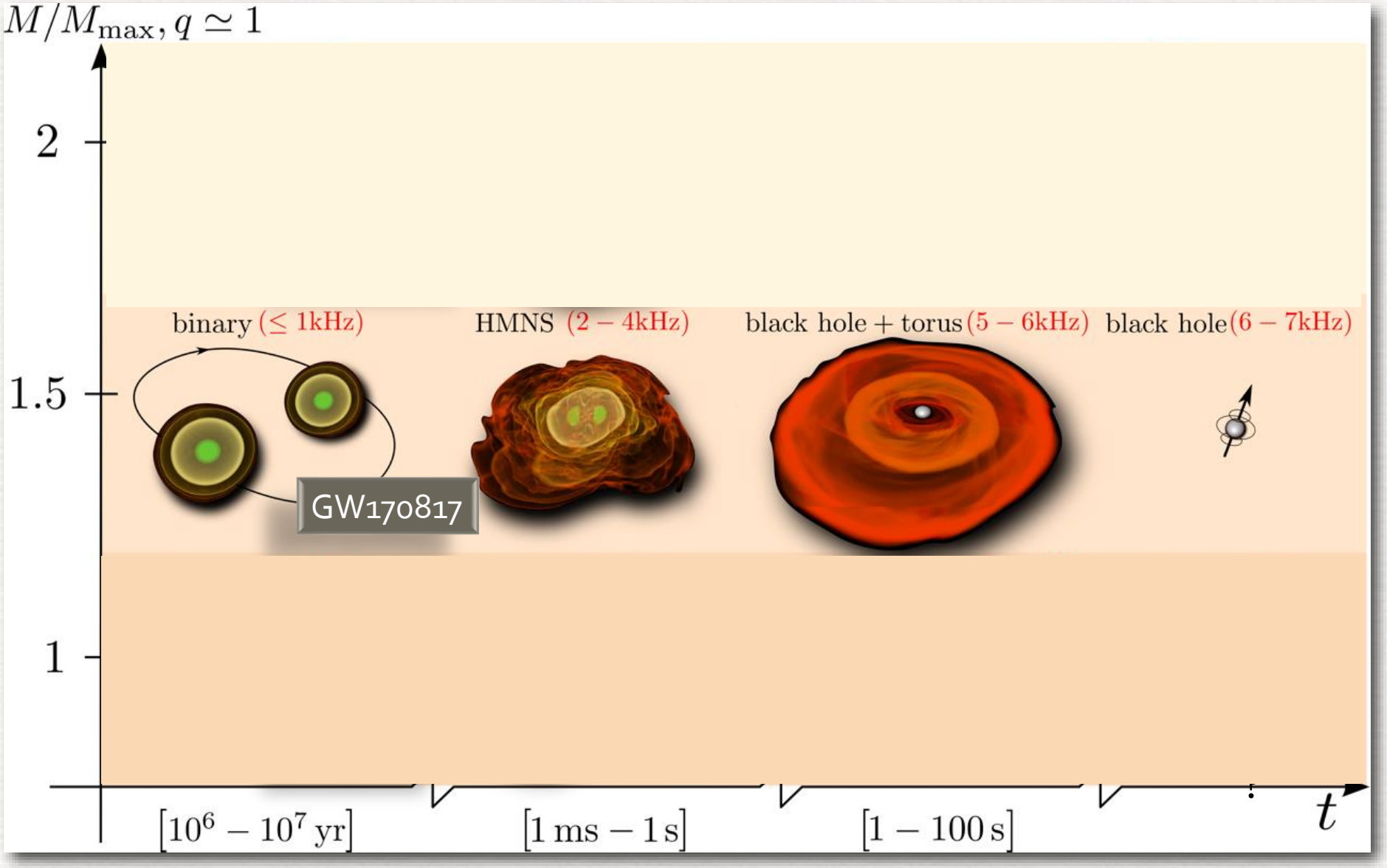

# Evolution of the density in the post merger phase

GNH3-EOS, initial NS mass: 1.35 $M_{solar}$

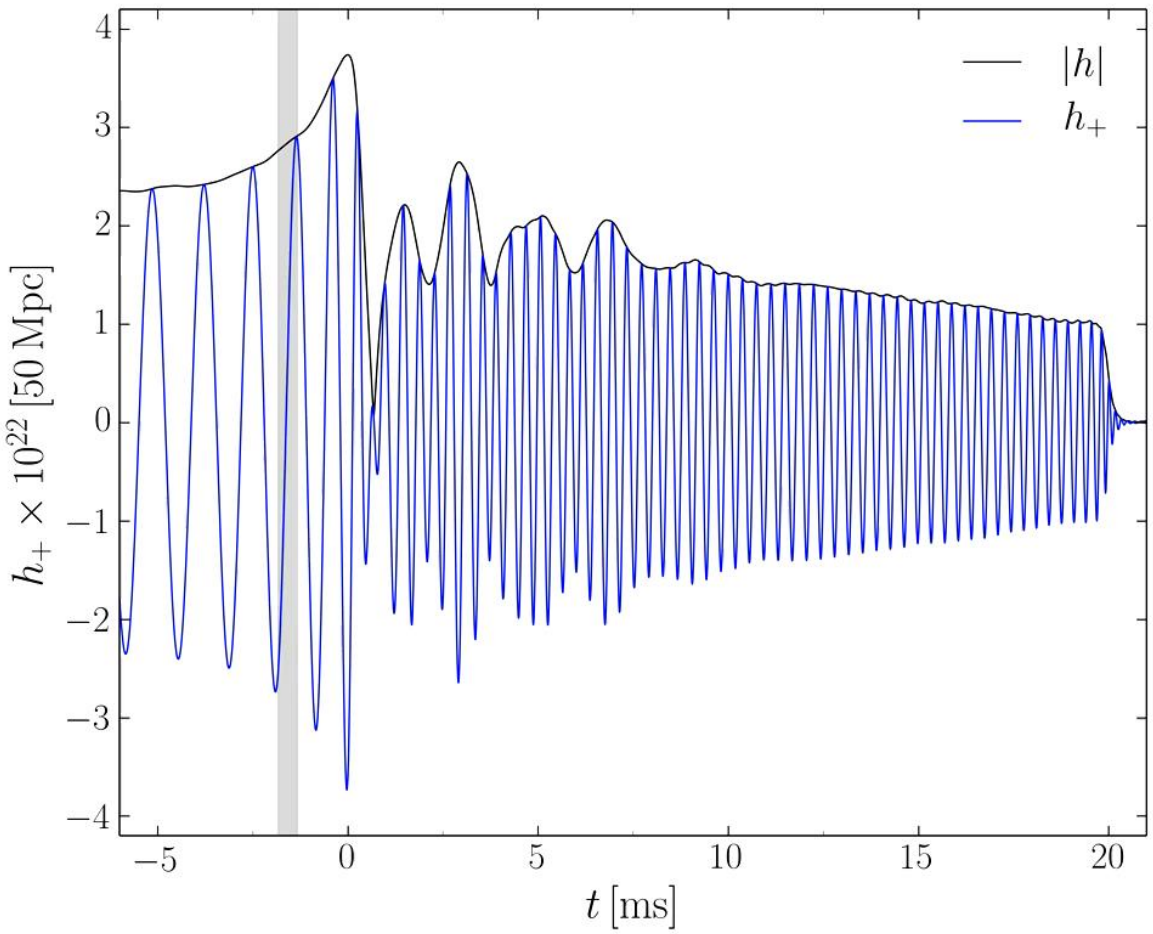


Gravitational wave amplitude
at a distance of 50 Mpc

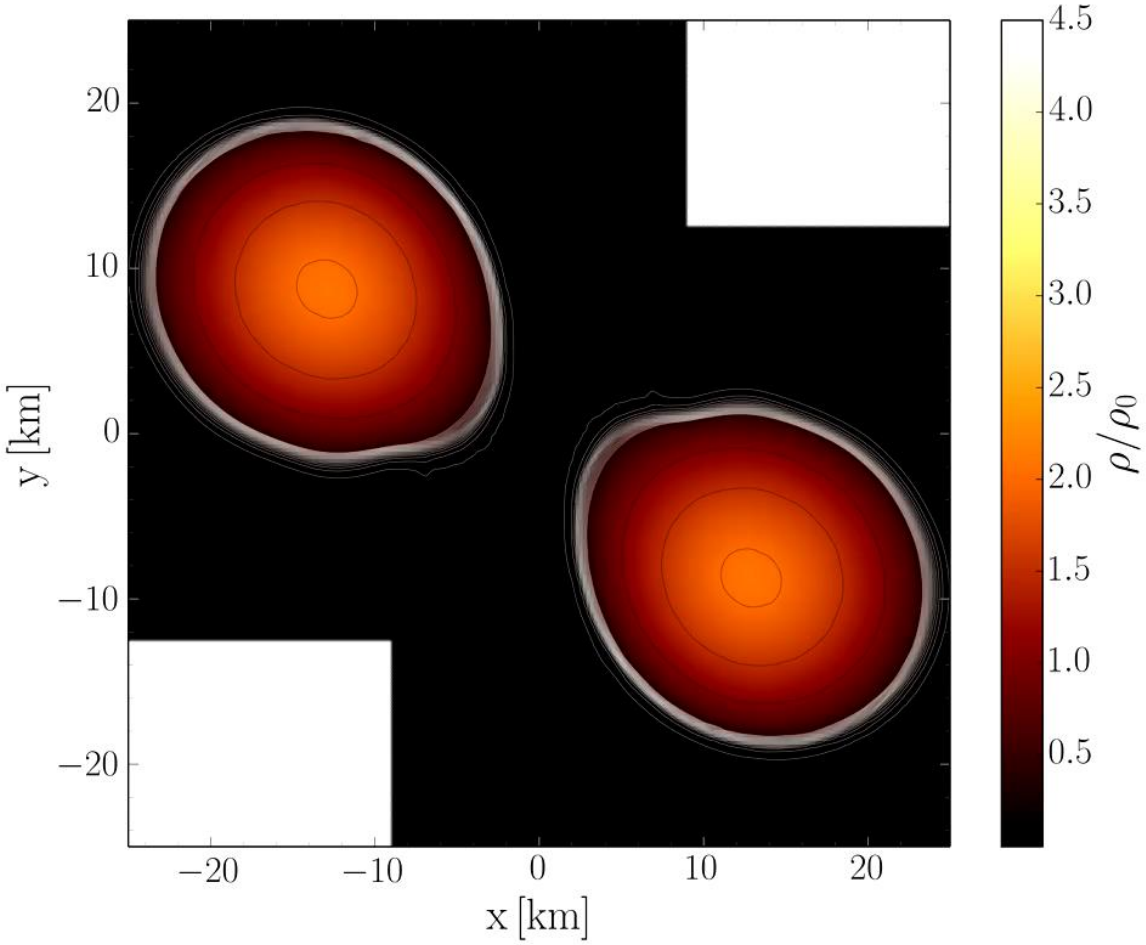


Rest mass density distribution ρ(x,y) in the equatorial plane
in units of the nuclear matter density $\rho_0$

# The different Phases of a Binary Compact Star Merger Event

Late inspiral and merger phase

Transient early postmerger phase

Postmerger phase

Collapse to the Kerr black hole and ringdown phase

Wiener Walzer

Disco-Fox

Merengue

Tango

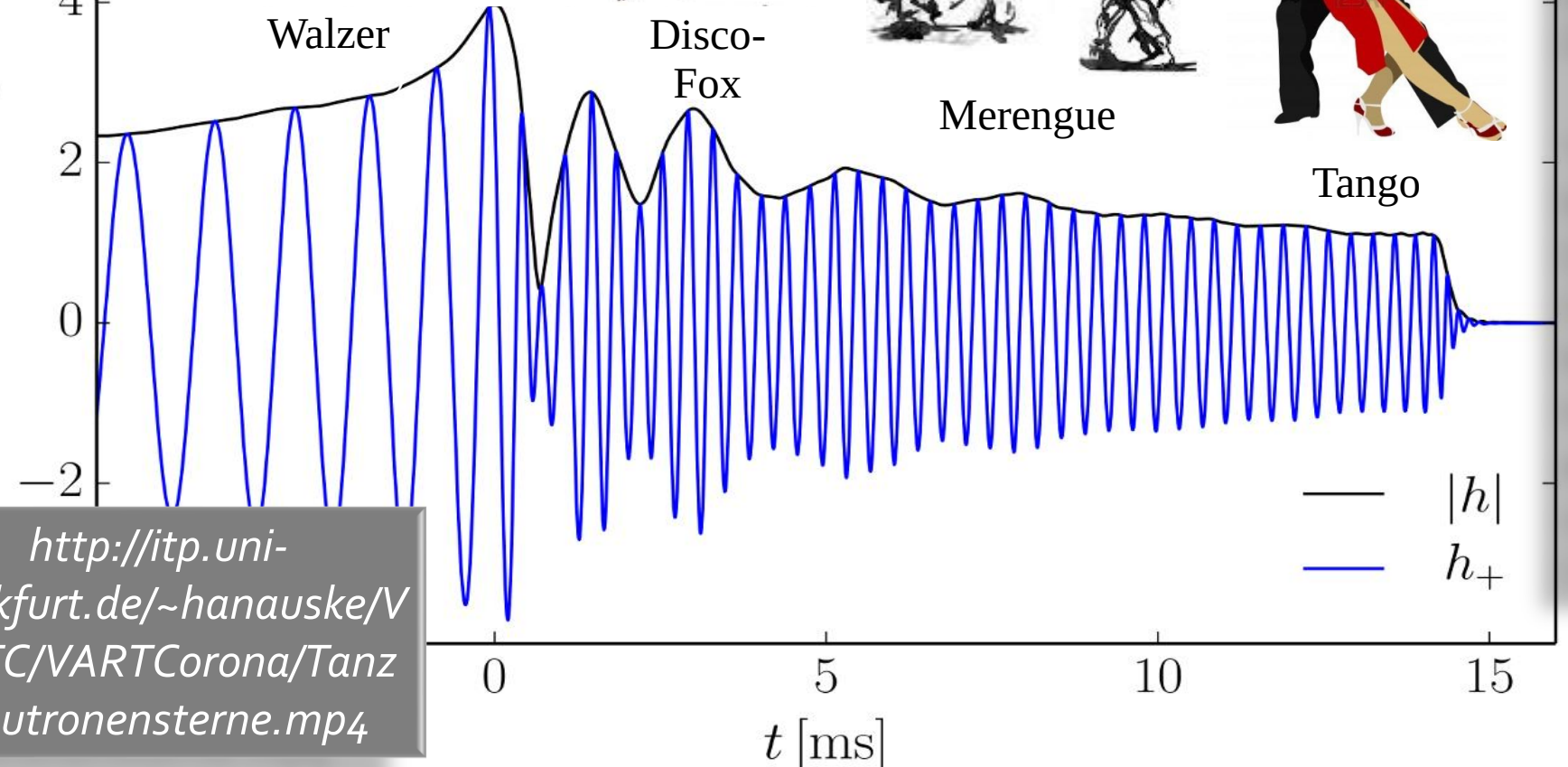


*http://itp.uni-frankfurt.de/~hanauske/VARTC/VARTCorona/TanzNeutronensterne.mp4*

*<u>Wy exactly these dances?</u>*
*Details in*

"Binary Compact Star Mergers and the Phase Diagram of Quantum Chromodynamics", Matthias Hanauske and Horst Stöcker, Discoveries at the Frontiers of Science, 107-132; Springer, Cham (2020)

# The different Phases during the Postmergerphase of the HMNS

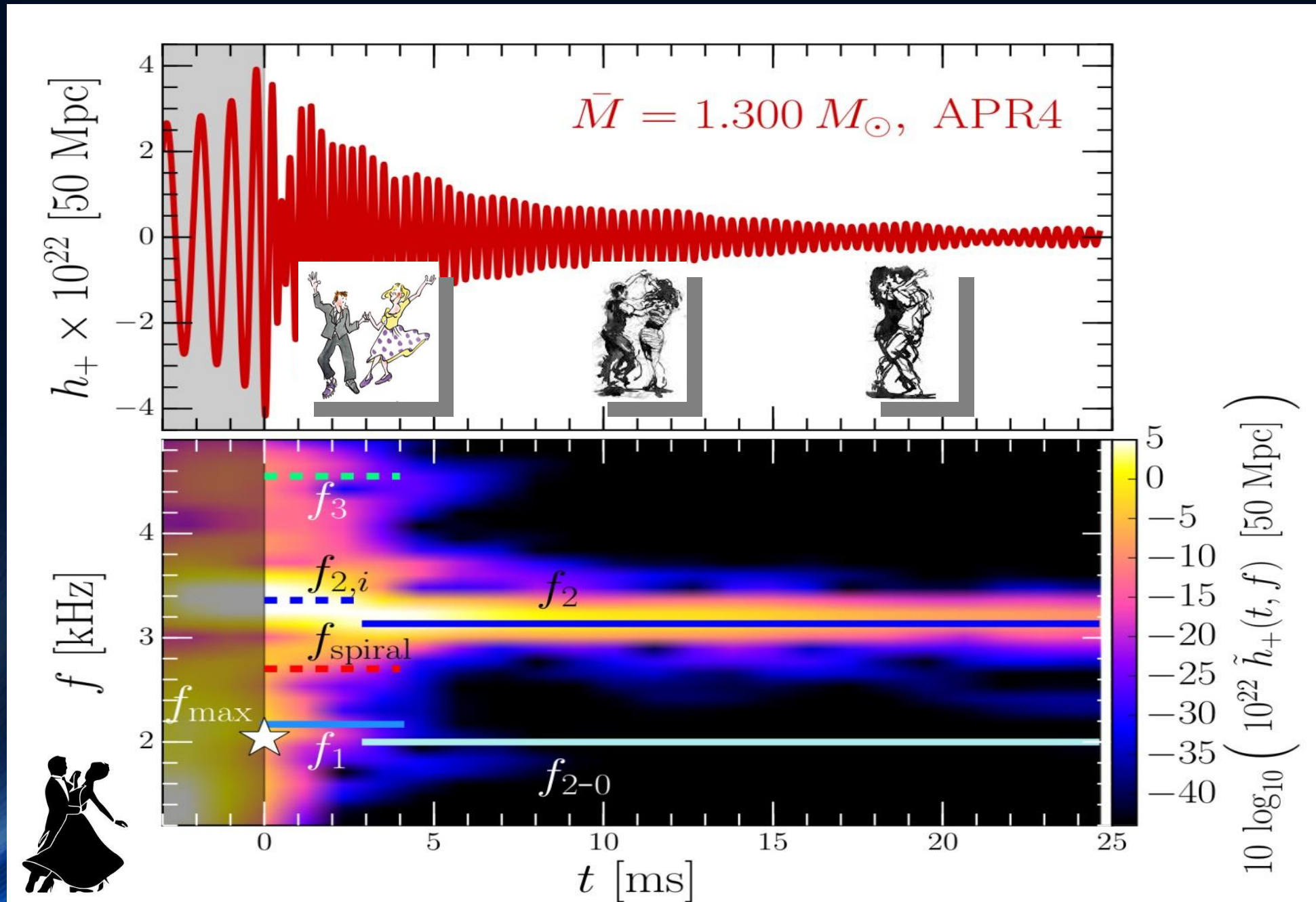

# Time Evolution of the GW-Spectrum

*Talk yesterday by L. Rezzolla*

The power spectral density profile of the post-merger emission is characterized by several distinct frequencies. Approximately 5 ms after merger, the only remaining dominant frequency is the $f_2$-frequency (see e.g. L.Rezzolla and K.Takami, PRD, 93(12), 124051 (2016))

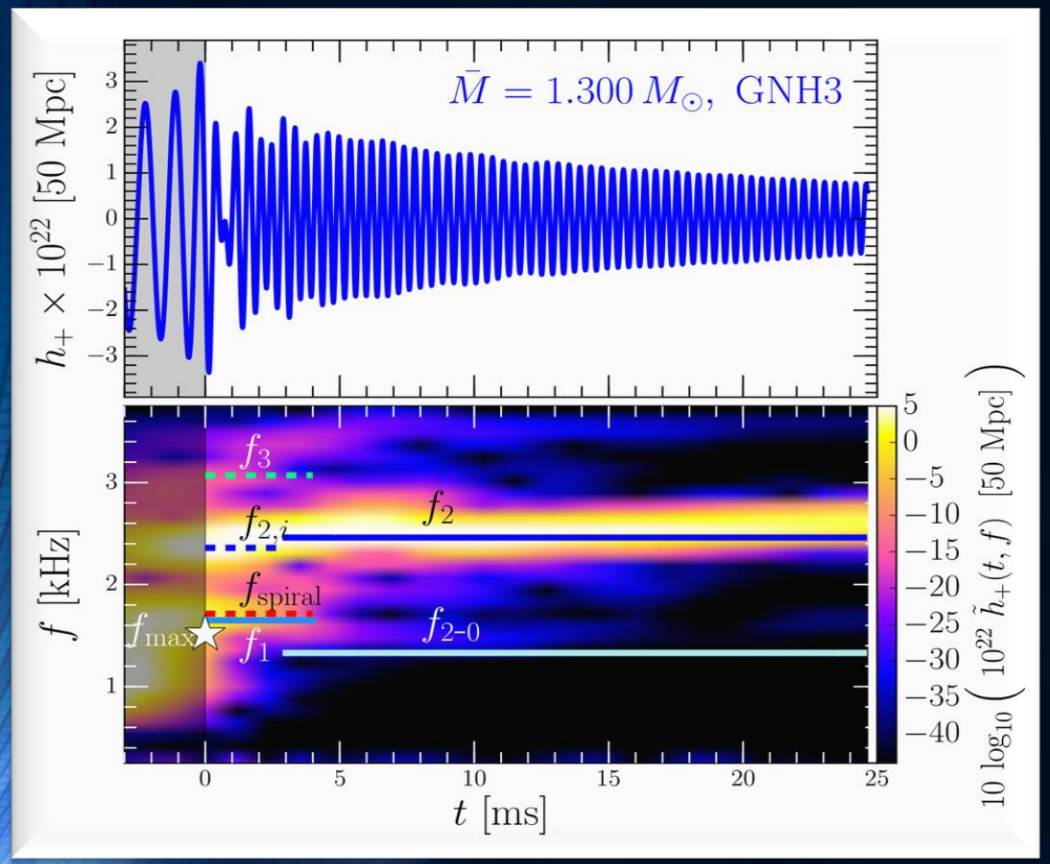


Stiff EOS

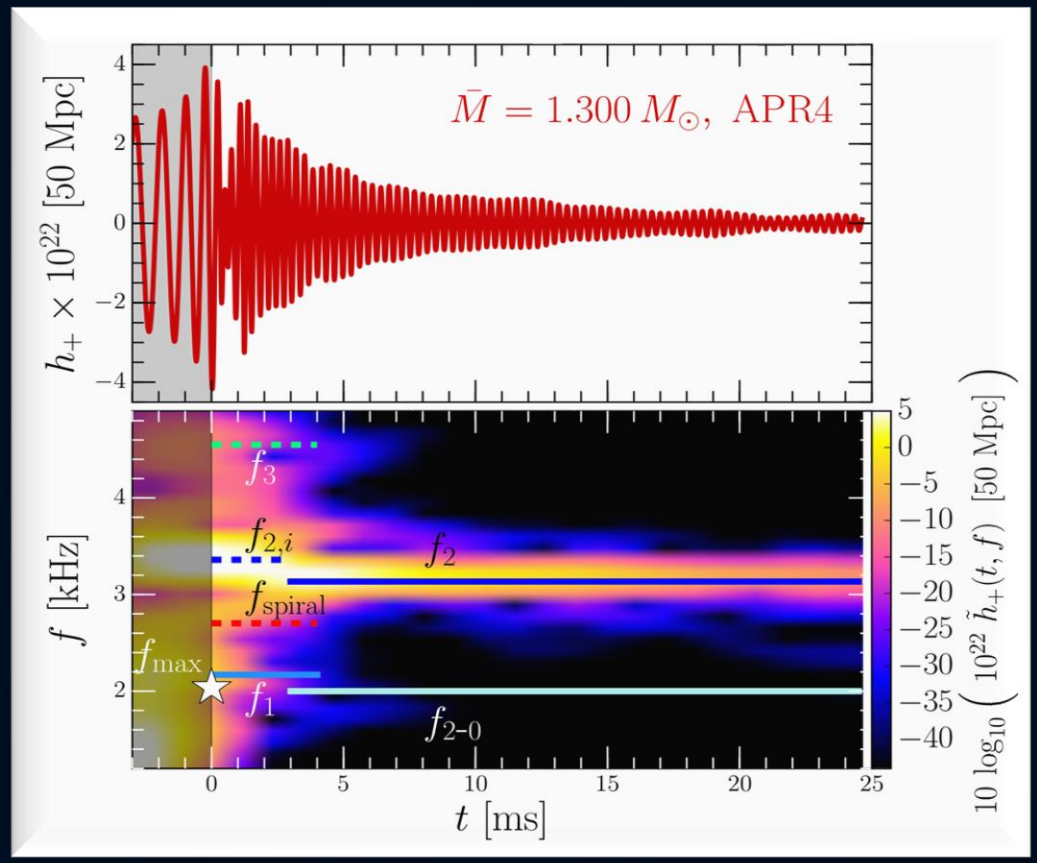


Soft EOS

Unfortunately, clow sensitivity at high gravitational wave frequencies, no post-merger signal has been found in GW170817.

But advanced detectors / next-generation detectors might be able to detect!!?

Evolution of the frequency spectrum of the emitted gravitational waves for the stiff GNH3 (left) and soft APR4 (right) EOS.

# The Co-Rotating Frame

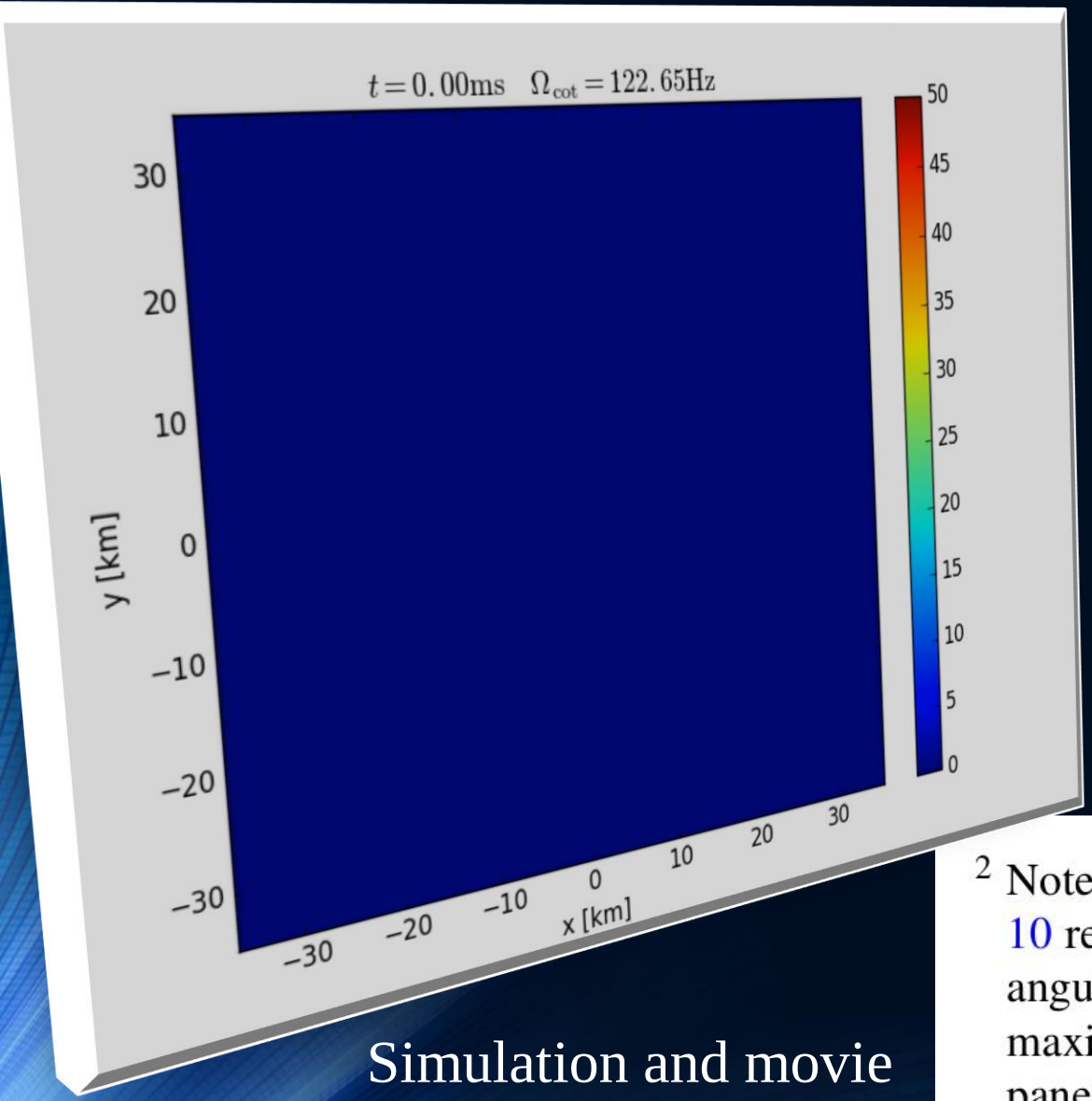


Simulation and movie has been produced by Luke Bovard

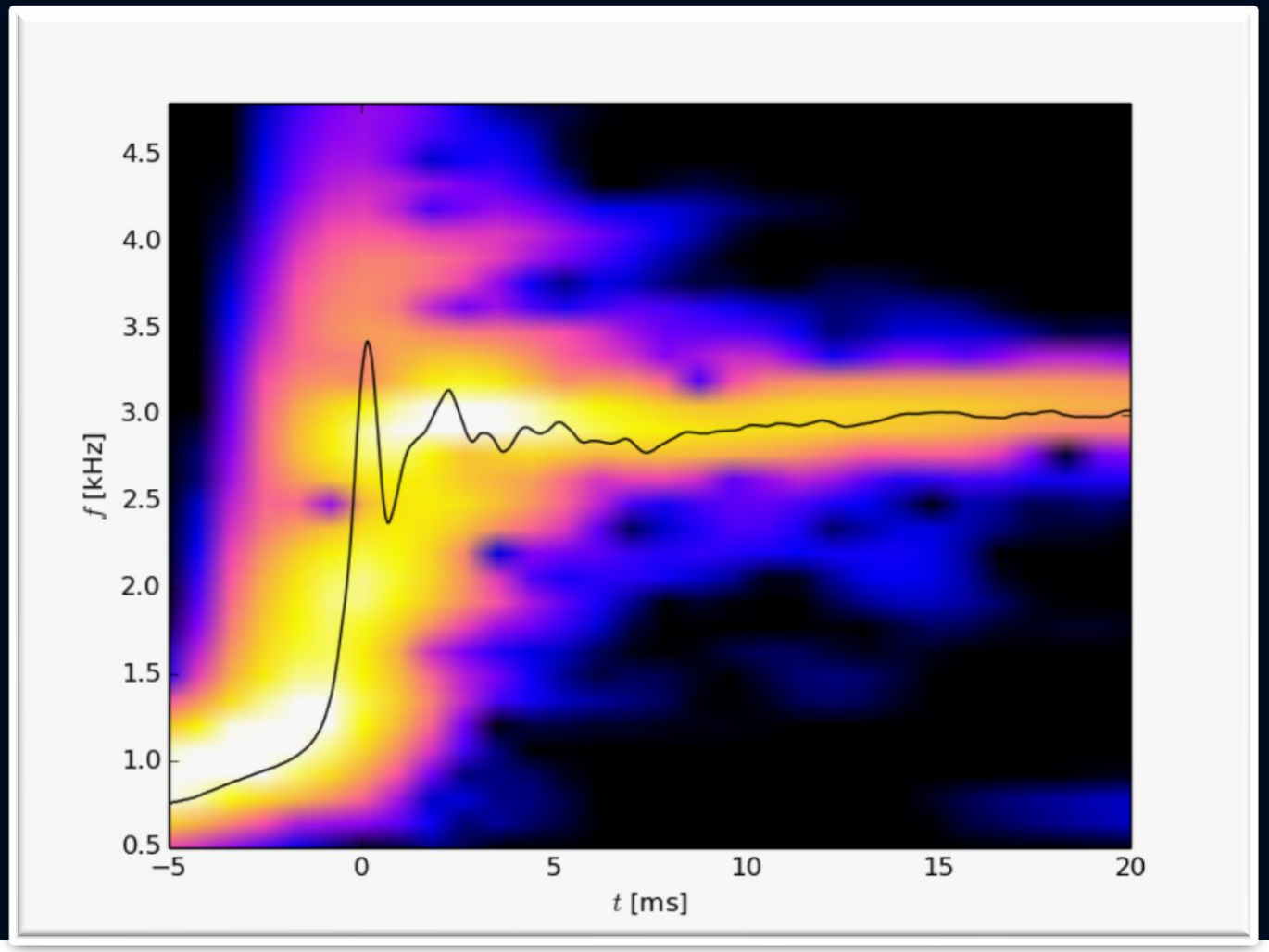


[2] Note that the angular-velocity distribution in the lower central panel of Fig. 10 refers to the corotating frame and that this frame is rotating at half the angular frequency of the emitted gravitational waves, $\Omega_{\rm GW}$. Because the maximum of the angular velocity $\Omega_{\rm max}$ is of the order of $\Omega_{\rm GW}/2$ (cf. left panel of Fig. 12), the ring structure in this panel is approximately at zero angular velocity.

# Density and Temperature Evolution inside the HMNS

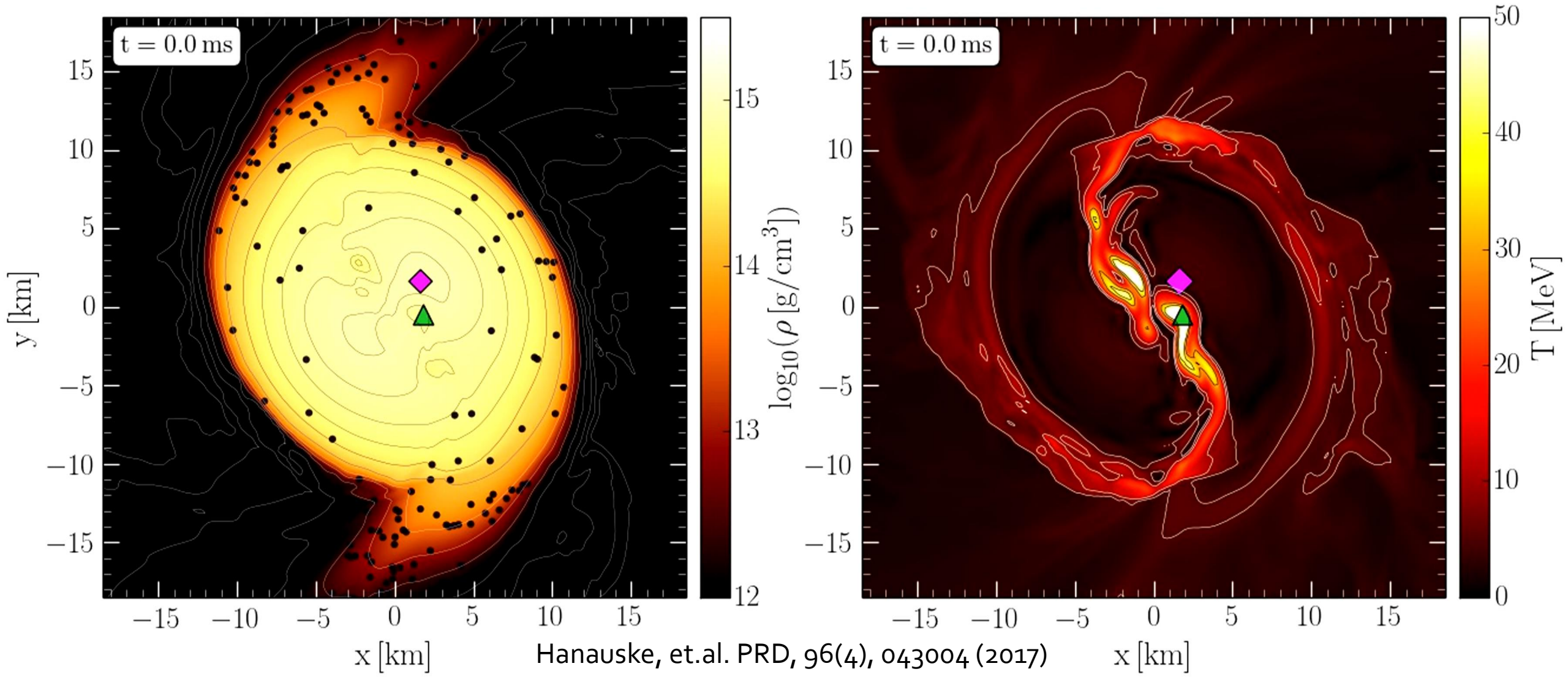


Hanauske, et.al. PRD, 96(4), 043004 (2017)

Rest mass density on the equatorial plane

Temperature on the equatorial plane

# Binary Neutron Star Mergers in the QCD Phase Diagram

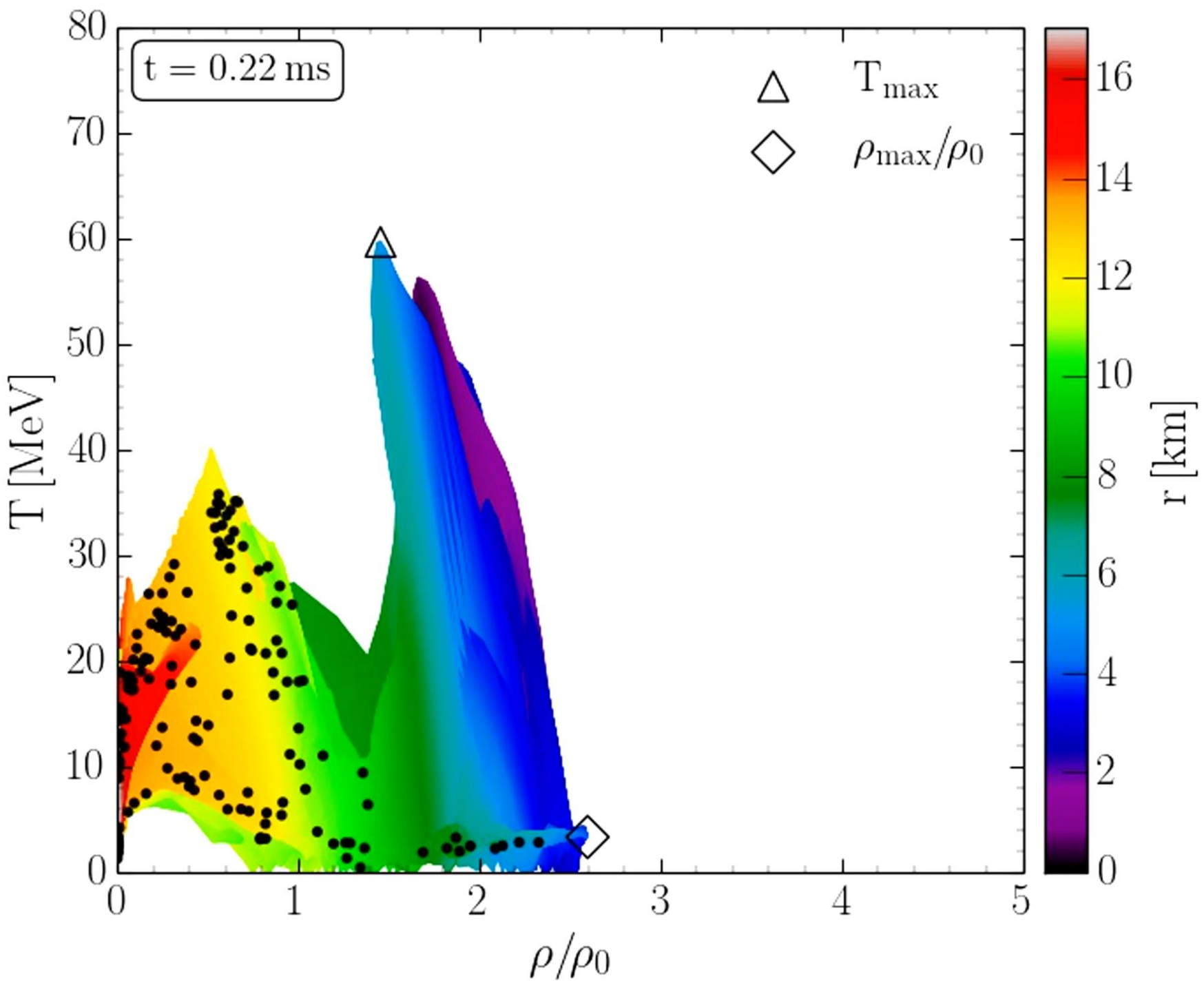


Evolution of hot and dense matter inside the inner area of a hypermassive neutron star simulated within the LS220 EOS with a total mass of $M_{total}=2.7\,M_\odot$ in the style of a (T- ρ) QCD phase diagram plot

The color-coding indicate the radial position r of the corresponding (T- ρ) fluid element measured from the origin of the simulation (x , y) = (0 , 0) on the equatorial plane at z = 0.

The open triangle marks the maximum value of the temperature while the open diamond indicates the maximum of the density.

# The Angular Velocity in the (3+1)-Split

The angular velocity Ω in th
function α , the ϕ-compone
$v^{\Phi}$ of the fluid (spatial proje

$$\Omega(x, y, z, t) =$$

Angular velocity Ω

Lapse

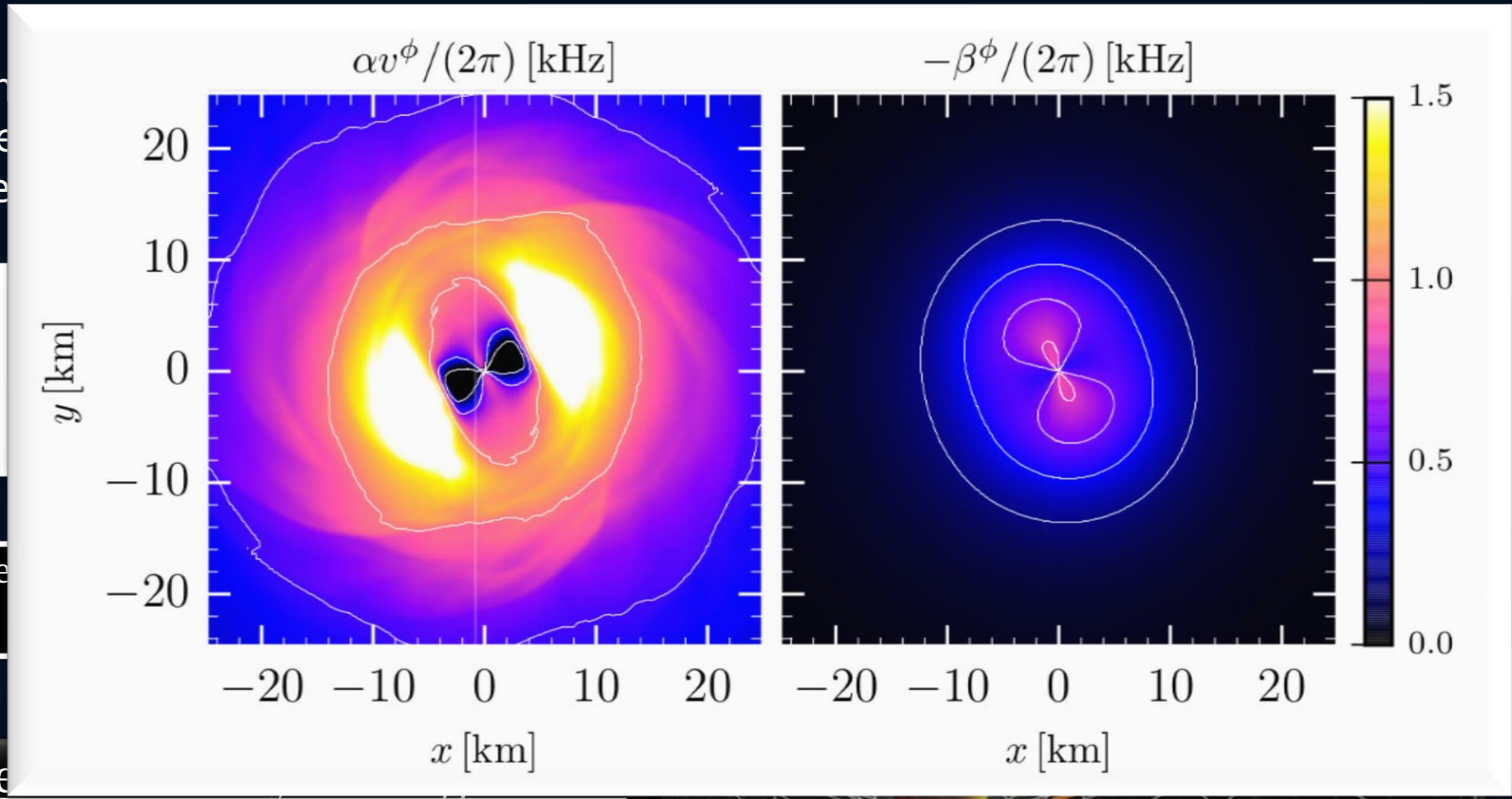


## Focus: Inner core of the


M. Shibata, K. Taniguchi, and K. Uryu, Phys. Rev. D 71, 084021 (2005)
M. Shibata and K. Taniguchi, Phys. Rev. D 73, 064027 (2006)
F. Galeazzi, S. Yoshida and Y. Eriguchi, A&A 541, p. A156 (2012)
W. Kastaun and F. Galeazzi, Phys. Rev. D 91, p. 064027 (2015)


# Temperature

# Angular Velocity

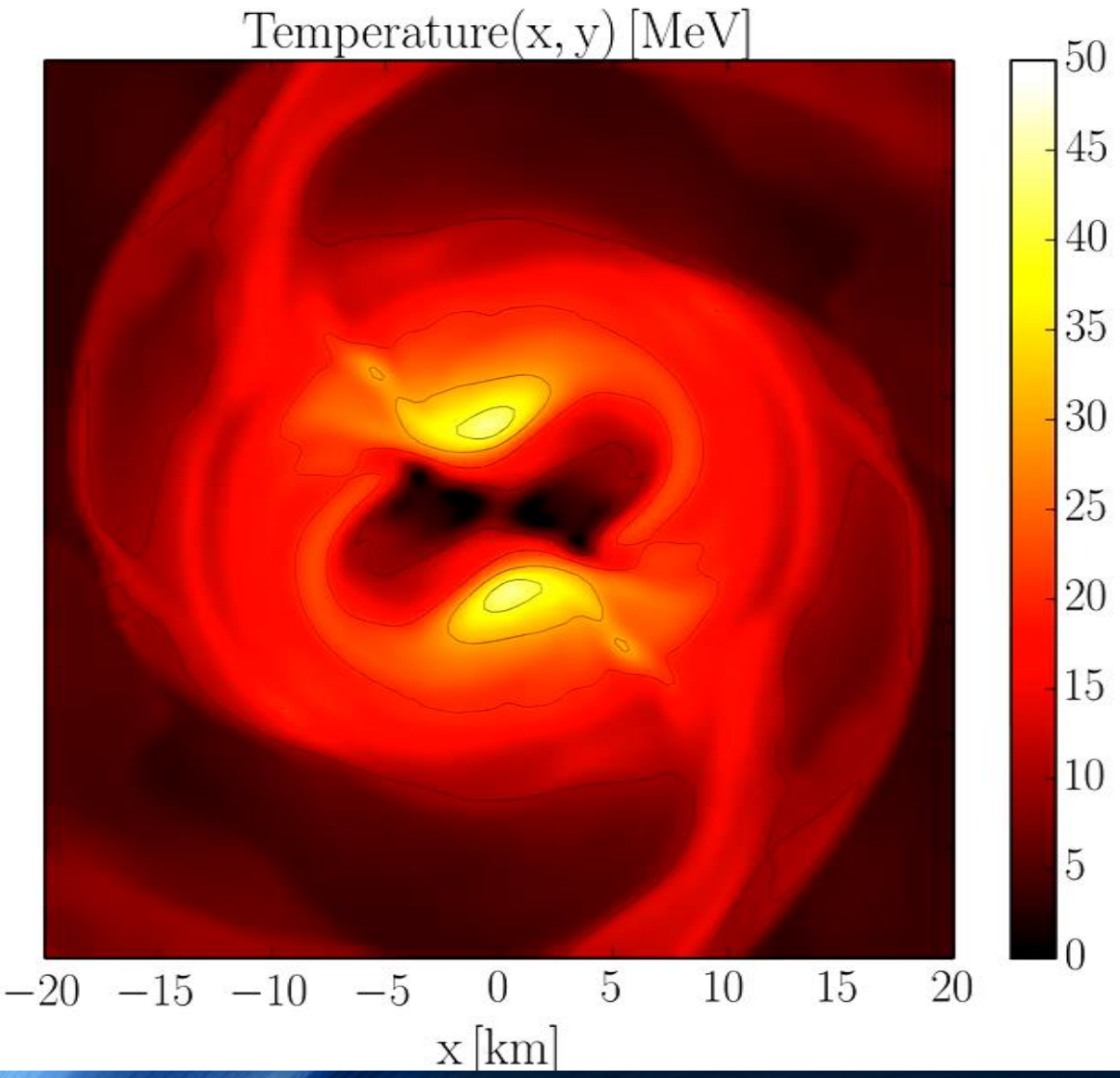


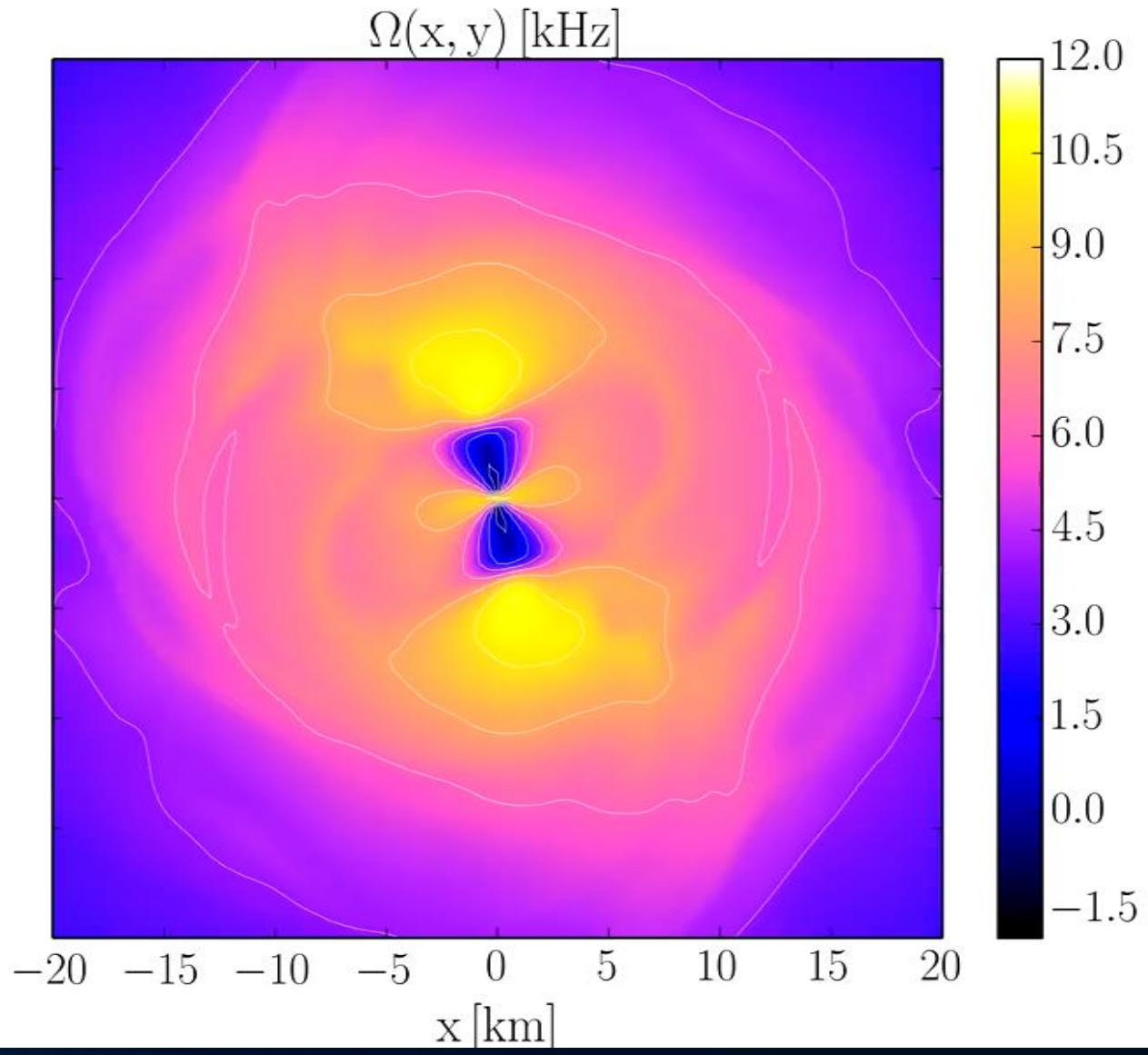


EOS: LS200 , Mass: 1.32 $M_{solar}$ , simulation with Pi-symmetry

# Time-averaged Rotation Profiles of the HMNSs

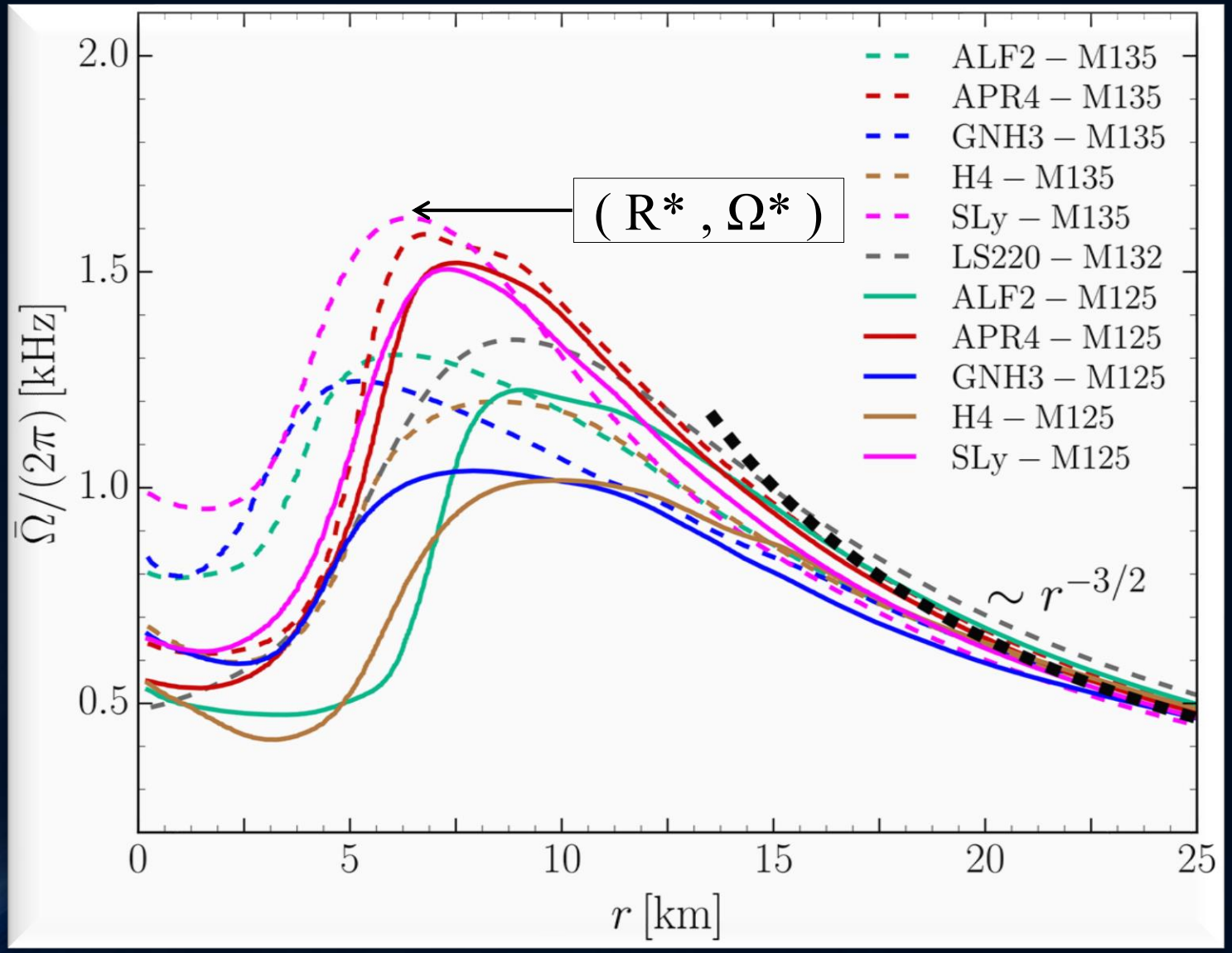


Soft EoSs:
Sly
APR4

Stiff EoSs:
GNH3
H4

Time-averaged rotation profiles for different EoS
Low mass runs (solid curves), high mass runs (dashed curves).

Hanauske, et.al. PRD, 96(4), 043004 (2017)

# Evolution of Tracer-particles tracking individual fluid elements in the equatorial plane of the HMNS at post-merger times

Mark G. Alford, Luke Bovard, Matthias Hanauske, Luciano Rezzolla, and Kai Schwenzer (2018) Viscous Dissipation and Heat Conduction in Binary Neutron-Star Mergers. Phys. Rev. Lett. 120, 041101

Different rotational behaviour of the quark-gluon-plasma produced in non-central ultra-relativistic heavy ion collisions
L. Adamczyk et.al., "Global Lambda-hyperon polarization in nuclear collisions: evidence for the most vortical fluid", Nature 548, 2017

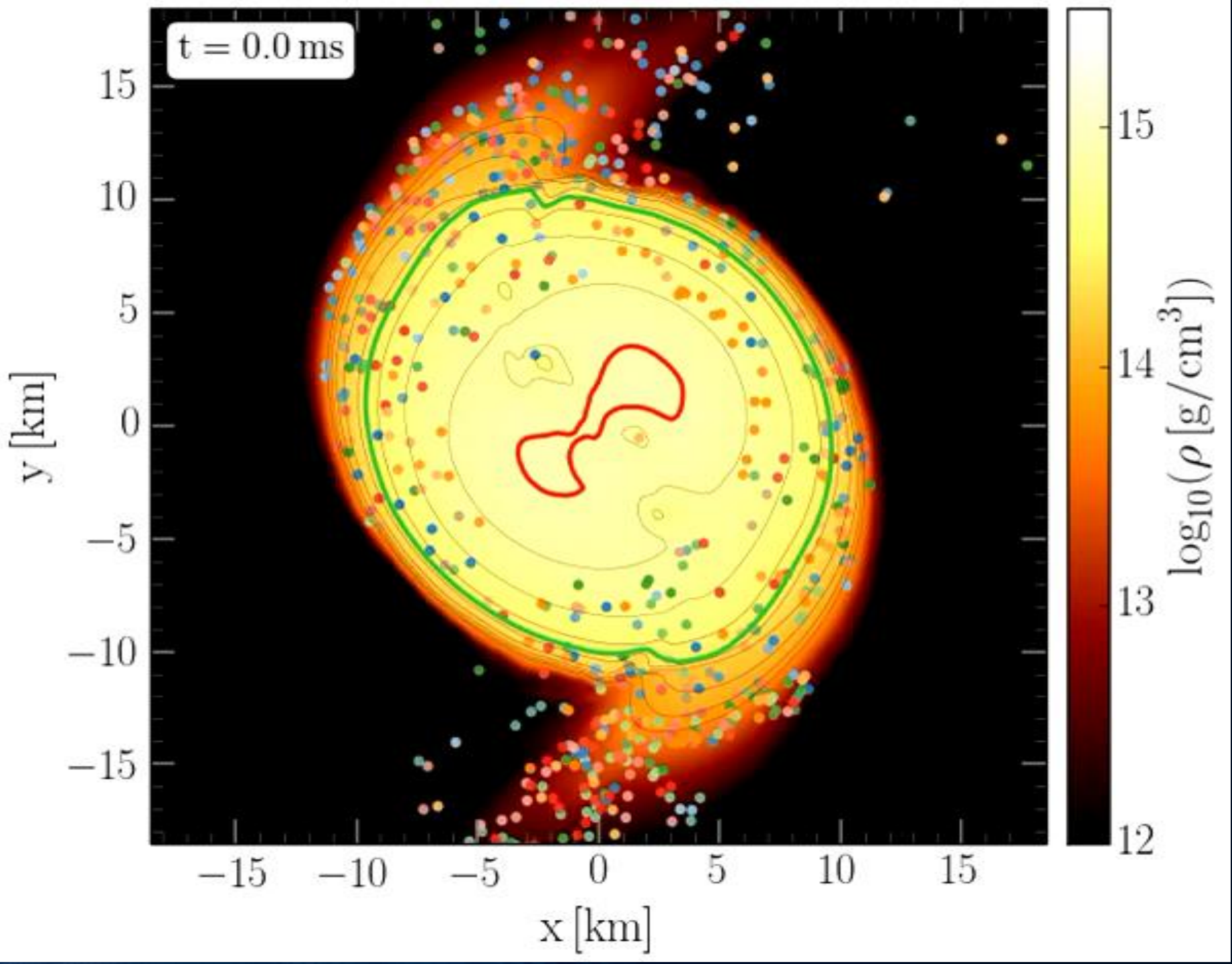

# Can we detect the quark-gluon plasma with gravitational waves?

- Gravitational-wave signatures of the hadron-quark ph
  compact star mergers
  - *Signatures within the late inspiral phase (premerger signals)*
    - Constraining twin stars with GW170817; G Montana, L Tolós, M Han
      99 (10), 103009 (2019)
  - *Signatures within the post-merger phase evolution*
    - **Phase-transition triggered collapse scenario**
      Signatures of quark-hadron phase transitions in general-relativistic neu
      Papenfort, V Dexheimer, M Hanauske, S Schramm, H Stöcker, L. Rezzol
      (2019)
    - **Delayed phase transition scenario**
      Postmerger Gravitational-Wave Signatures of Phase Transitions in Bina
      Rezzolla; Physical Review Letters 124 (17), 171103 (2020)
    - **Prompt phase transition scenario**
      Identifying a first-order phase transition in neutron-star mergers through gr
      Bastian, DB Blaschke, K Chatziioannou, JA Clark, JA Clark, T Fischer, M Oerte
      (2019)

# Can we detect the quark-gluon plasma with gravitational waves?

- Gravitational-wave signatures of the hadron-quark phase transition in binary compact star mergers
  - *Signatures within the late inspiral phase (premerger signals)*
    - Constraining twin stars with GW170817; G Montana, L Tolós, M Hanauske, L Rezzolla; Physical Review D 99 (10), 103009 (2019)
  - *Signatures within the post-merger phase evolution*
    - **Phase-transition triggered collapse scenario**
      Signatures of quark-hadron phase transitions in general-relativistic neutron-star mergers; ER Most, LJ Papenfort, V Dexheimer, M Hanauske, S Schramm, H Stöcker, L. Rezzolla; Physical review letters 122 (6), 061101 (2019)
    - **Delayed phase transition scenario**
      Postmerger Gravitational-Wave Signatures of Phase Transitions in Binary Mergers; LR Weih, M Hanauske, L Rezzolla; Physical Review Letters 124 (17), 171103 (2020)
    - **Prompt phase transition scenario**
      Identifying a first-order phase transition in neutron-star mergers through gravitational waves; A Bauswein, NUF Bastian, DB Blaschke, K Chatziioannou, JA Clark, JA Clark, T Fischer, M Oertel; Physical review letters 122 (6), 061102 (2019)

# Sig
## Phas

ER Most et al., PRL 122 (6), 061101 (2019)

(CMF)

) sigma

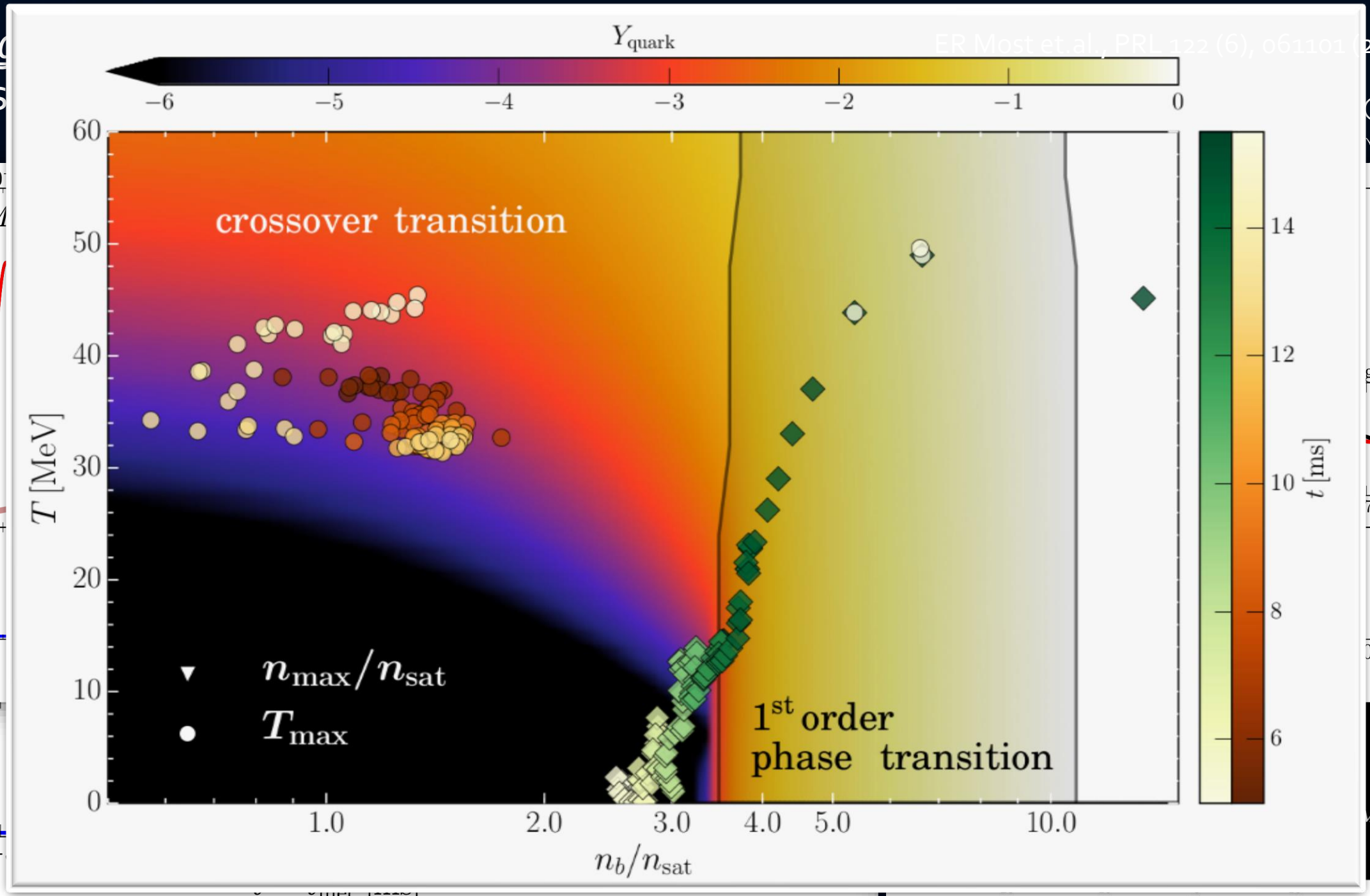


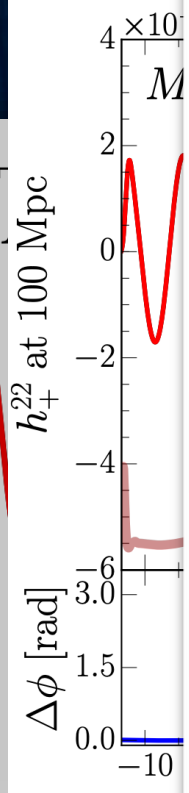


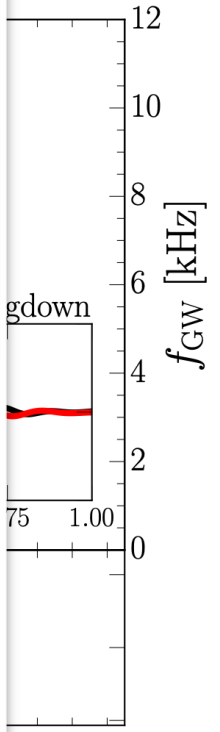


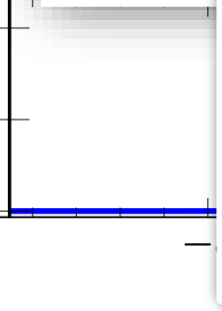

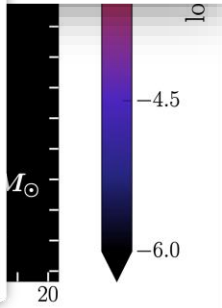

**Phase-transition triggered collapse scenario**

*Signatures of quark-hadron phase transitions in general-relativistic neutron-star mergers*

ER Most, LJ Papenfort, V Dexheimer, M Hanauske, S Schramm, H Stöcker and L. Rezzolla

Physical review letters 122 (6), 061101 (2019)

Density-Temperature-Composition dependent EOS within the CMFΩ model.

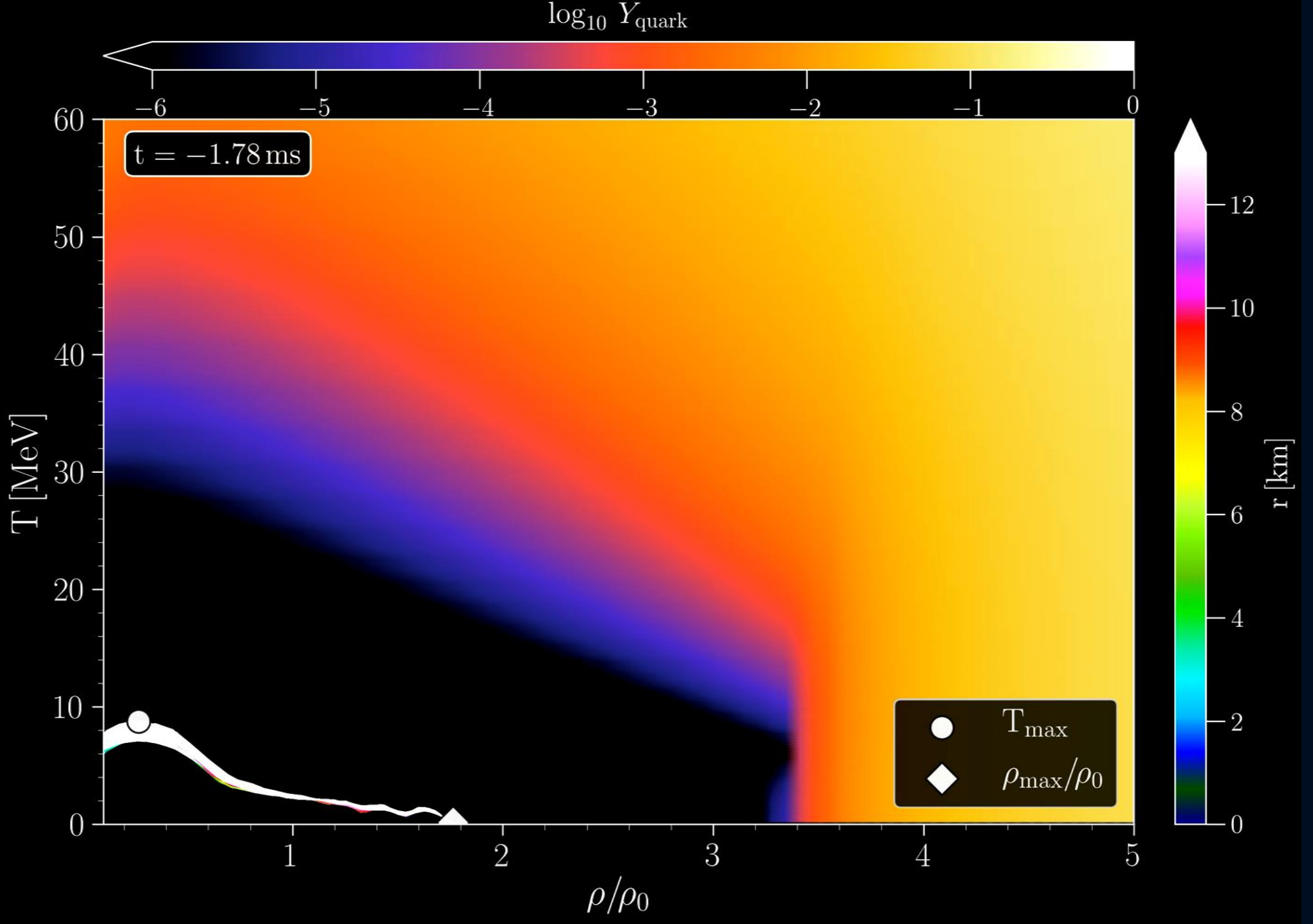

The last simu

r (HMHS)

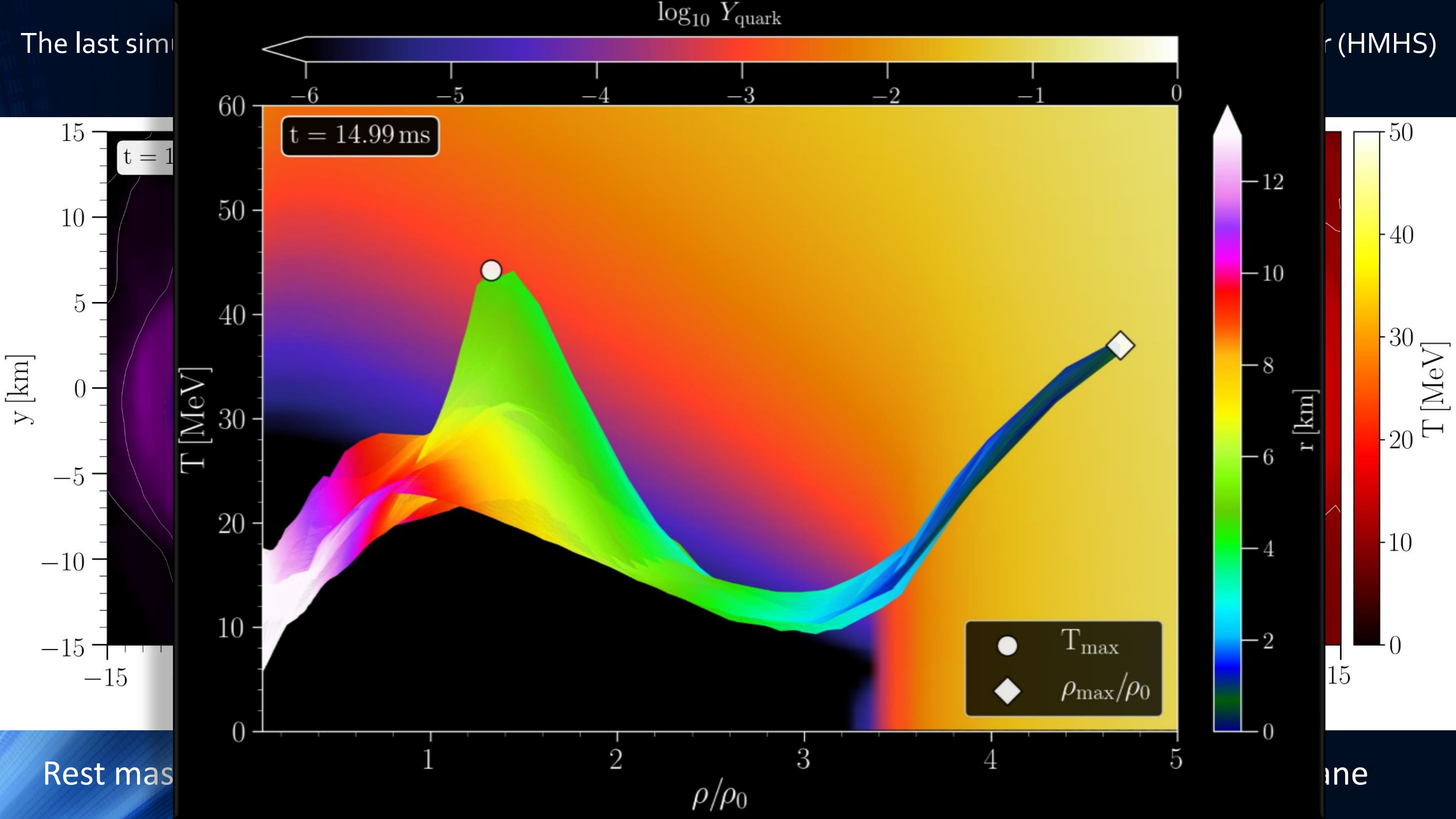


Rest mas

ane

The last sim

(HMHS)

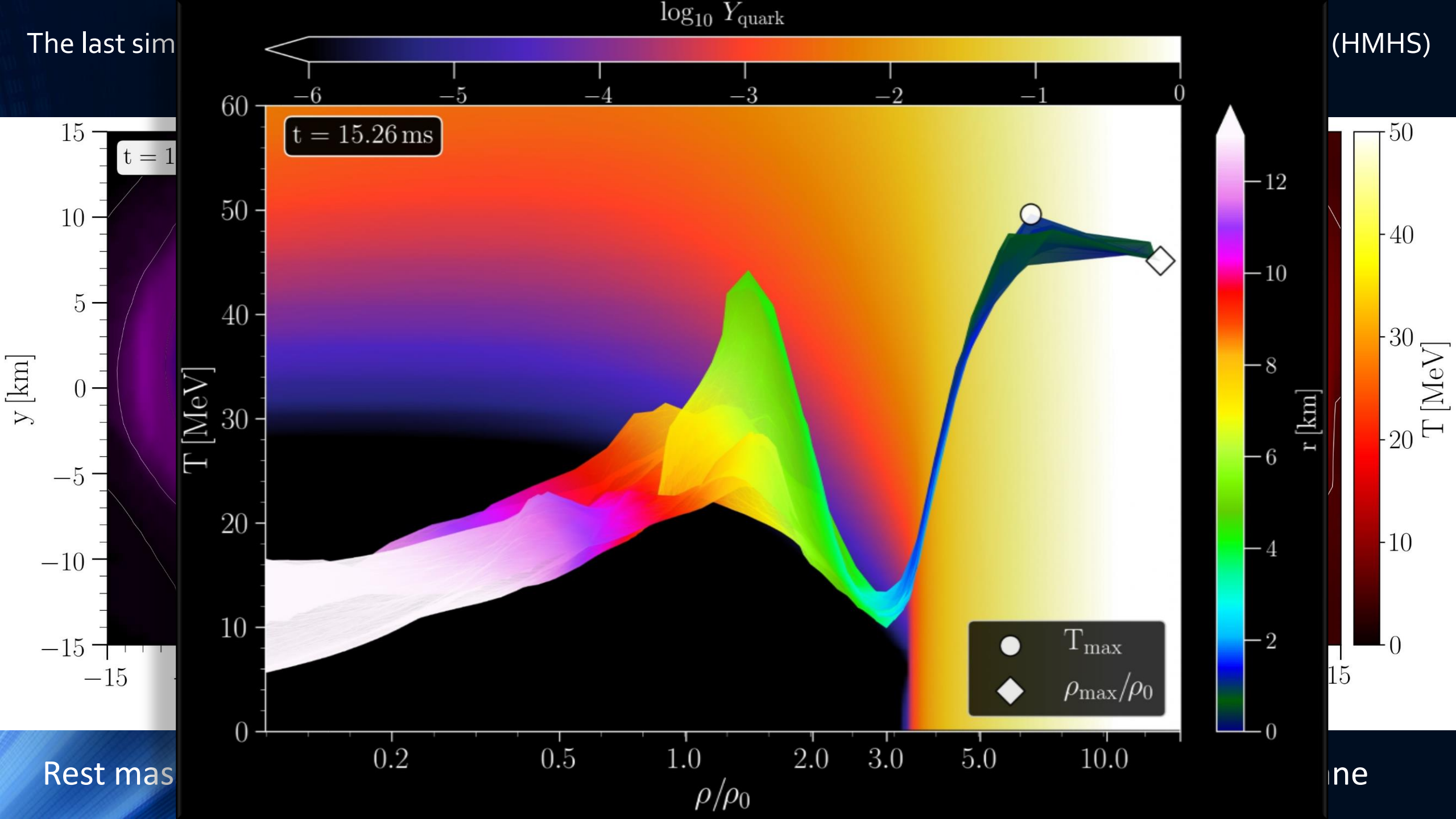


Rest mas

ne

# The Strange Bird Plot

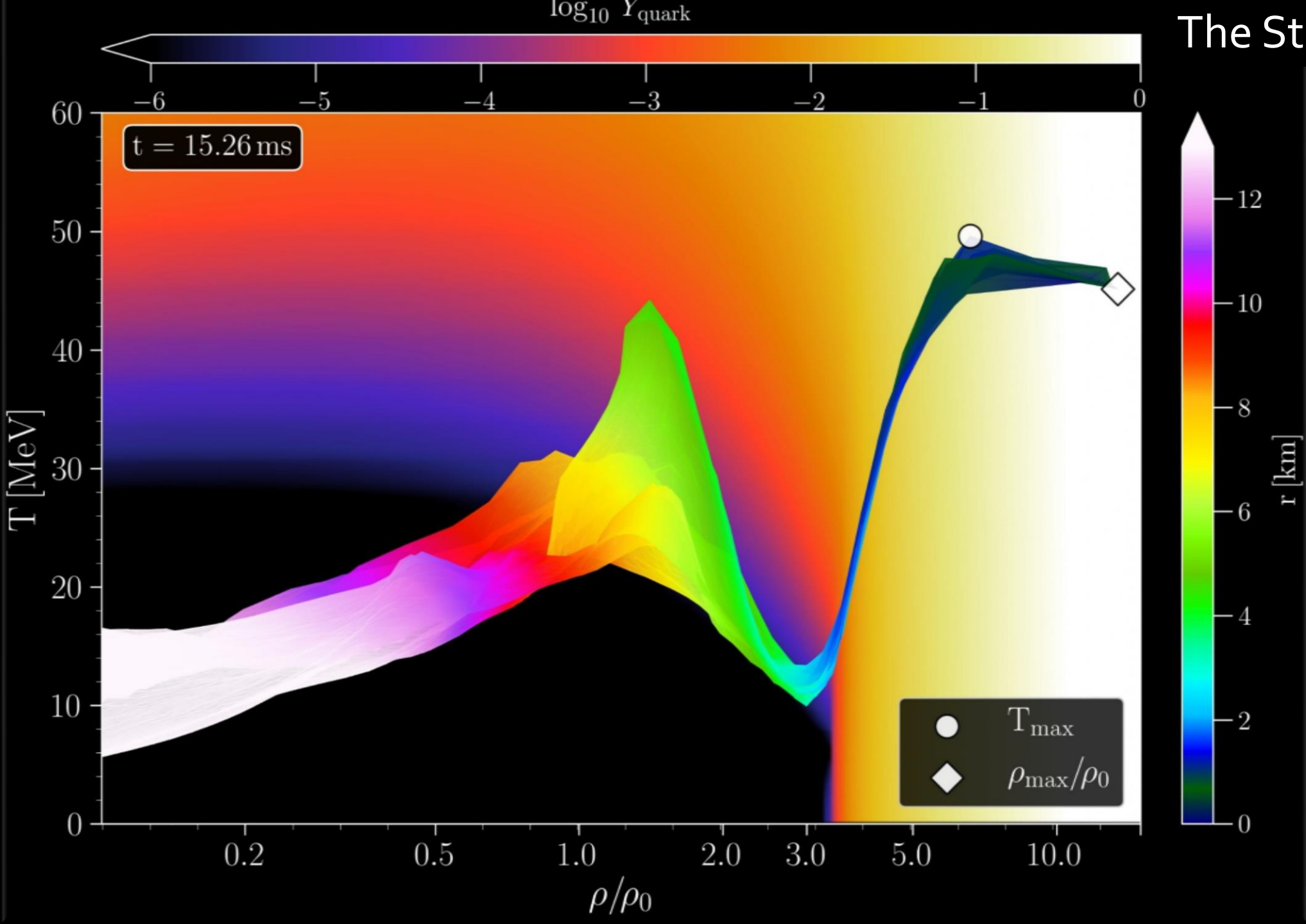


While the quarks in the pelican's head have already rescued themselves from their confinement cage, his body still largely consists of hadronic particles. It is precisely at this point in time that the apparent horizon is formed around the dense and hot head of the strange bird and the free strange quark matter is macroscopically confined by the formation of the black hole.

# GRAVITATIONAL COLLAPSE AND SPACE- TIME SINGULARITIES

Nobel Price 2020: R.Penrose, PRL Vol.14 No.3 (1965)

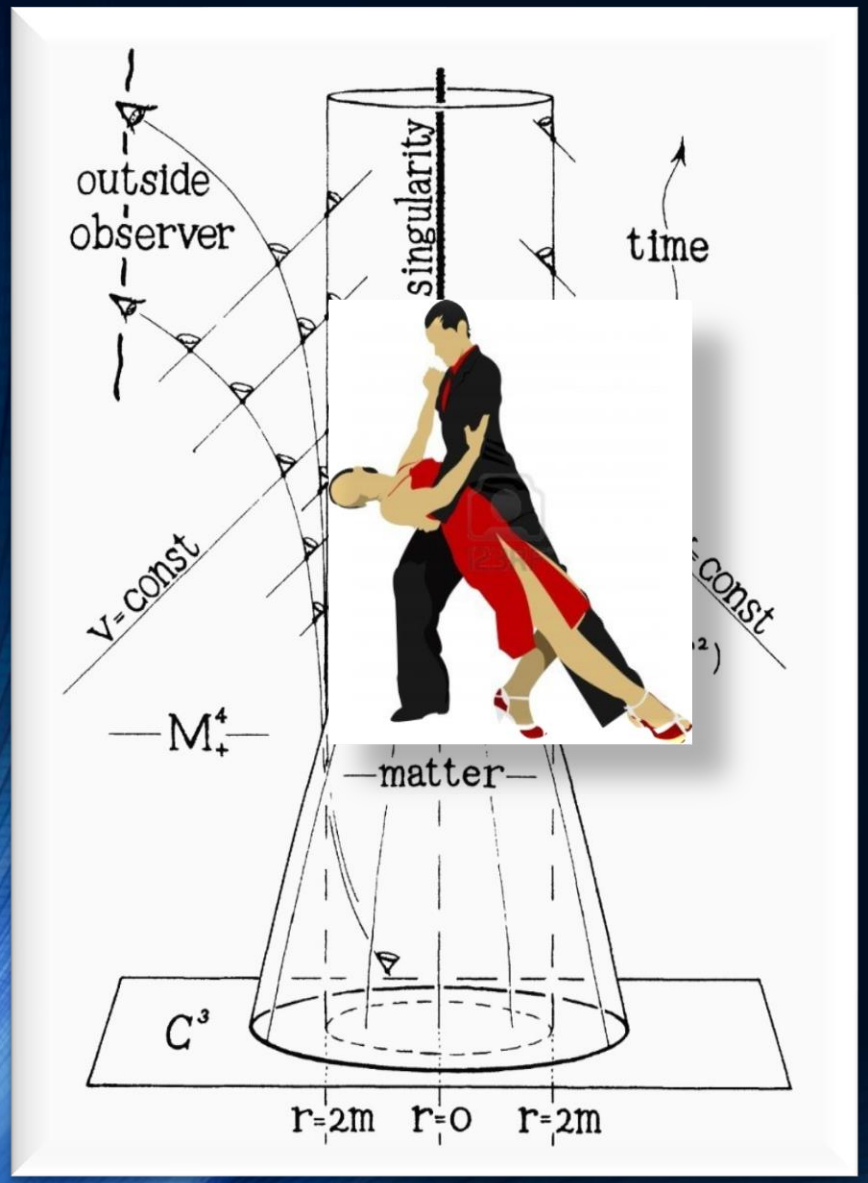


Self-drawn space-time diagram by R.Penrose (1965)

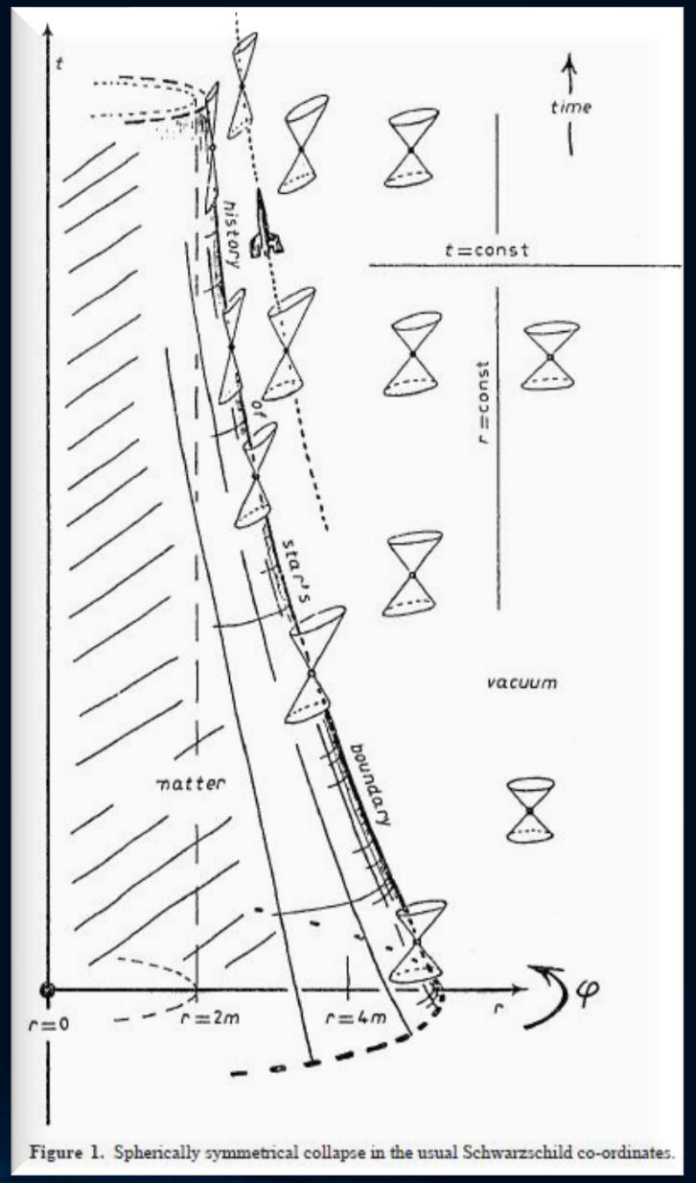


Figure 1. Spherically symmetrical collapse in the usual Schwarzschild co-ordinates.

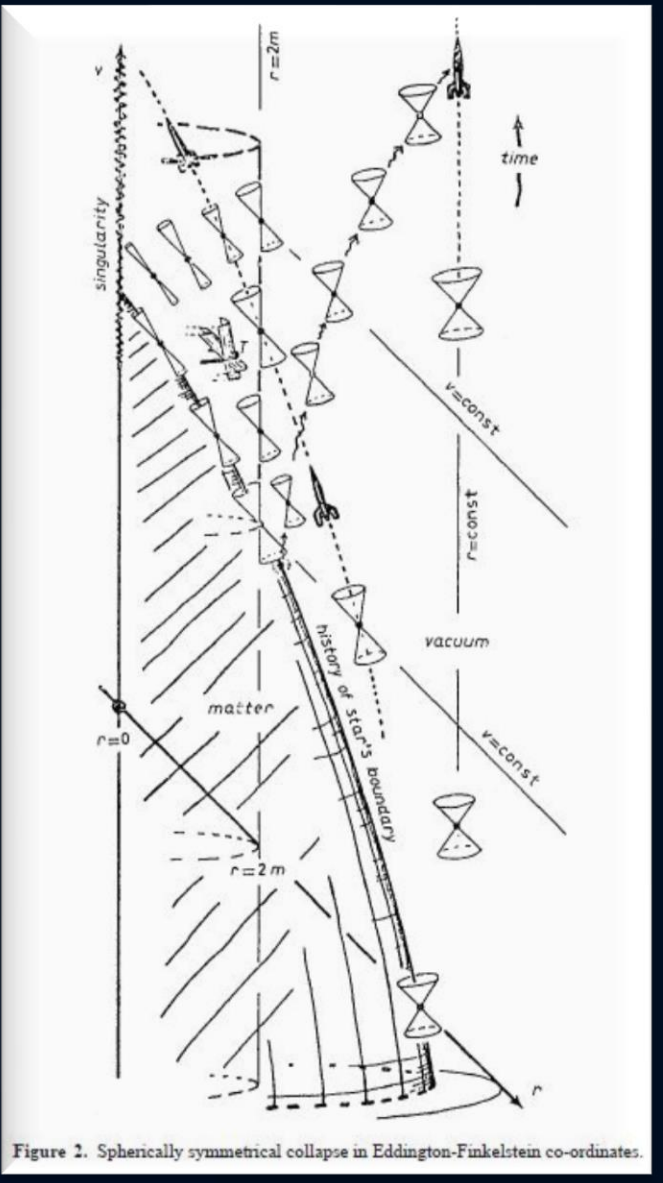


Figure 2. Spherically symmetrical collapse in Eddington-Finkelstein co-ordinates.

R.Penrose in Rivista del Nuovo Cimento, Num.Spez. I, 257 (1969)

Probably the best illustration of the essential properties of the black hole that is created

The spacetime funnel
in the
German parliament building

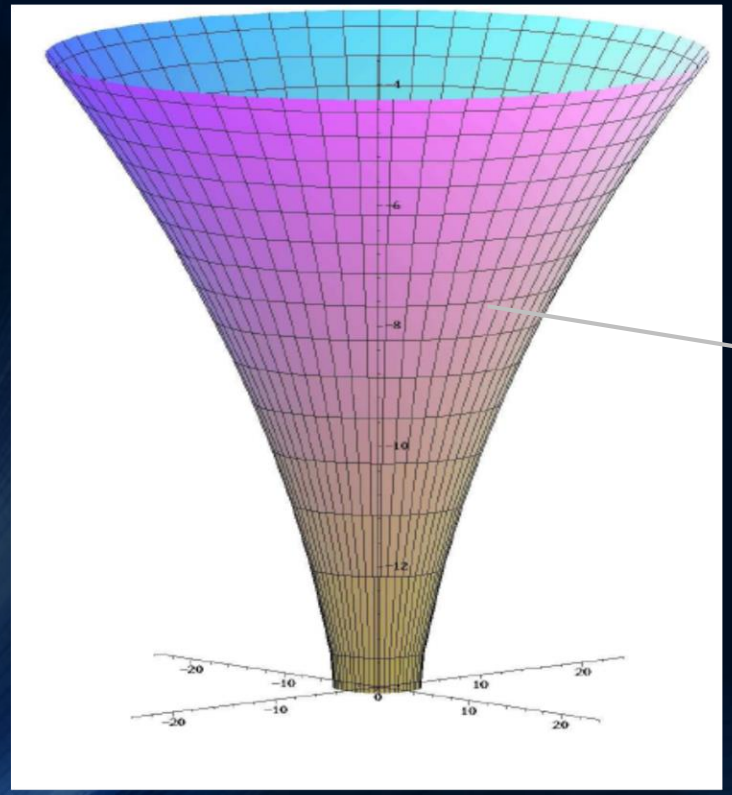


Lateral Thoughts: Matthias Hanauske

physicsweb.org

M. Hanauske, Physics World 18 (10), 64 (2005)

# Black holes and the German Reichstag

One day a couple of years ago I was attending a meeting of the German Astronomical Society in Berlin, when I was gripped with an almost irrepressible sense of inner unrest. There was no other option – I simply had to leave the lecture halls of the Technical University and enjoy the gorgeous day outside. Before I left, however, I carefully taped my poster to the wall between the entrances to the men's and women's toilets, which seemed the perfect spot for it. Every congress delegate would now be forced – subliminally at least – to notice my creation.

After leaving the university buildings, I first soaked up the summer sunshine in the zoological gardens [illegible] heading towards the Reichstag – the home of the G[illegible] parliament. As I did so, my thoughts wandered off i[illegible] ferent direction. What a waste of time, it occurred [illegible] all those boring lectures are. What physics despe[illegible] needs, I reasoned, is a new and exciting way of pres[illegible] the subject.

Unfortunately, modern physics is impossible to com-prehend using intuition alone. How can bizarre concepts such as the curvature of space–time or the event horizon of a black hole be understood? What possible imagery could help non-scientists to grasp the significance and vital importance of some of the major insights of theoretical physics? Finding a simple way of conveying those ideas seemed an impossible task.

Lost in thought, I looked up and realized I had almost reached my desired destination as the modern glass dome of the newly constructed core of the Reichstag building swung into view. As I examined the dome more closely, I noticed it contained a huge funnel on the inside. To my

The funnel looks exactly like the diagrams used to illustrate the curvature of a black hole

Space-time funnel

Frozen images of engraving events in German history

Event Horizon

Ereignishorizont

Real Singularity

http://th.physik.uni-frankfurt.de/~hanauske/new/LateralThougts.html

# Can we detect the quark-gluon plasma with gravitational waves?

- Gravitational-wave signatures of the hadron-quark phase transition in binary compact star mergers
  - *Signatures within the late inspiral phase (premerger signals)*
    - Constraining twin stars with GW170817; G Montana, L Tolós, M Hanauske, L Rezzolla; Physical Review D 99 (10), 103009 (2019)
  - *Signatures within the post-merger phase evolution*
    - **Phase-transition triggered collapse scenario**
      Signatures of quark-hadron phase transitions in general-relativistic neutron-star mergers; ER Most, LJ Papenfort, V Dexheimer, M Hanauske, S Schramm, H Stöcker, L. Rezzolla; Physical review letters 122 (6), 061101 (2019)
    - **Delayed phase transition scenario**
      Postmerger Gravitational-Wave Signatures of Phase Transitions in Binary Mergers; LR Weih, M Hanauske, L Rezzolla; Physical Review Letters 124 (17), 171103 (2020)
    - **Prompt phase transition scenario**
      Identifying a first-order phase transition in neutron-star mergers through gravitational waves; A Bauswein, NUF Bastian, DB Blaschke, K Chatziioannou, JA Clark, JA Clark, T Fischer, M Oertel; Physical review letters 122 (6), 061102 (2019)

# *Signatures within the post-merger phase evolution*

## Delayed phase transition scenario

Postmerger Gravitational-Wave Signatures of Phase Transitions in Binary Mergers; LR Weih, M Hanauske, L Rezzolla; Physical Review Letters 124 (17), 171103 (2020)

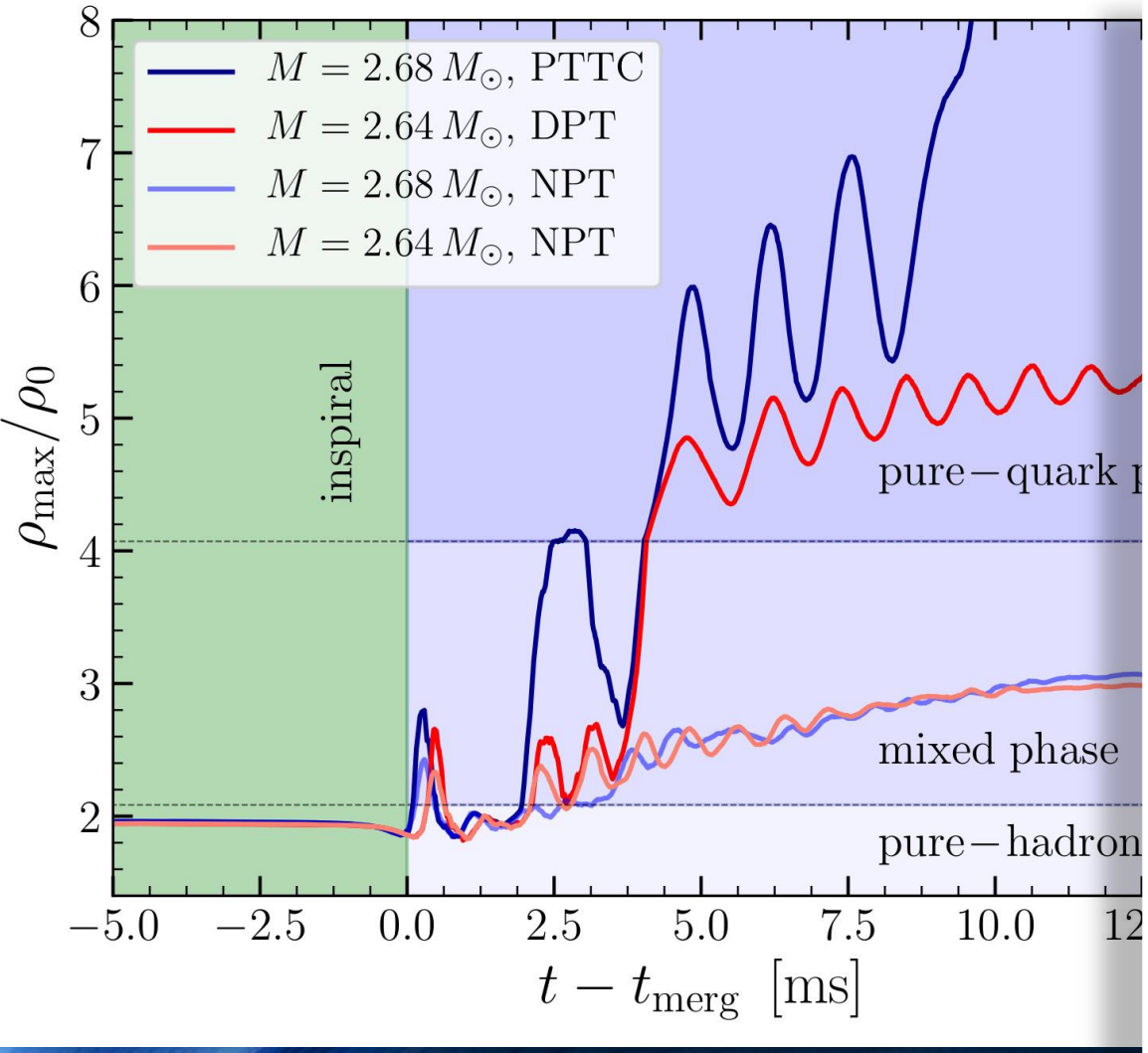


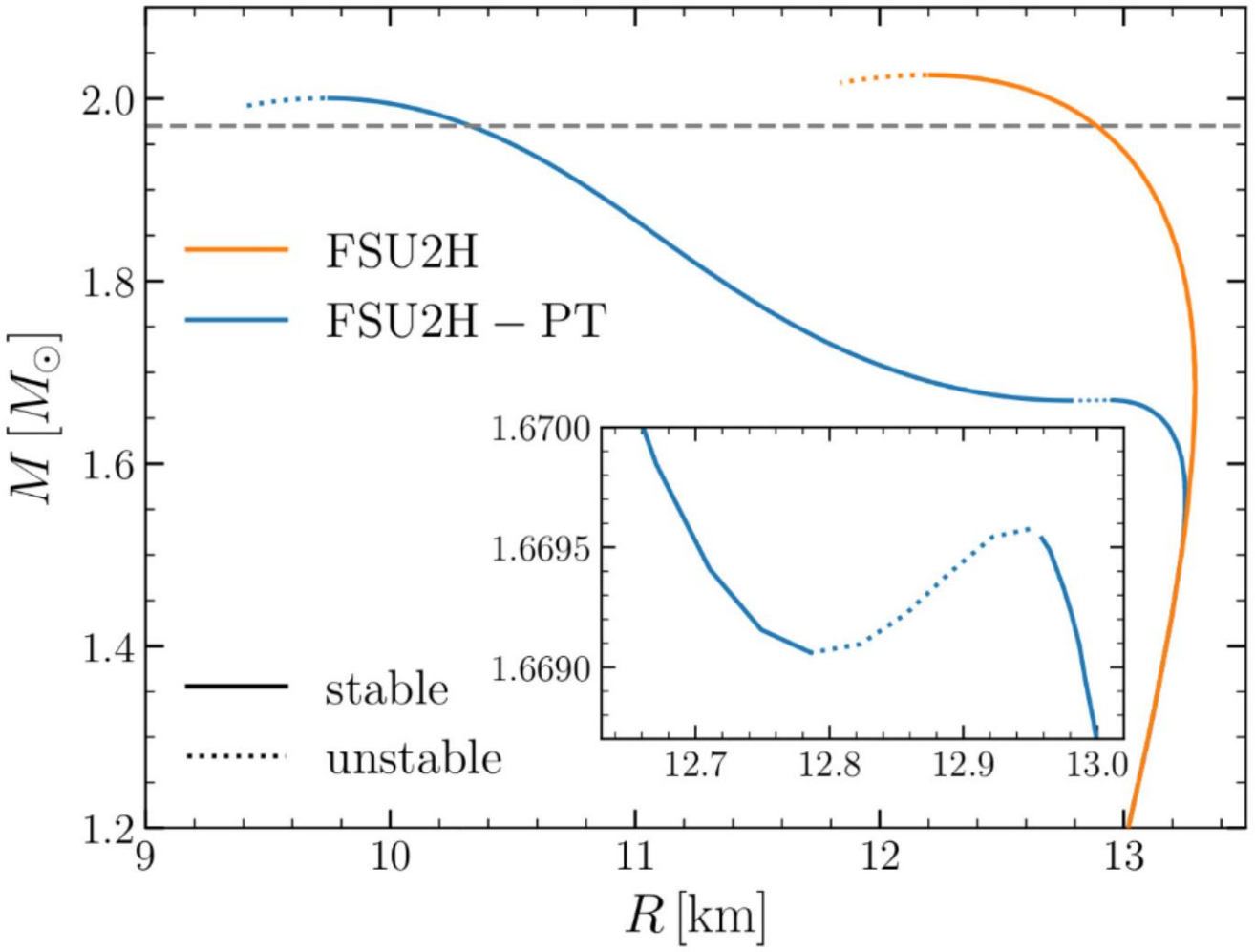

# Binary Neutron Star Mergers in the QCD Phase Diagram

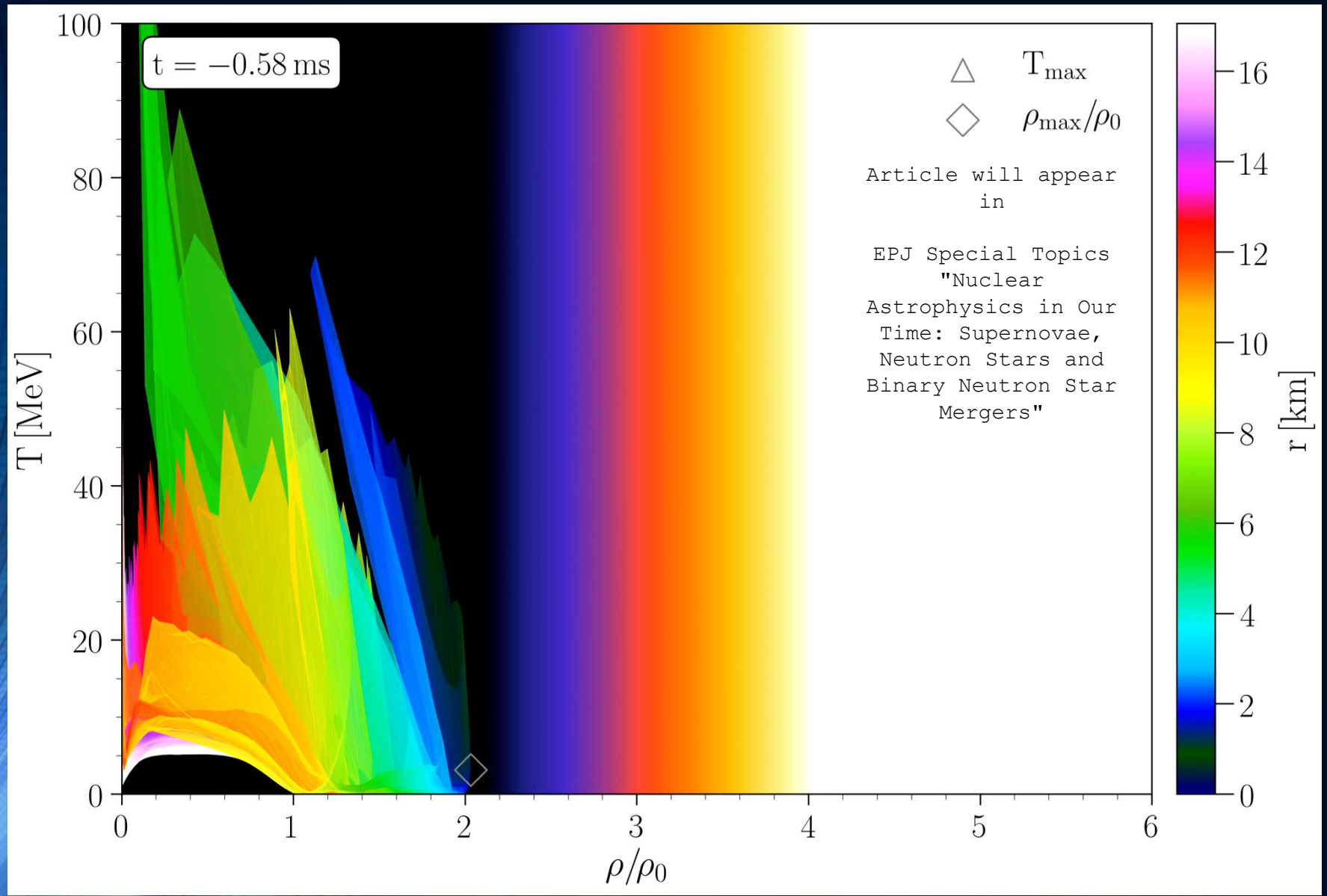


Evolution of hot and dense matter inside the inner area of a hypermassive hybrid star simulated within the ( FSU2H-PT + thermal ideal fluid ) EOS with a total mass of $M_{total}=2.64\ M_{\odot}$ in the style of a (T- ρ) QCD phase diagram plot

The color-coding indicate the radial position r of the corresponding (T- ρ) fluid element measured from the origin of the simulation (x , y) = (o , o) on the equatorial plane at z = o.

The open triangle marks the maximum value of the temperature while the open diamond indicates the maximum of the density.

These figures show the configuration of the HMHS at a time right before the collapse to the more compact star. The small asymmetry in the density profile and especially the double-core structure is amplified by the collapse resulting in a large one-sided asymmetry (i.e., an m = 1 asymmetry in a spherical-harmonics decomposition), which triggers a sizeable h21 GW strain.

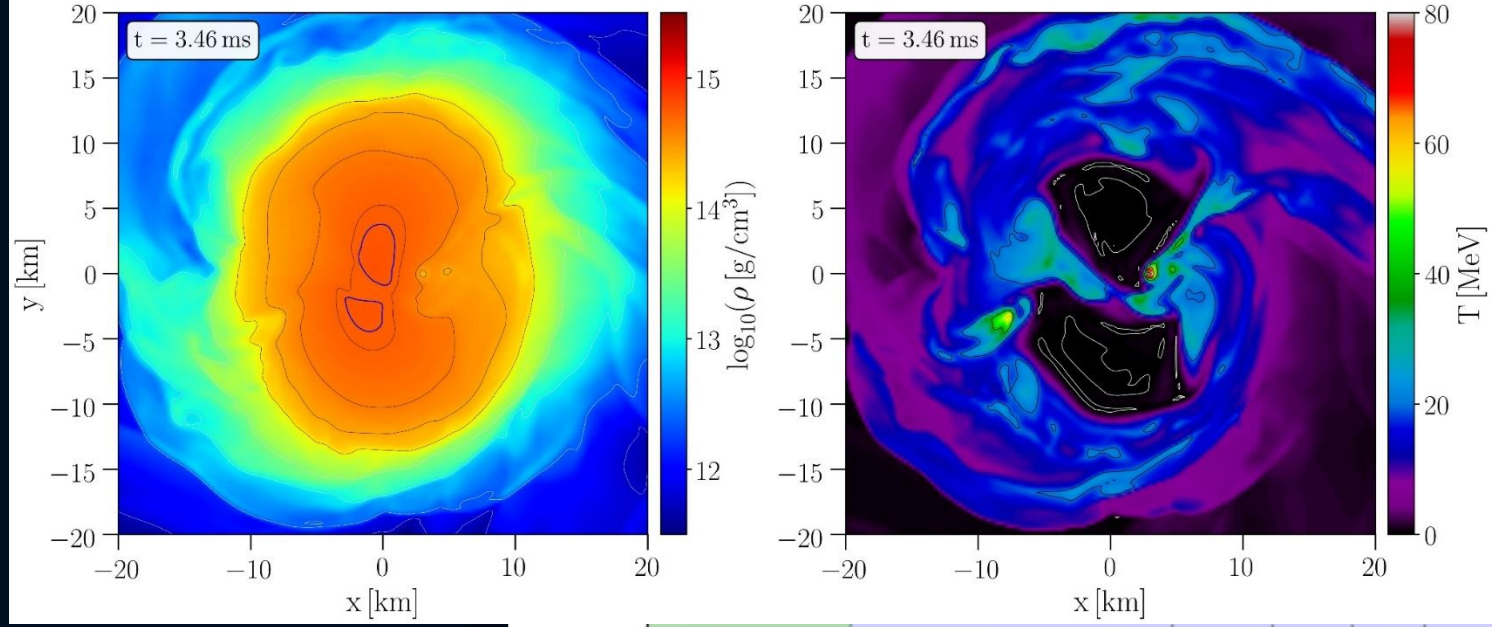


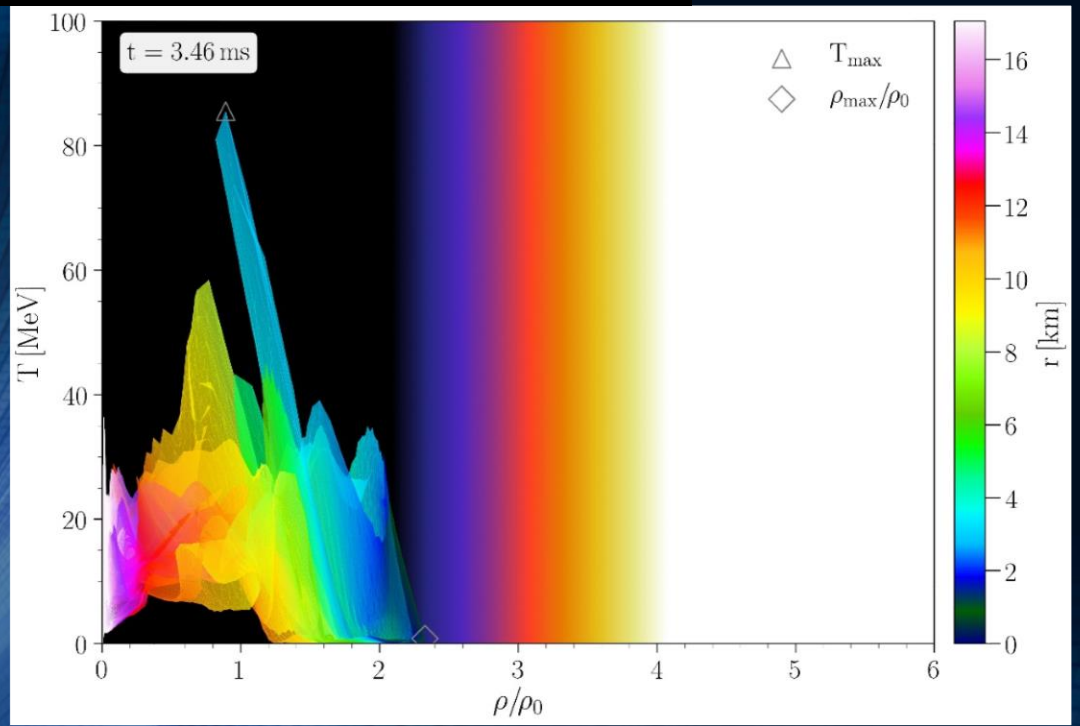


Density maximum

Instantaneous GW frequency

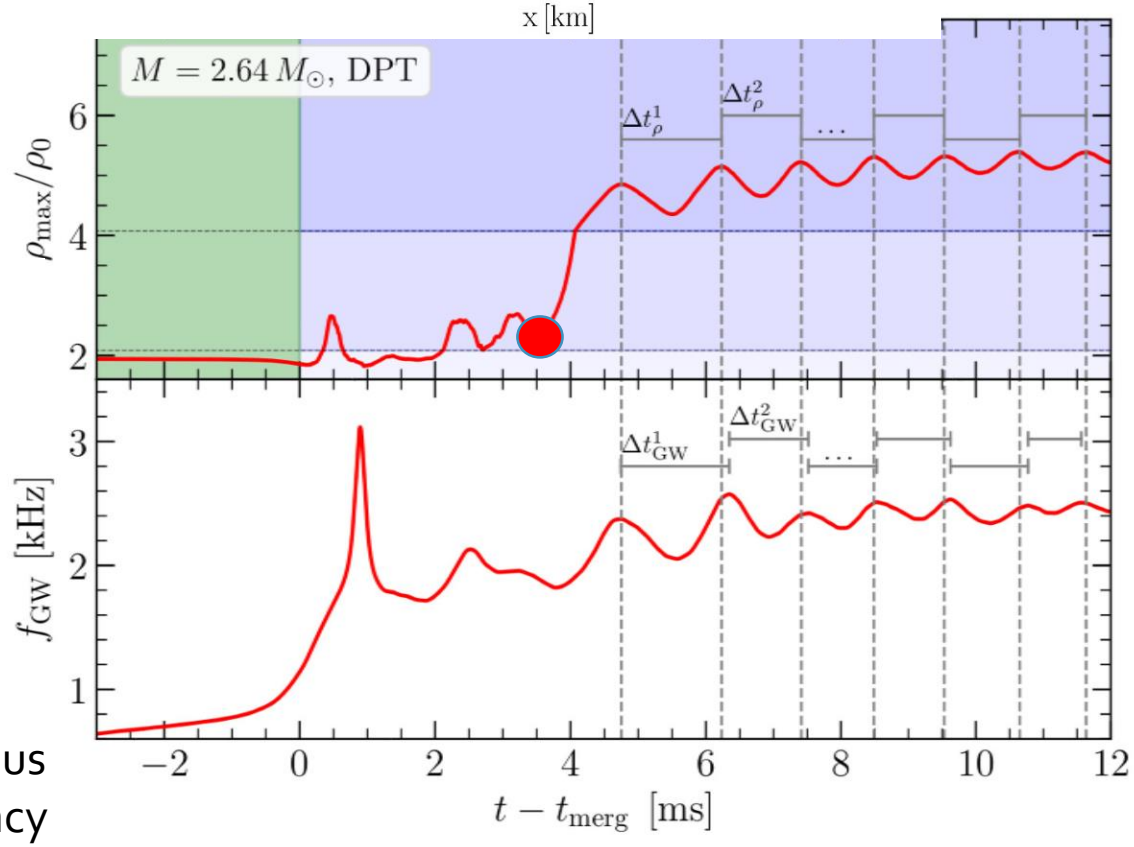

The figures correspond to a time near the first density maximum at t = 4.8ms (see red marker). The large m = 1 contribution can be seen by looking at the asymmetry of the spatial location of the quark core, which is marked with the second blue contour line. As a result of this asymmetry, the location of the two temperature are at different radial distances from the grid center.

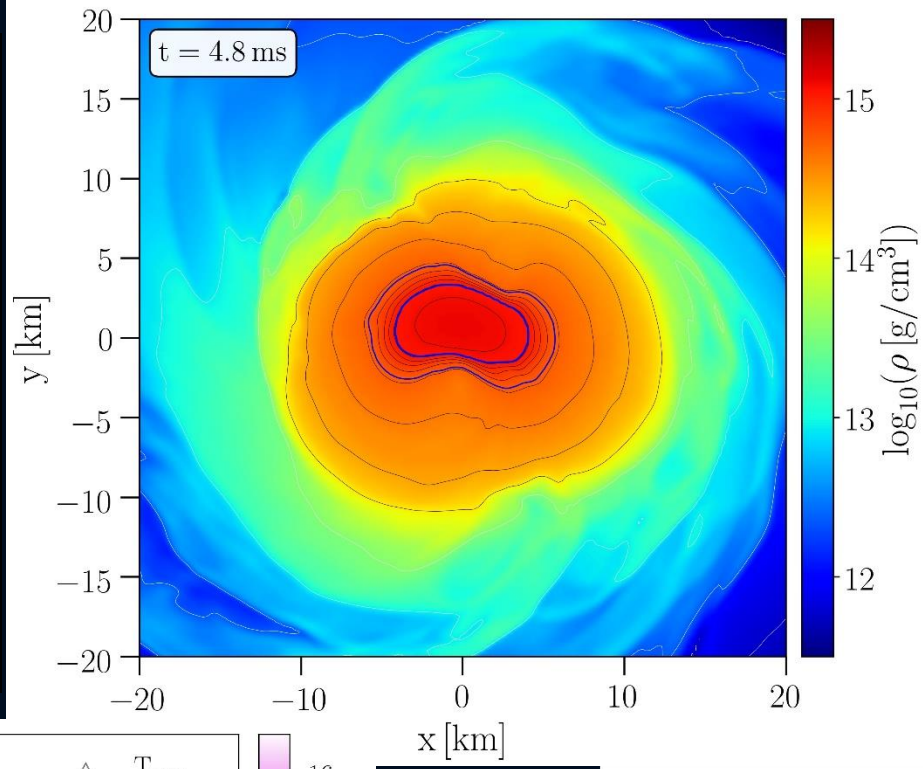


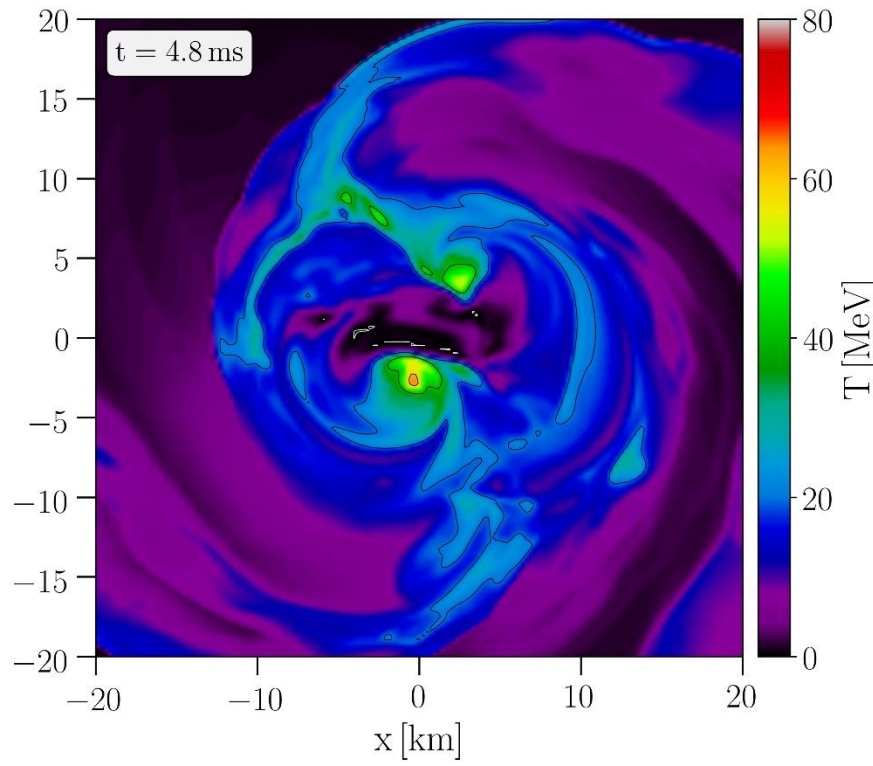


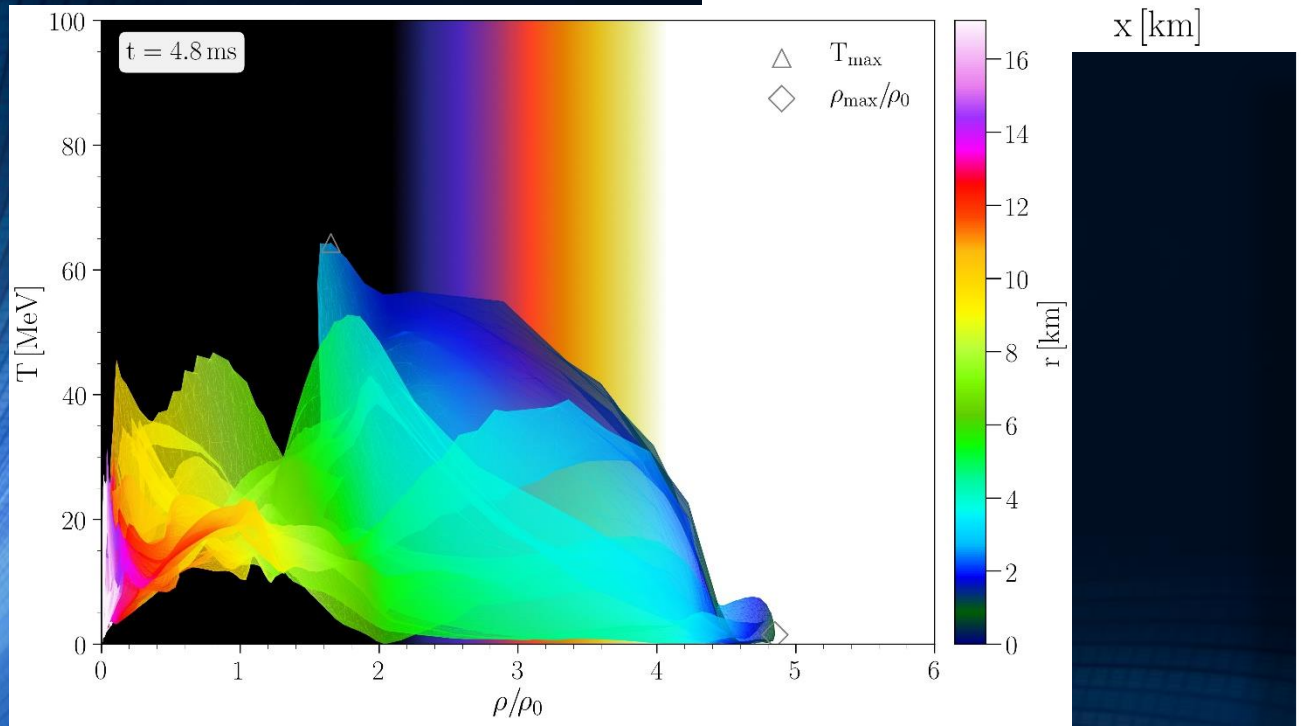


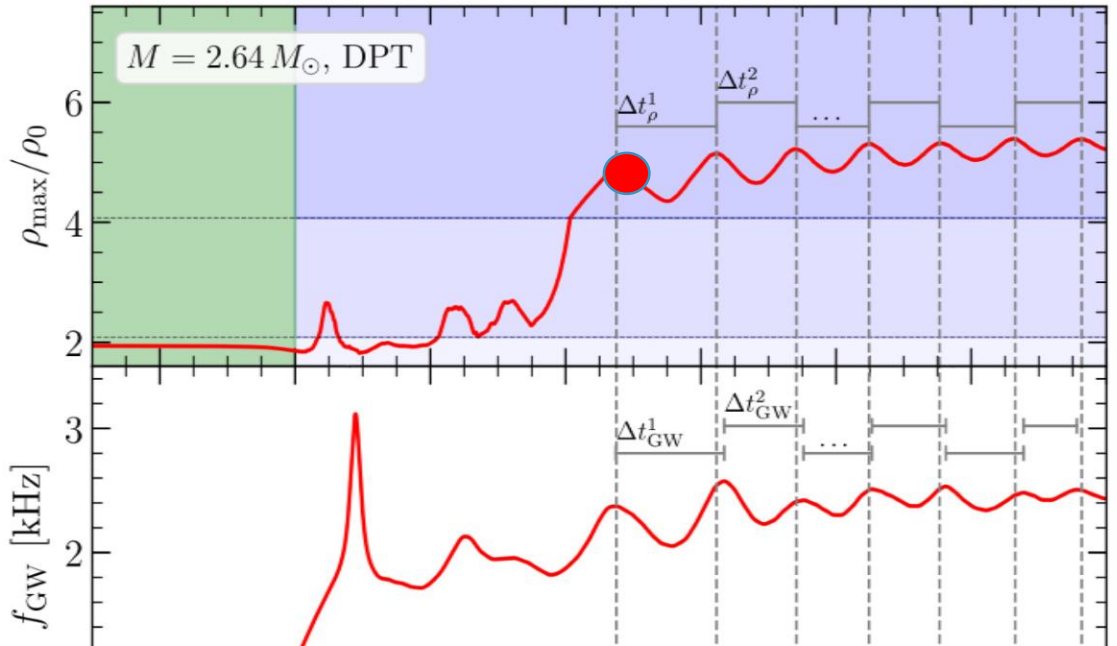

The figures correspond to a time near the first density minimum at t = 5.52ms (see red marker). The large m = 1 contribution can be seen by looking at the asymmetry of the spatial location of the quark core, which is marked with the second blue contour line. As a result of this asymmetry, the location of the two temperature are at different radial distances from the grid center.

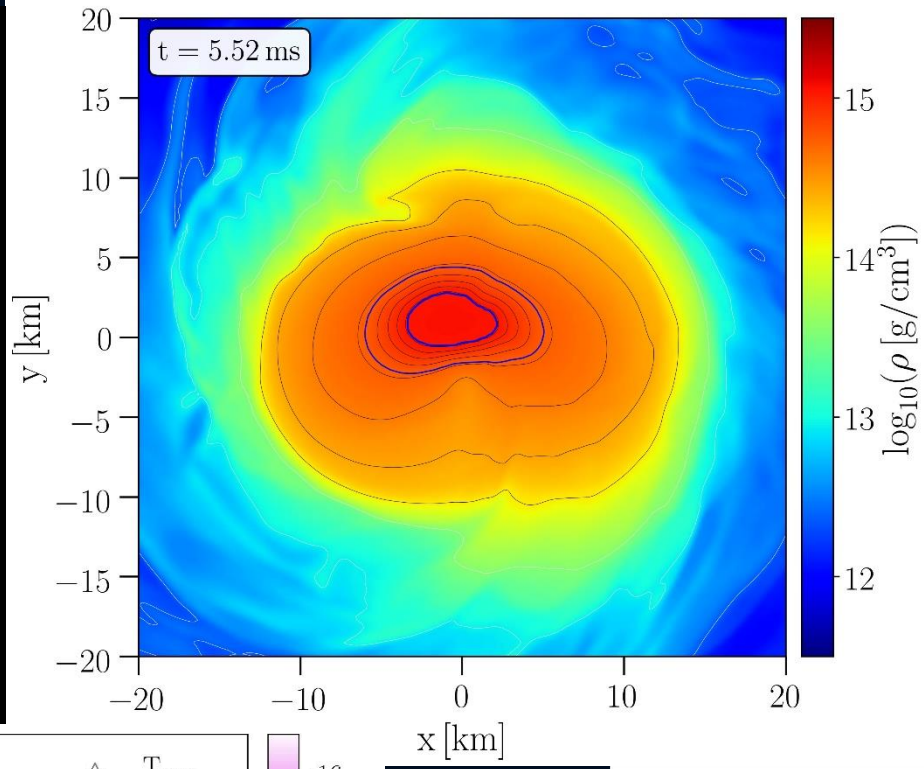


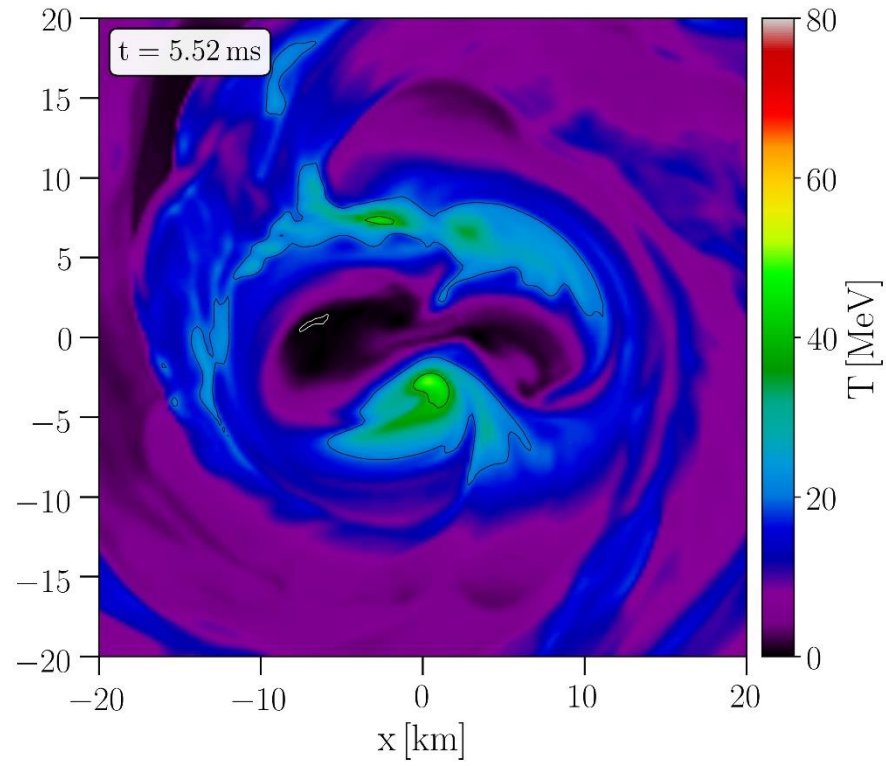


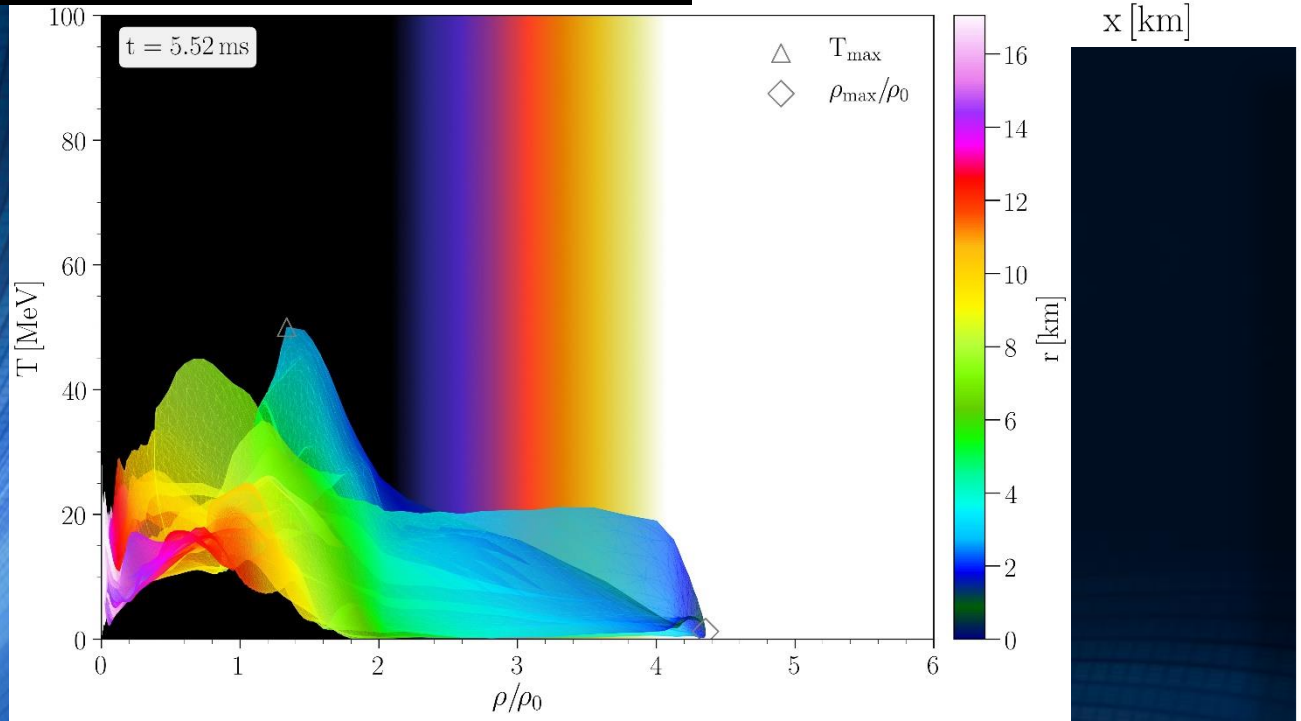


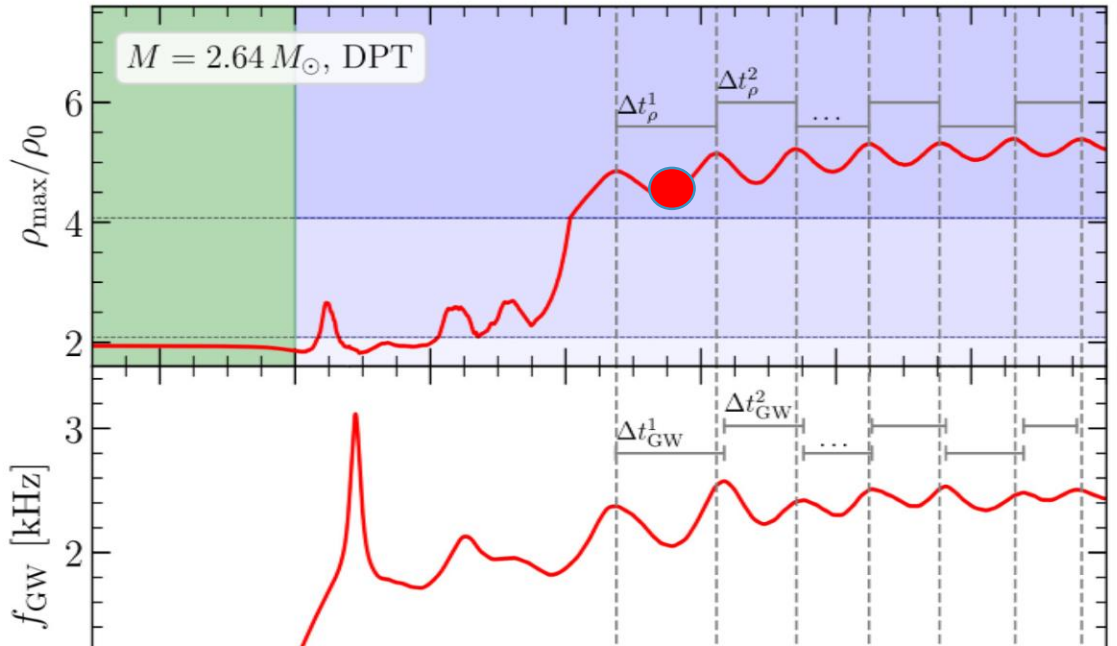

The collapse of the HMNS to the HMHS causes the system to vibrate. At the times when the maximum of the central density is reached, the pure quark core with its stiffer equation of state presses violently against the gravitational pressure and the star expands again and, as a result, its central density decreases.

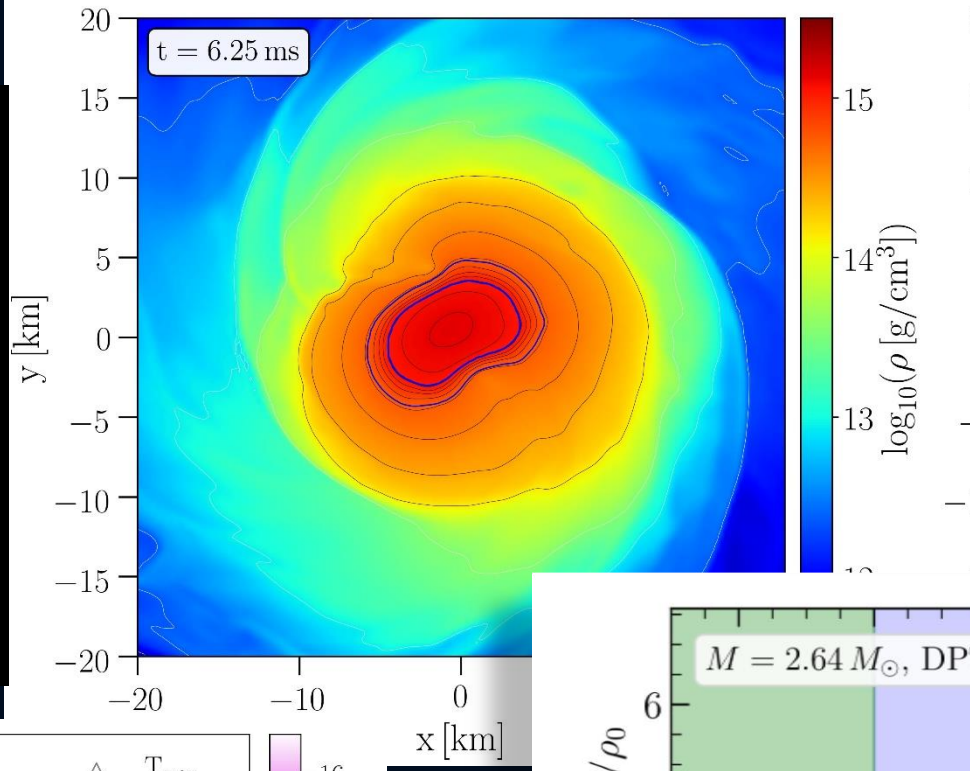


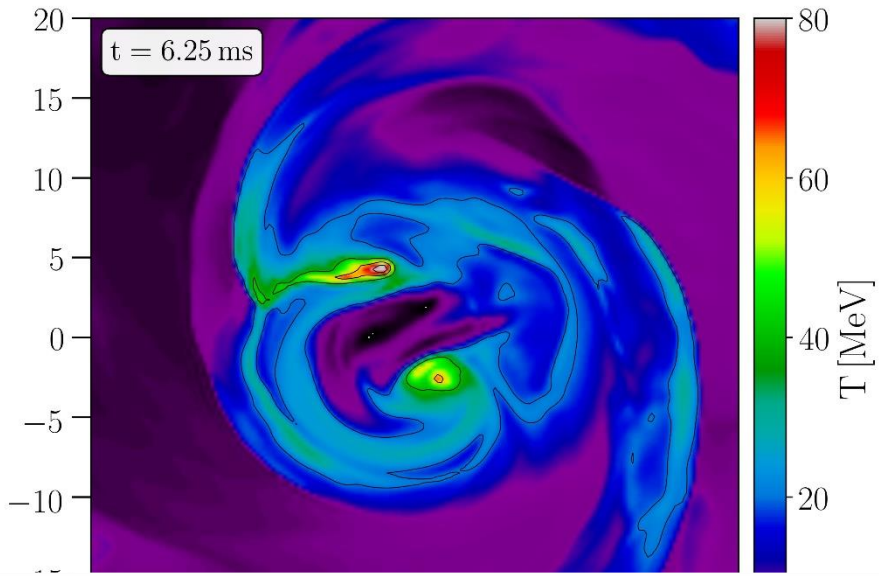


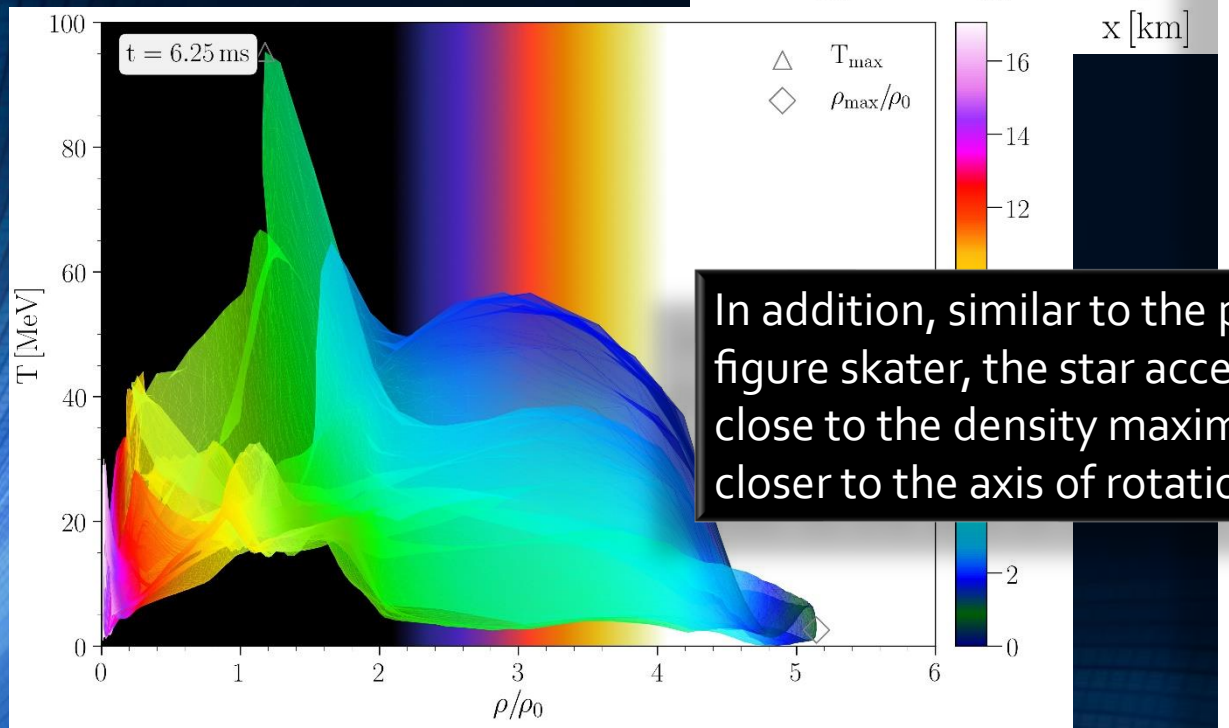


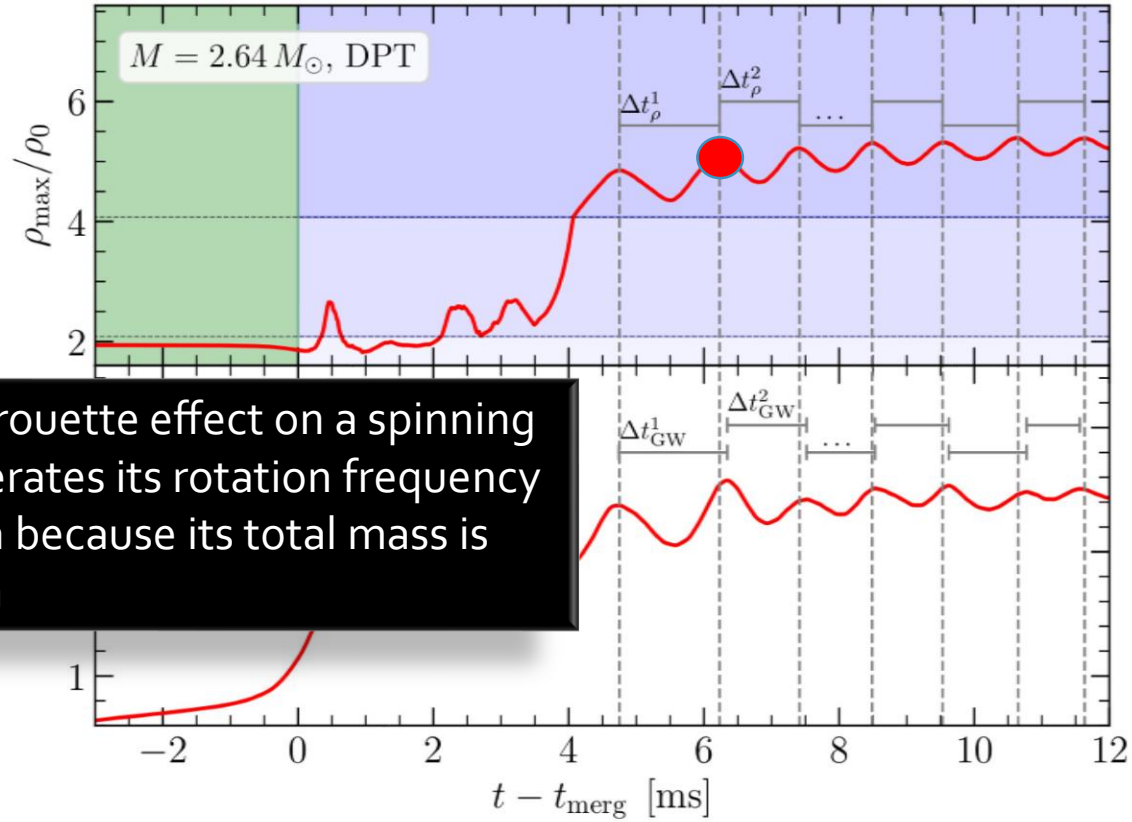


In addition, similar to the pirouette effect on a spinning figure skater, the star accelerates its rotation frequency close to the density maxima because its total mass is closer to the axis of rotation

These figures report the HMHS properties at t = 13.15 ms and shows that in addition to the two temperature hot-spots, a new high temperature shell surrounding a cold core appears within the mixed phase region of the remnant . For subsequent post-merger times, the two temperature hot-spots will be smeared out to become a ring like structure on the equatorial plane

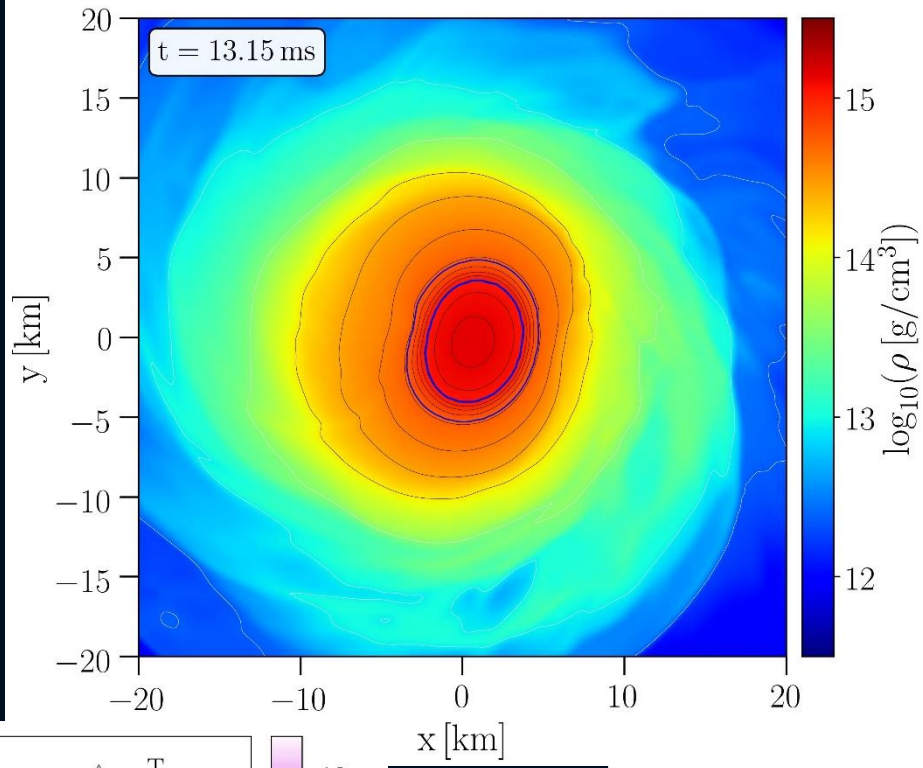


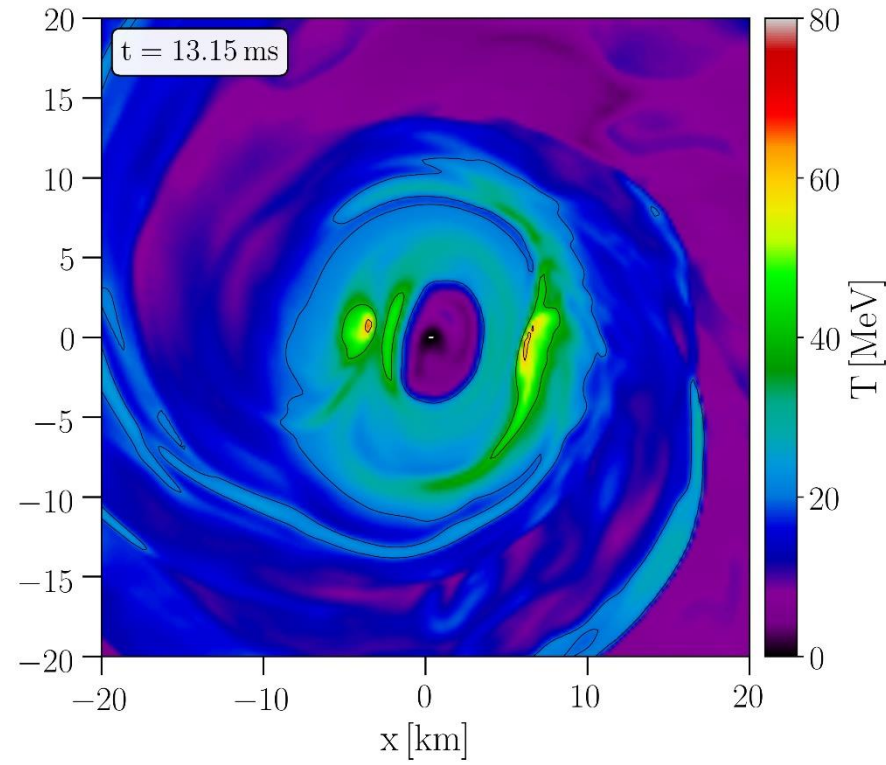


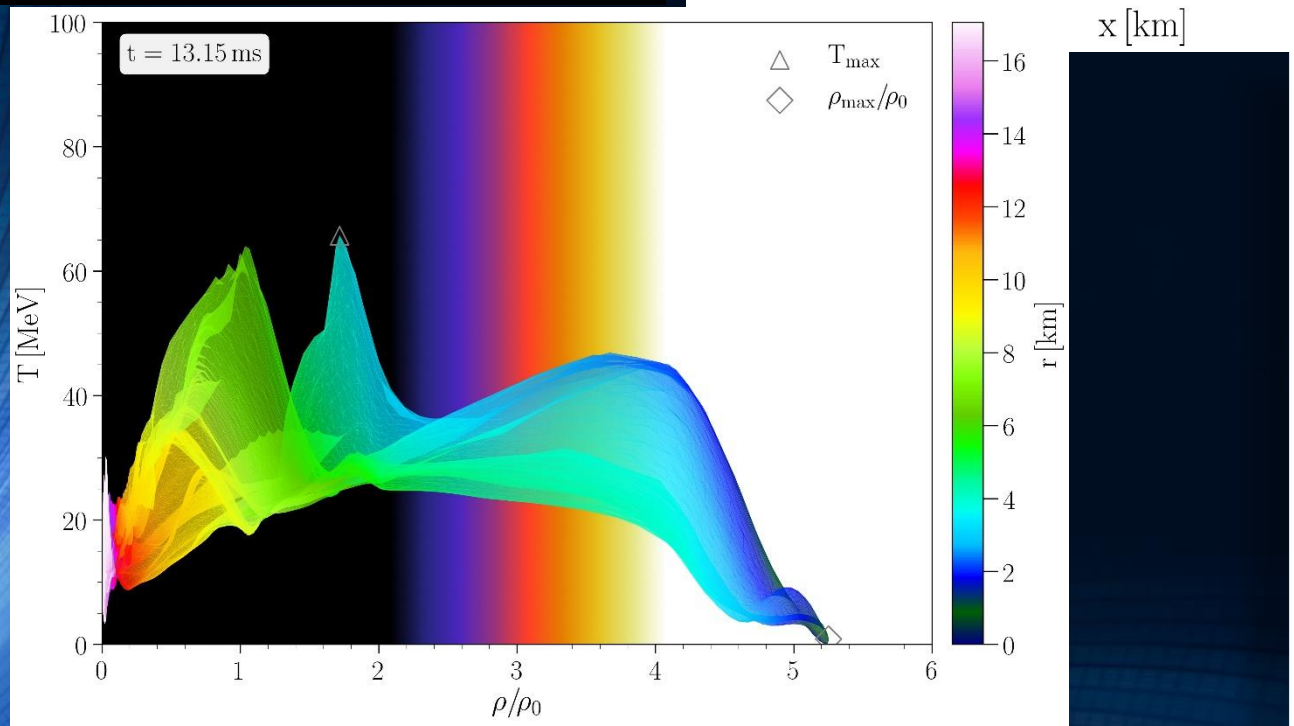


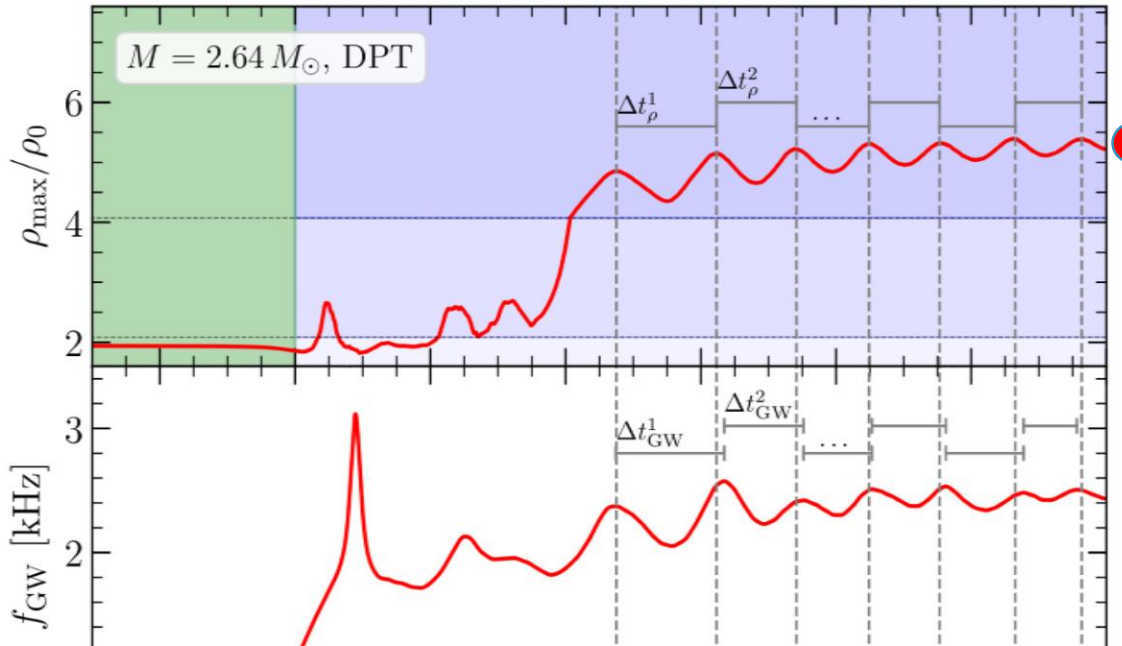

Density Temperature Rotation-profile Frame dragging

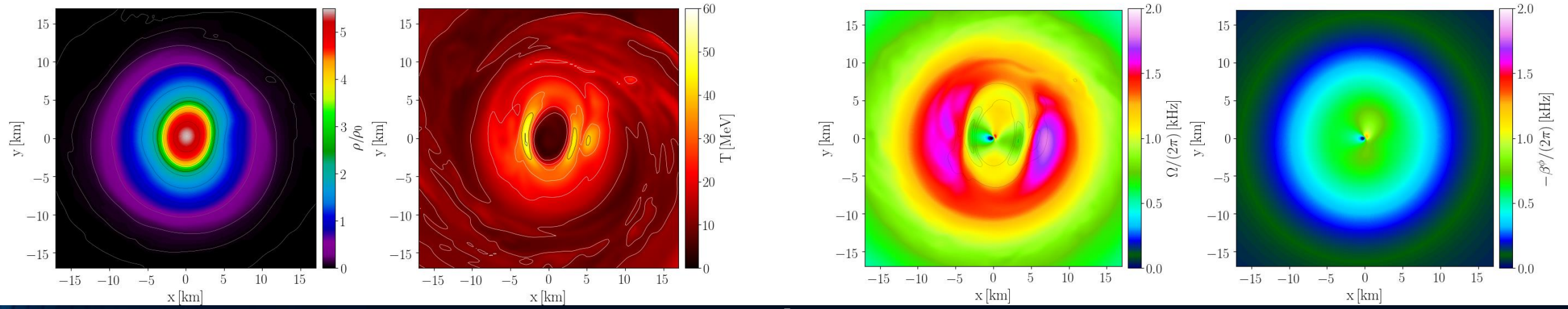


xy-plane

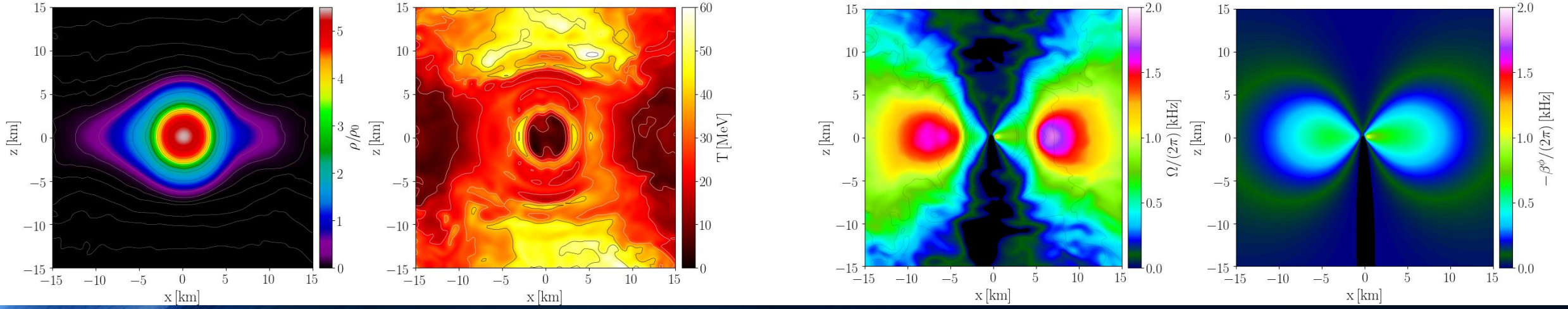


xz-plane

Density Temperature Rotation-profile Frame dragging

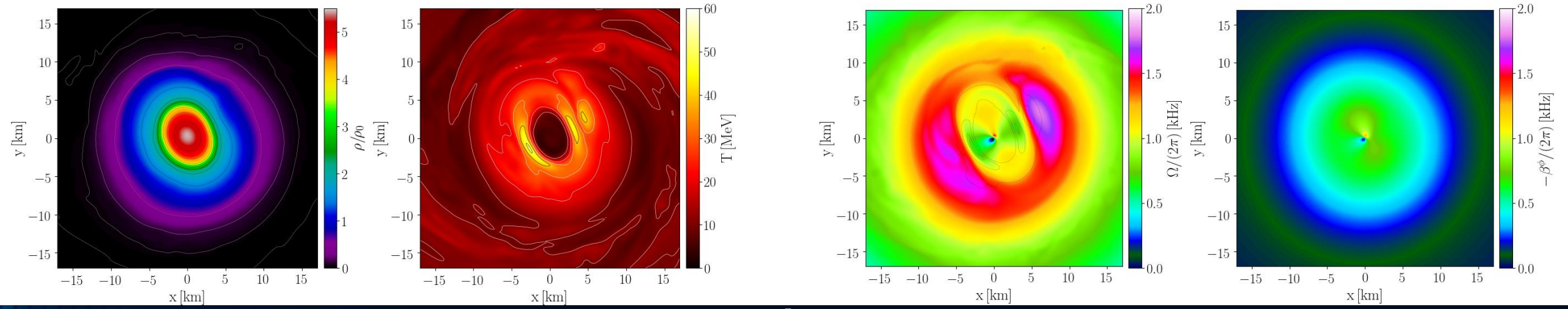


xy-plane

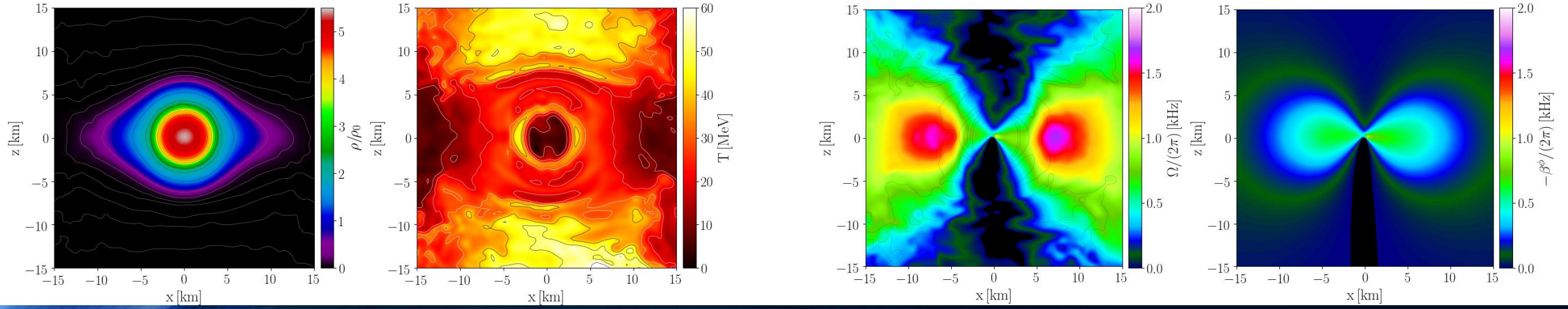


xz-plane

Density Temperature Rotation-profile Frame dragging

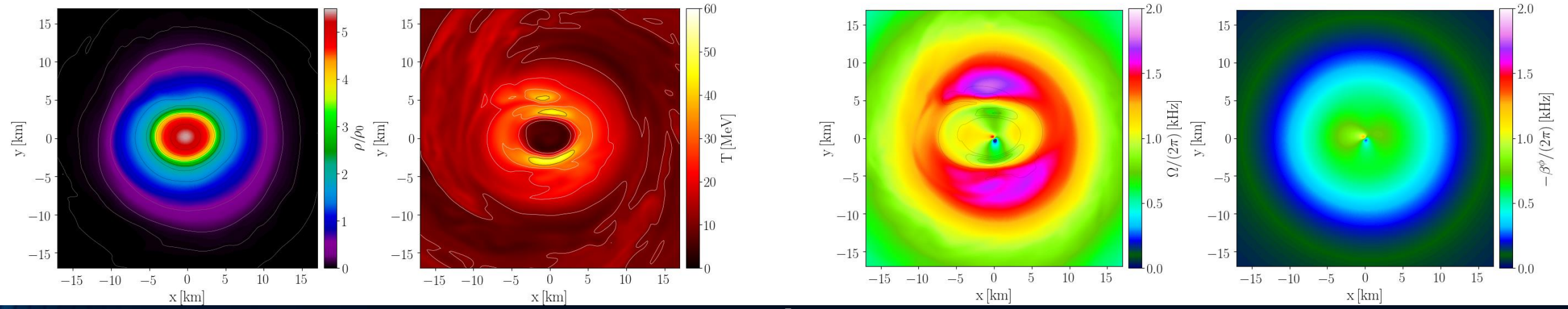


xy-plane

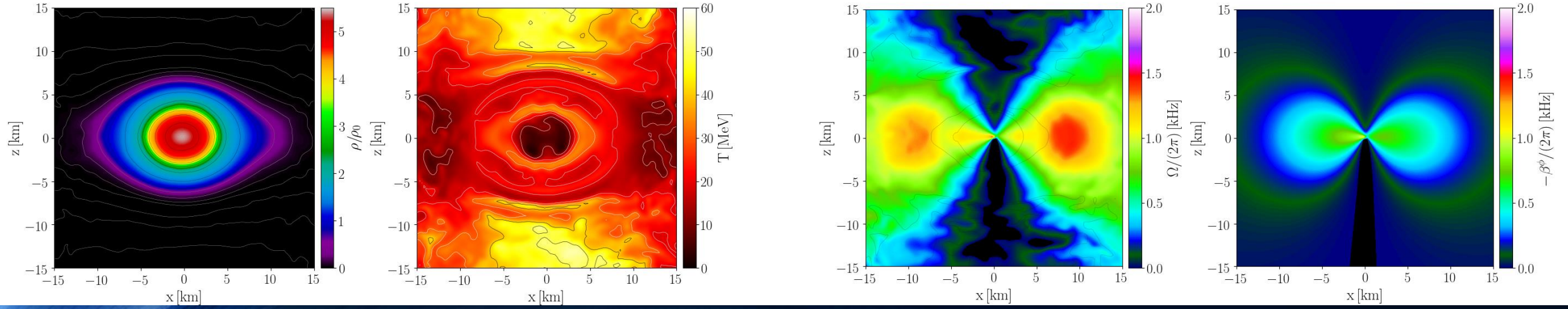


xz-plane

Density Temperature Rotation-profile Frame dragging

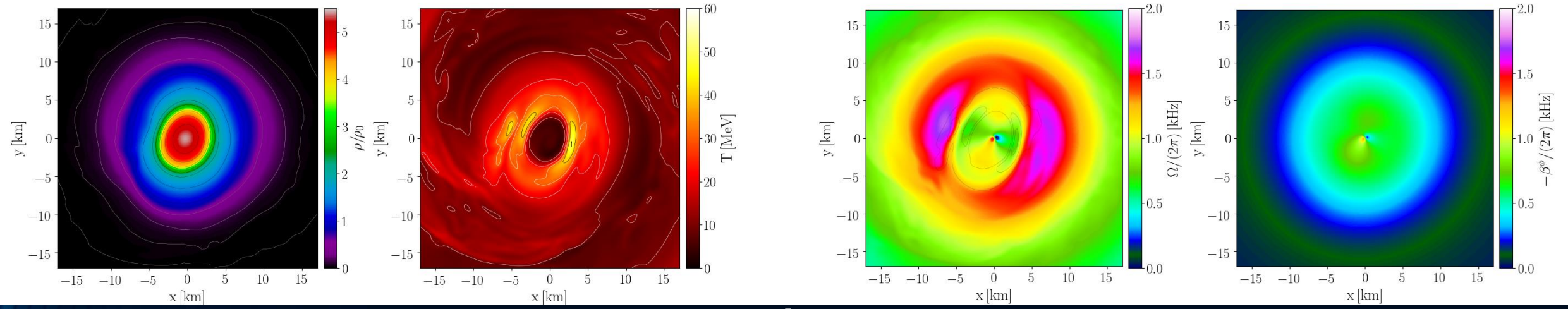


xy-plane

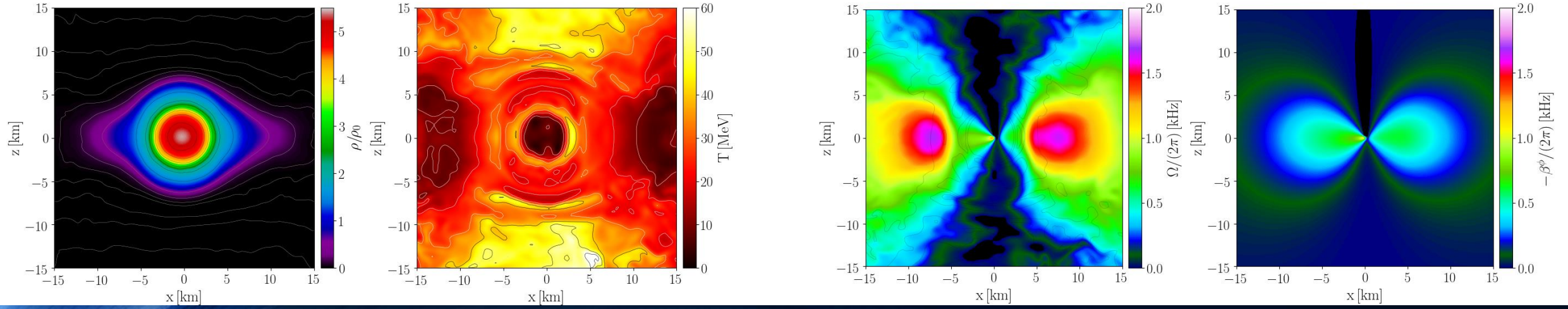


xz-plane

# Postmerger Gravitational-Wave Signatures of Phase Transitions in Binary Mergers; LR Weih, M Hanauske, L Rezzolla; Physical Review Letters 124 (17), 171103 (2020)

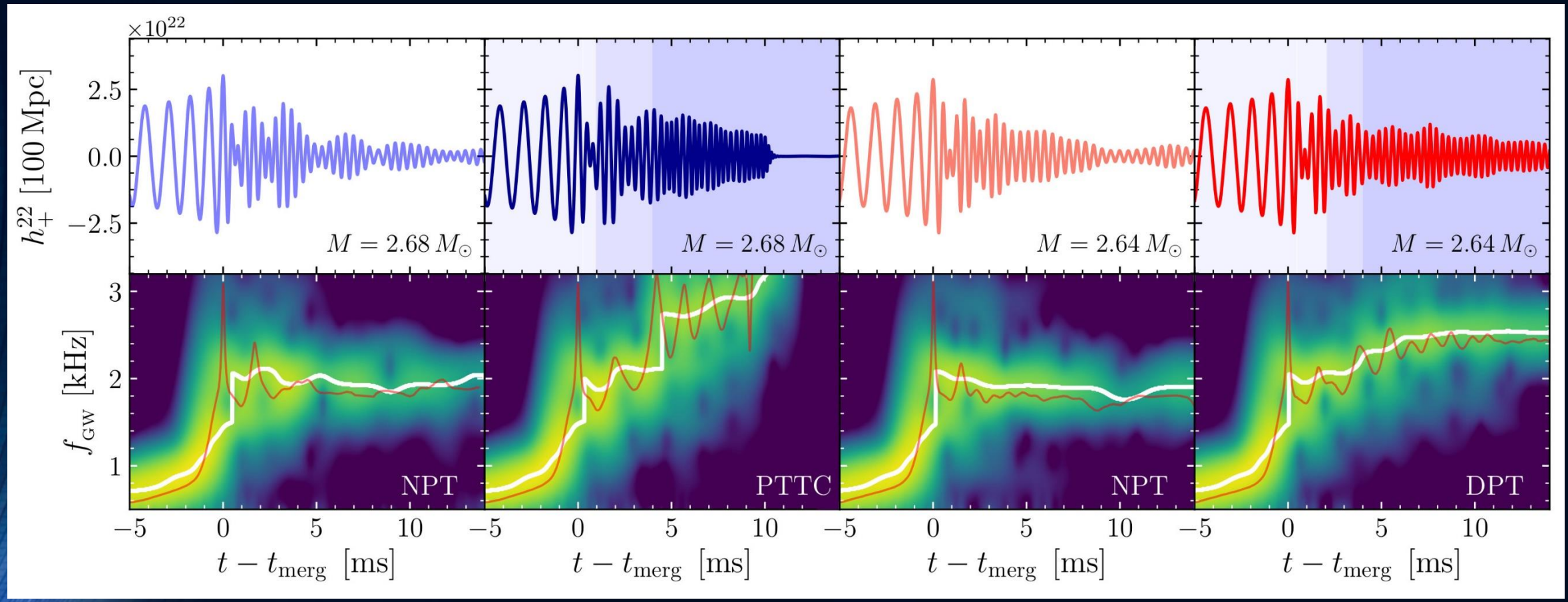


Strain h+ (top) and its spectrogram (bottom) for the four BNSs considered. In the top panels the different shadings mark the times when the HMNS core enters the mixed and quark phases the NPT models are always purely hadronic. In the bottom panels, the white lines trace the maximum of the spectrograms, while the red lines show the instantaneous gravitational-wave frequency.

# Differnce in the $h_+^{12}$ – gravitational wave mode

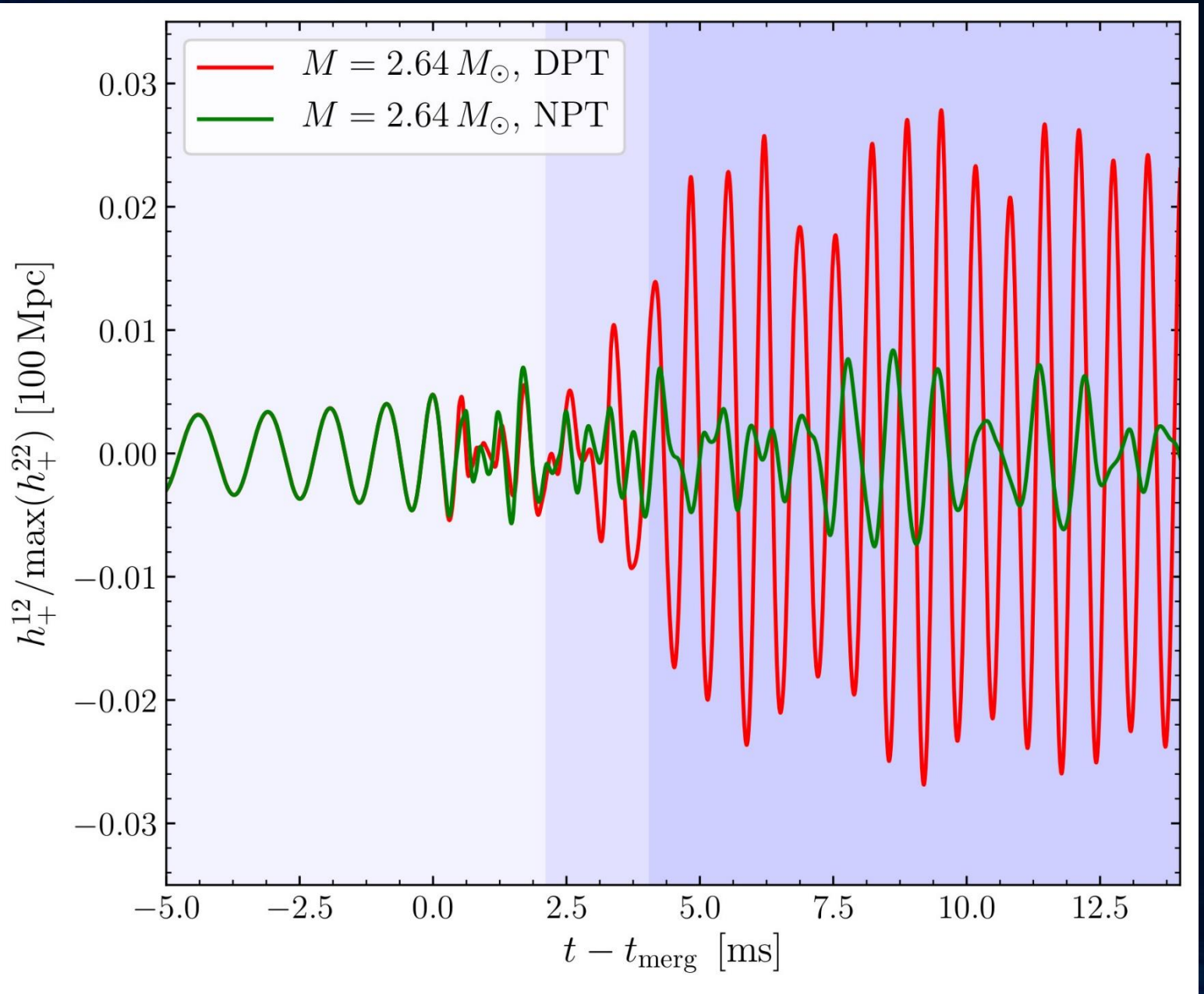


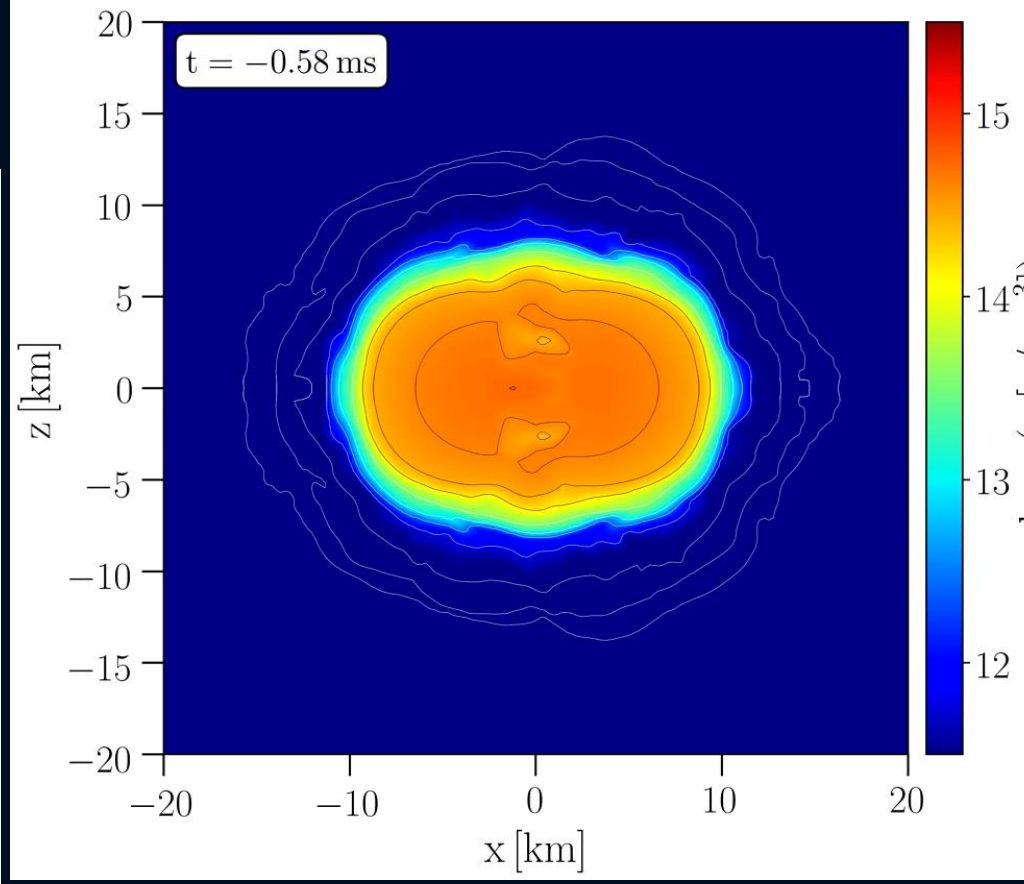


Due to the large m=1 mode of the emitted gravitational wave in the DPT case, a qualitative difference to the NPT scenario might be observable in future by focusing on the $h_+^{12}$ – gravitational wave mode during the post-merger evolution.

# Can we detect the quark-gluon plasma with gravitational waves?

- Gravitational-wave signatures of the hadron-quark phase transition in binary compact star mergers
  - *Signatures within the late inspiral phase (premerger signals)*
    - Constraining twin stars with GW170817; G Montana, L Tolós, M Hanauske, L Rezzolla; Physical Review D 99 (10), 103009 (2019)
  - *Signatures within the post-merger phase evolution*
    - **Phase-transition triggered collapse scenario**
      Signatures of quark-hadron phase transitions in general-relativistic neutron-star mergers; ER Most, LJ Papenfort, V Dexheimer, M Hanauske, S Schramm, H Stöcker, L. Rezzolla; Physical review letters 122 (6), 061101 (2019)
    - **Delayed phase transition scenario**
      Postmerger Gravitational-Wave Signatures of Phase Transitions in Binary Mergers; LR Weih, M Hanauske, L Rezzolla; Physical Review Letters 124 (17), 171103 (2020)
    - **Prompt phase transition scenario**
      Identifying a first-order phase transition in neutron-star mergers through gravitational waves; A Bauswein, NUF Bastian, DB Blaschke, K Chatziioannou, JA Clark, JA Clark, T Fischer, M Oertel; Physical review letters 122 (6), 061102 (2019)

# Can we detect the quark-gluon plasma with gravitational waves?

- Gravitational-wave signatures of the hadron-quark phase transition in binary compact star mergers
  - *Signatures within the late inspiral phase (premerger signals)*
    - Constraining twin stars with GW170817; G Montana, L Tolós, M Hanauske, L Rezzolla; Physical Review D 99 (10), 103009 (2019)
  - *Signatures within the post-merger phase evolution*
    - **Phase-transition triggered collapse scenario**
      Signatures of quark-hadron phase transitions in general-relativistic neutron-star mergers; ER Most, LJ Papenfort, V Dexheimer, M Hanauske, S Schramm, H Stöcker, L. Rezzolla; Physical review letters 122 (6), 061101 (2019)
    - **Delayed phase transition scenario**
      Postmerger Gravitational-Wave Signatures of Phase Transitions in Binary Mergers; LR Weih, M Hanauske, L Rezzolla; Physical Review Letters 124 (17), 171103 (2020)
    - **Prompt phase transition scenario**
      Identifying a first-order phase transition in neutron-star mergers through gravitational waves; A Bauswein, NUF Bastian, DB Blaschke, K Chatziioannou, JA Clark, JA Clark, T Fischer, M Oertel; Physical review letters 122 (6), 061102 (2019)

Additional results from observing run O3

Black Hole

Neutron Star

&

?

Black Hole

$M_2 \sim 2.6\ M_\odot$

Laser Interferometer Space Antenna
LISA (2034)

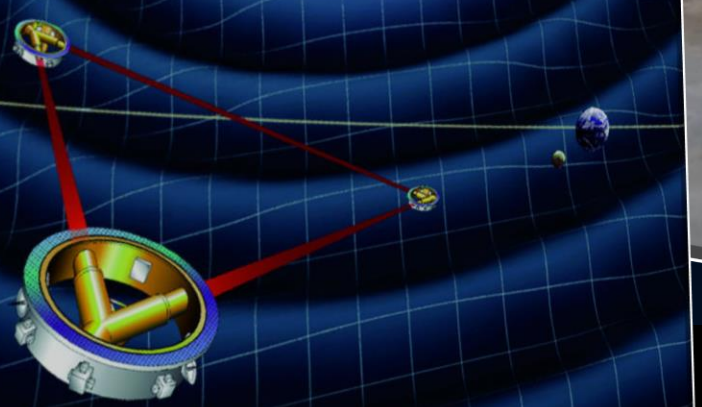

Cosmic Explorer (2035?)

The next observing runs (O4,O5,..)


Einstein Telescope (2035?)

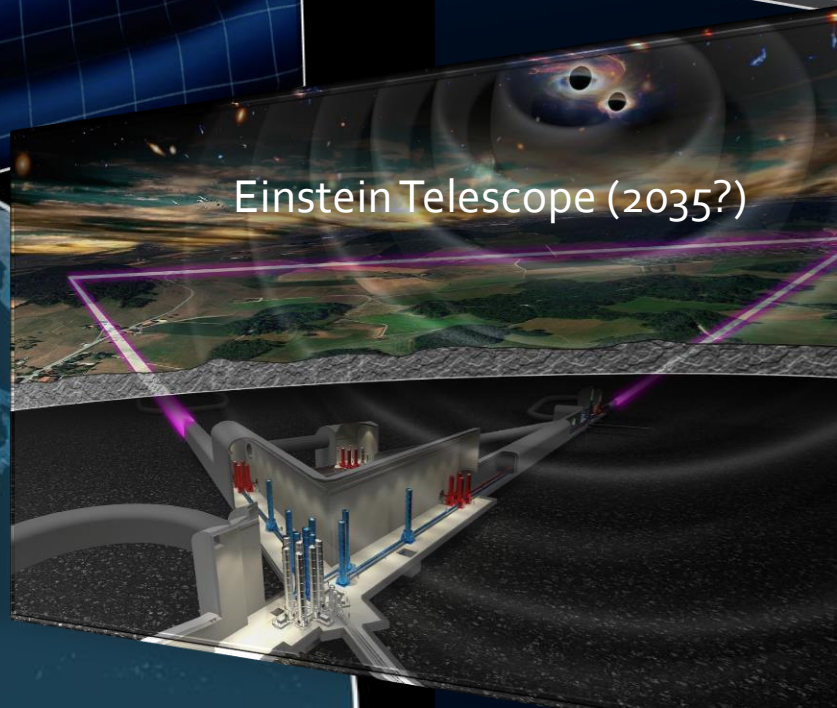

- Additional Slides

# *Signatures within the post-merger phase evolution*

## Prompt phase transition scenario

IWARA Conference
Talk by David Blaschke

Identifying a first-order phase transition in neutron-star mergers through gravitational waves; A Bauswein, NUF Bastian, DB Blaschke, K Chatziioannou, JA Clark, JA Clark, T Fischer, M Oertel; Physical review letters 122 (6), 061102 (2019)

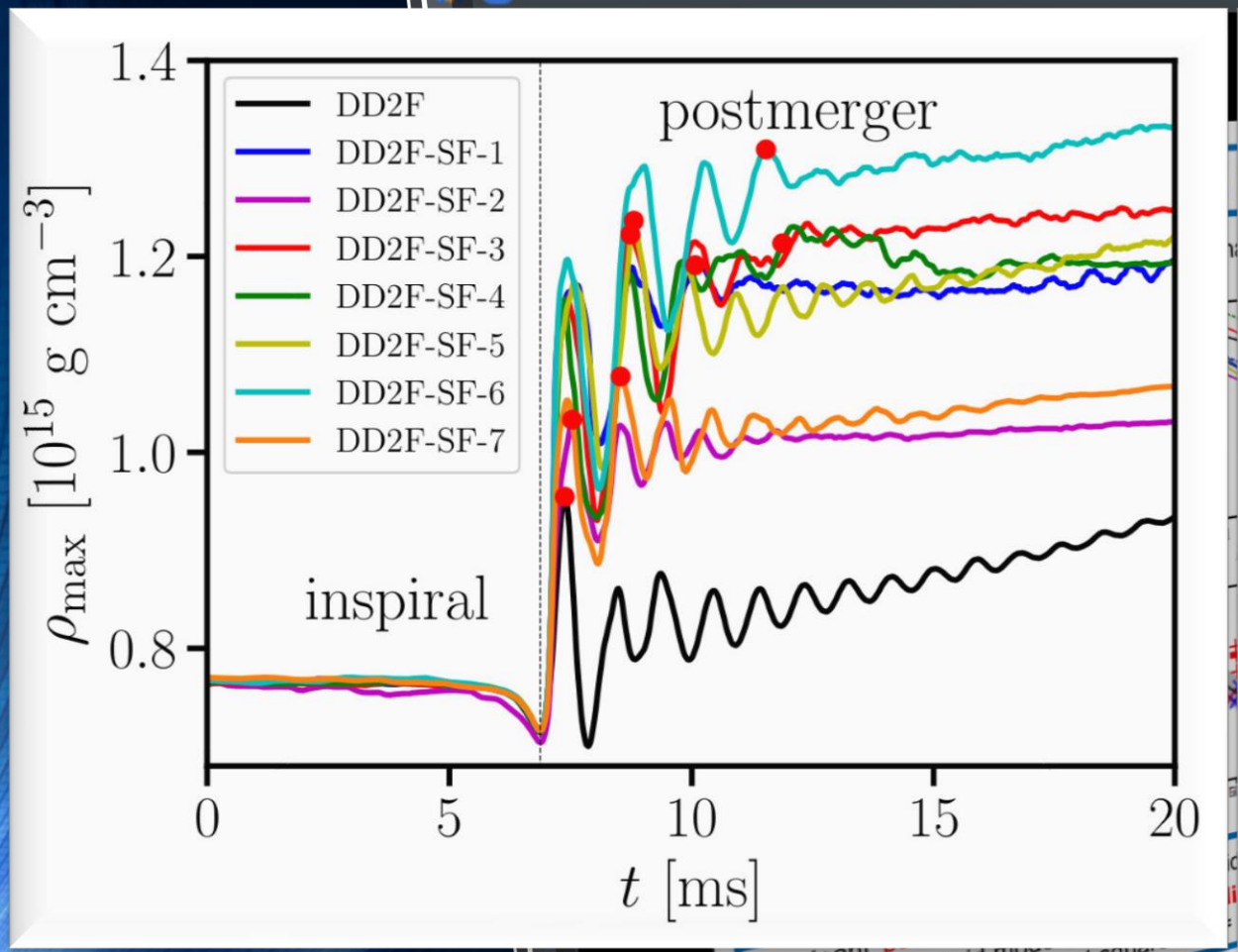


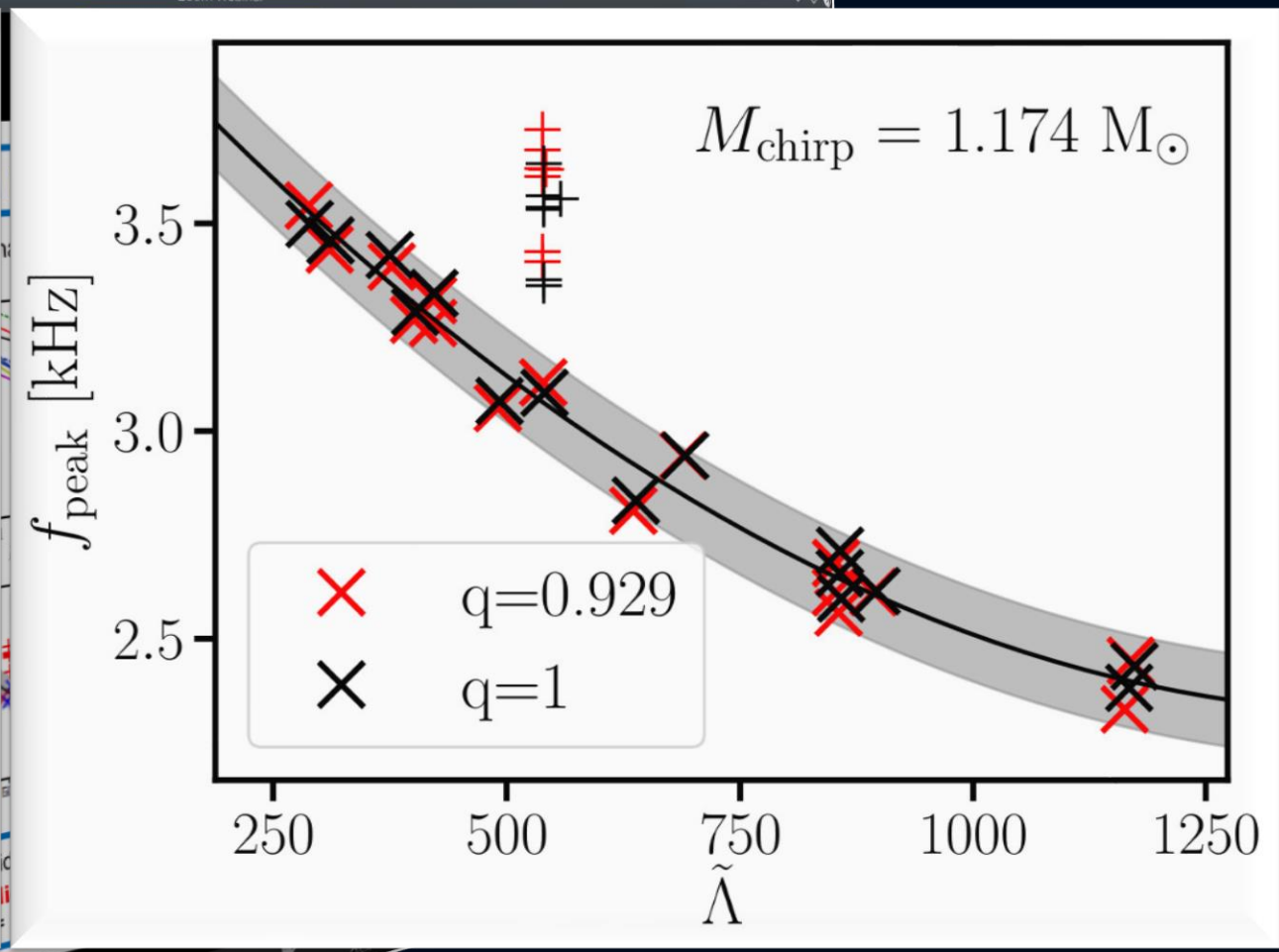

# Gravitational-wave signatures within the late inspiral phase

## Construction of the EOS with a hadron-quark phase transition

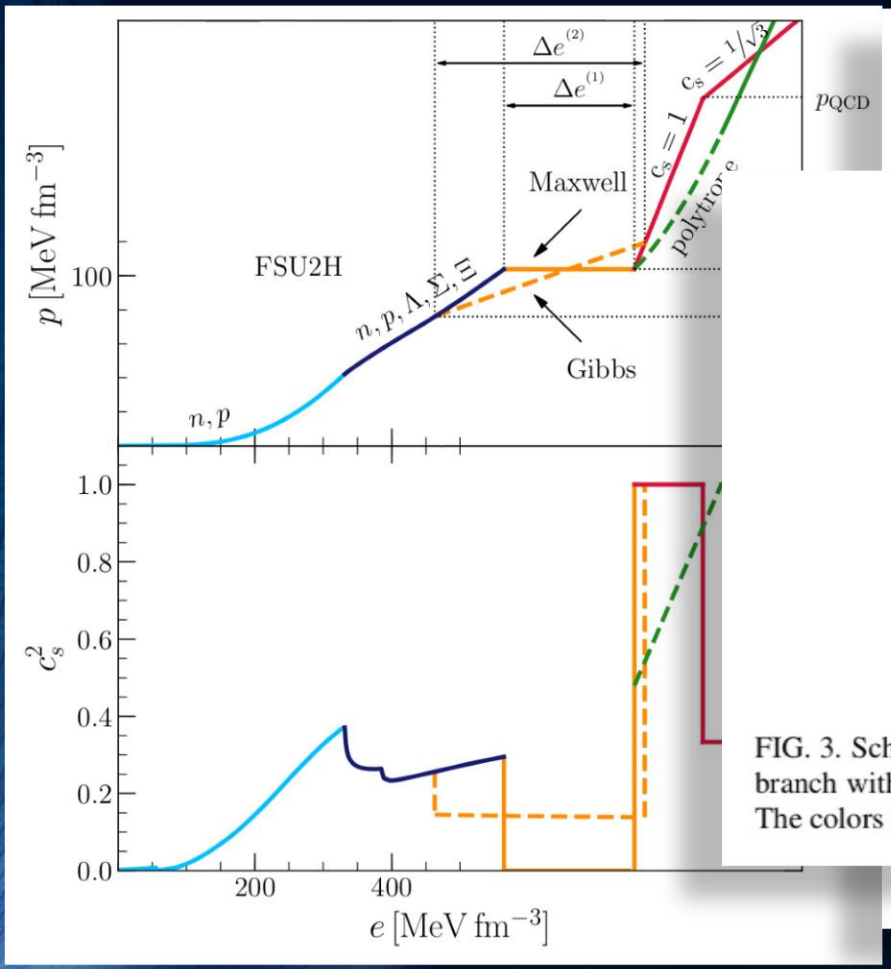


## The Mass-Radius relation and the twin star property

Maxwell Construction  Gibbs Construction

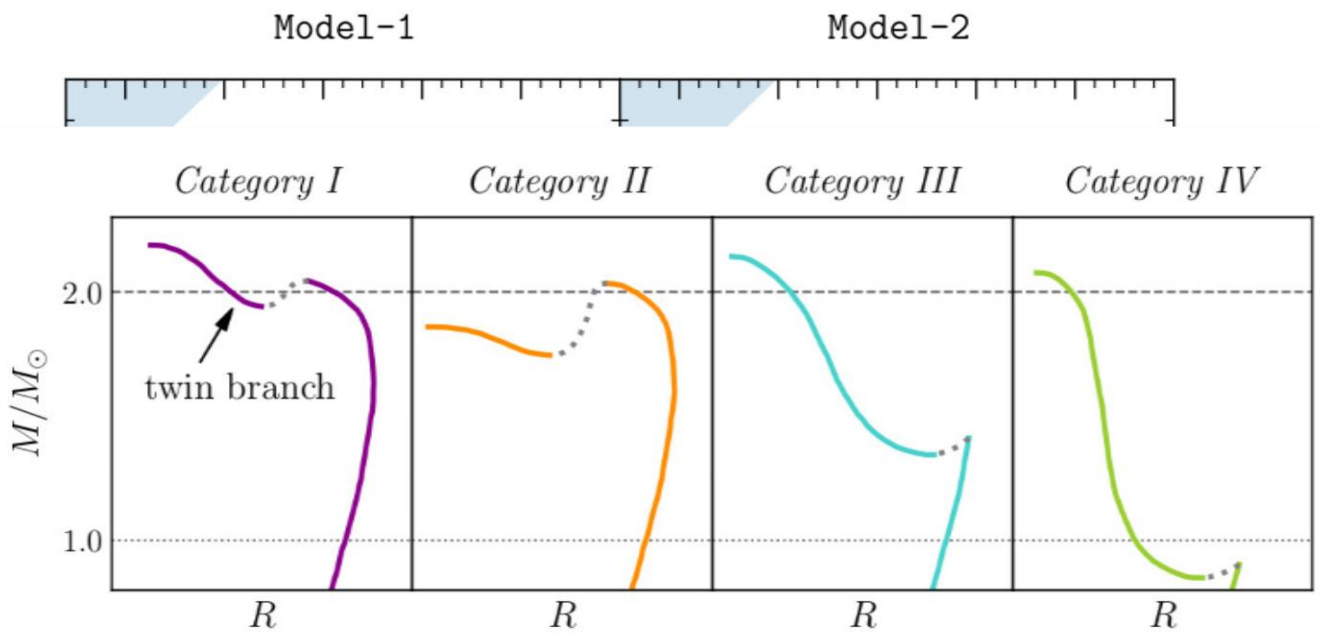


FIG. 3. Schematic behaviour of the mass–radius relation for the twin-star categories *I–IV* defined in the text. Note the appearance of a "twin" branch with a mixed or pure-quark phase; the twin branch has systematically smaller radii than the branch with a nuclear or hadronic phase. The colors used for these categories will be employed also in the subsequent figures.

G. Montana, L.Tolos, M.Hanauske and L.Rezzolla
„Constraining twin stars with GW170817", PRD 99(10), 2019

G. Montana, L.Tolos, M.Hanauske

*tars*

9

bility

Λ of a
f its mass

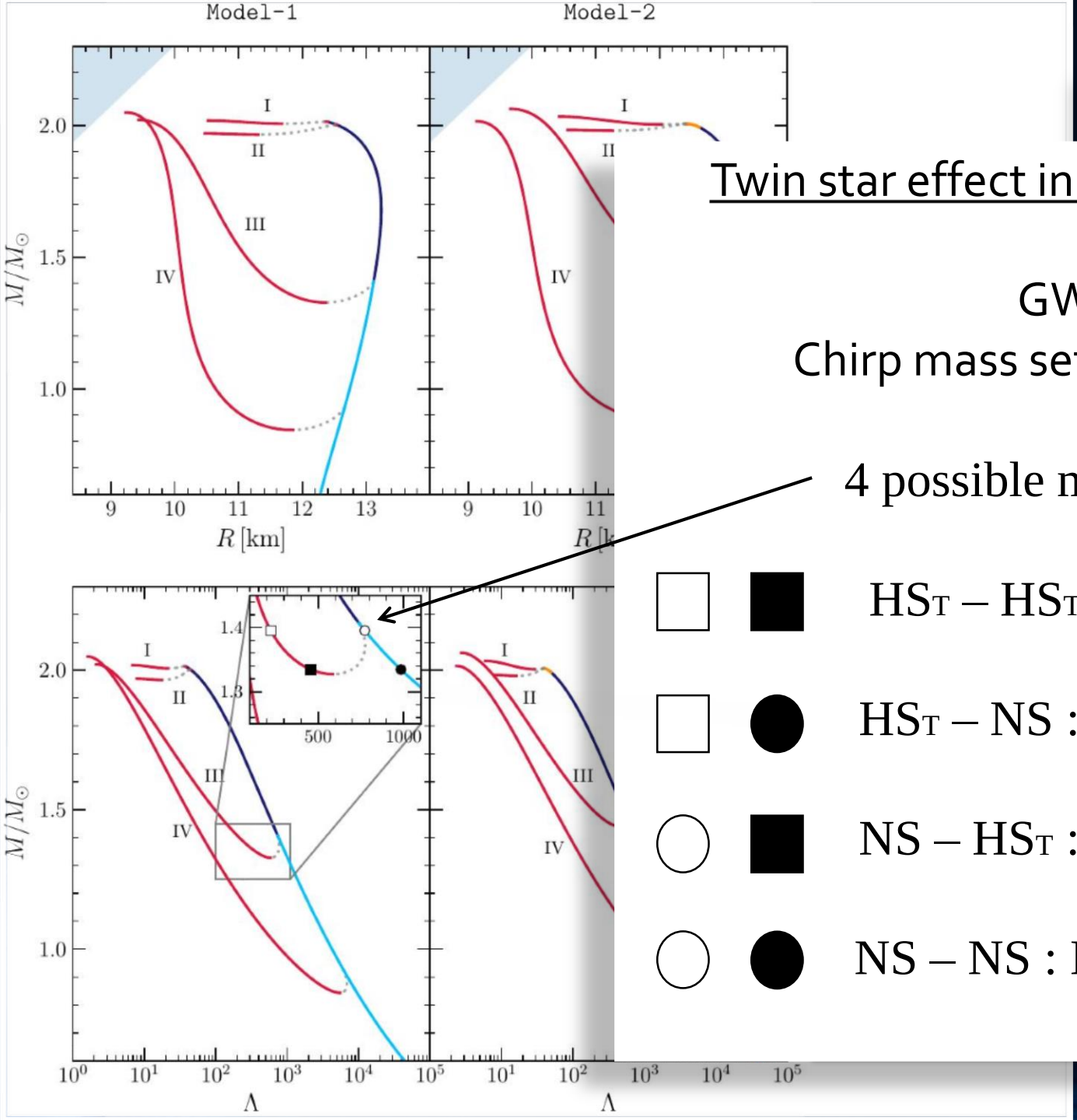


## Twin star effect in the tidal deformability

GW170817:
Chirp mass set to $M_{ch} = 1.188\ M_\odot$

4 possible merger scenarios:

- HS$_T$ – HS$_T$ : Hybrid star – Hybrid Star
- HS$_T$ – NS : Hybrid star – Neutron Star
- NS – HS$_T$ : Neutron star – Hybrid Star
- NS – NS : Neutron star – Neutron Star

# Constraining the hadron-quark phase transition with GW170817

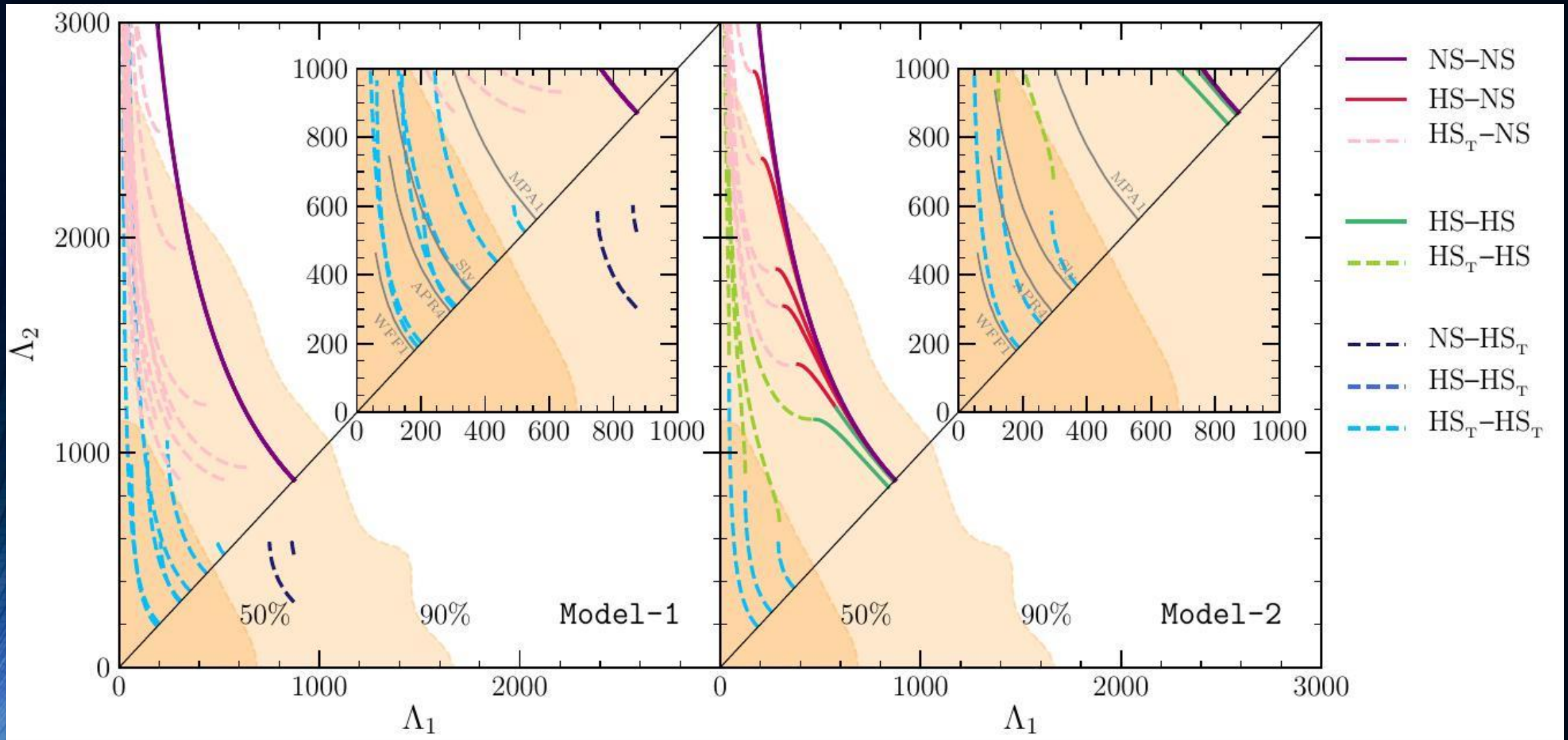


Assuming that the hadronic part of the EOS is given by the FSU2H model, the phase transition takes place already in the inspiral phase -> GW170817 was a hybrid star merger

# *Pre-merger signatures of the hadron-quark phase transition*

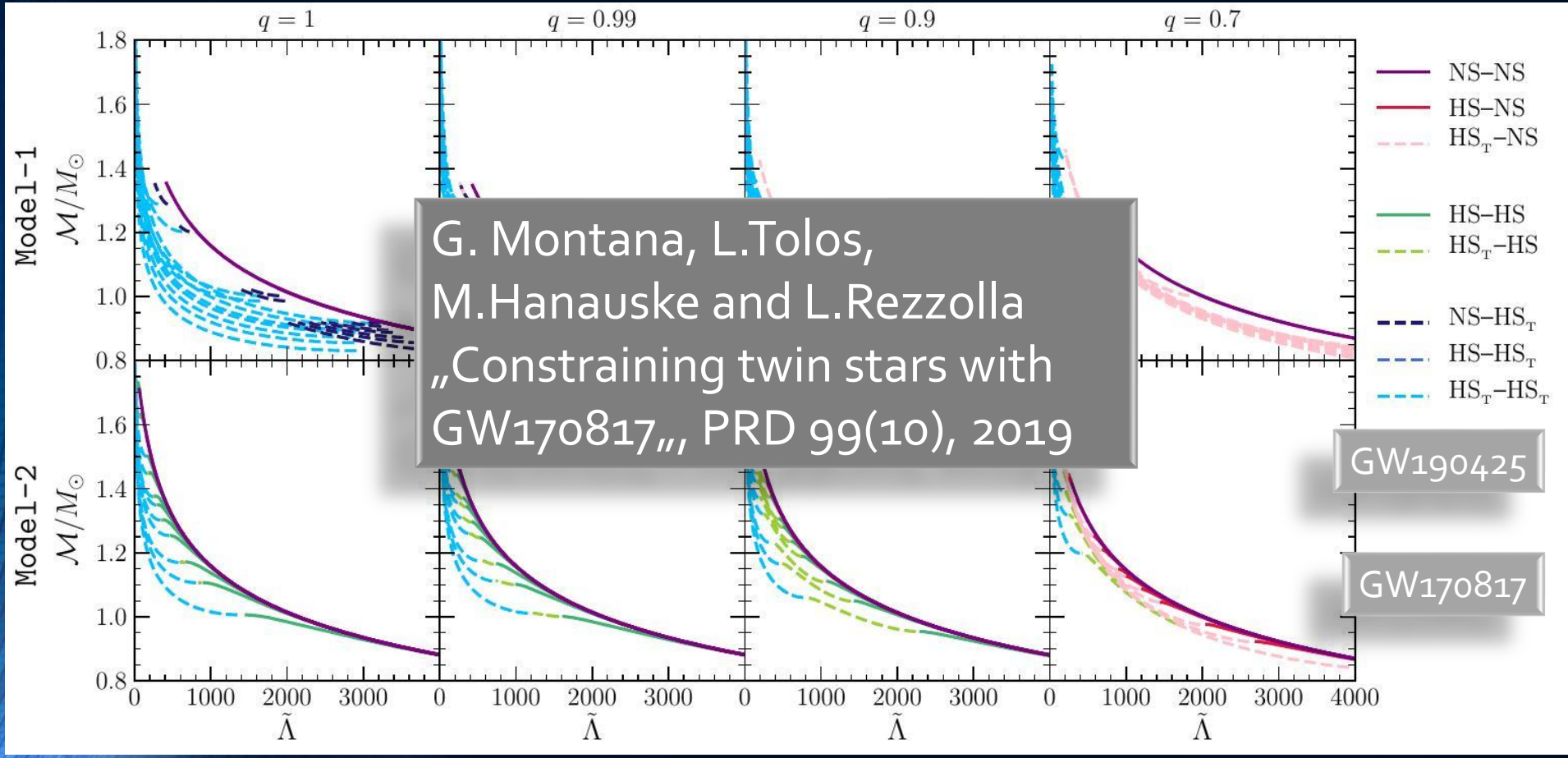


G. Montana, L.Tolos, M.Hanauske and L.Rezzolla „Constraining twin stars with GW170817„, PRD 99(10), 2019

Chirp mass set to $\mathcal{M}_{ch}$ as a function of the weighted dimensionless tidal deformability $\tilde{\Lambda} = \tilde{\Lambda}(M1, M2, \Lambda1, \Lambda2)$ for different mass ratios q

In the next few years, further gravitational waves from binary neutron star collisions with different chirp masses and mass ratios will be detected and thus the equation of state will be further restricted.

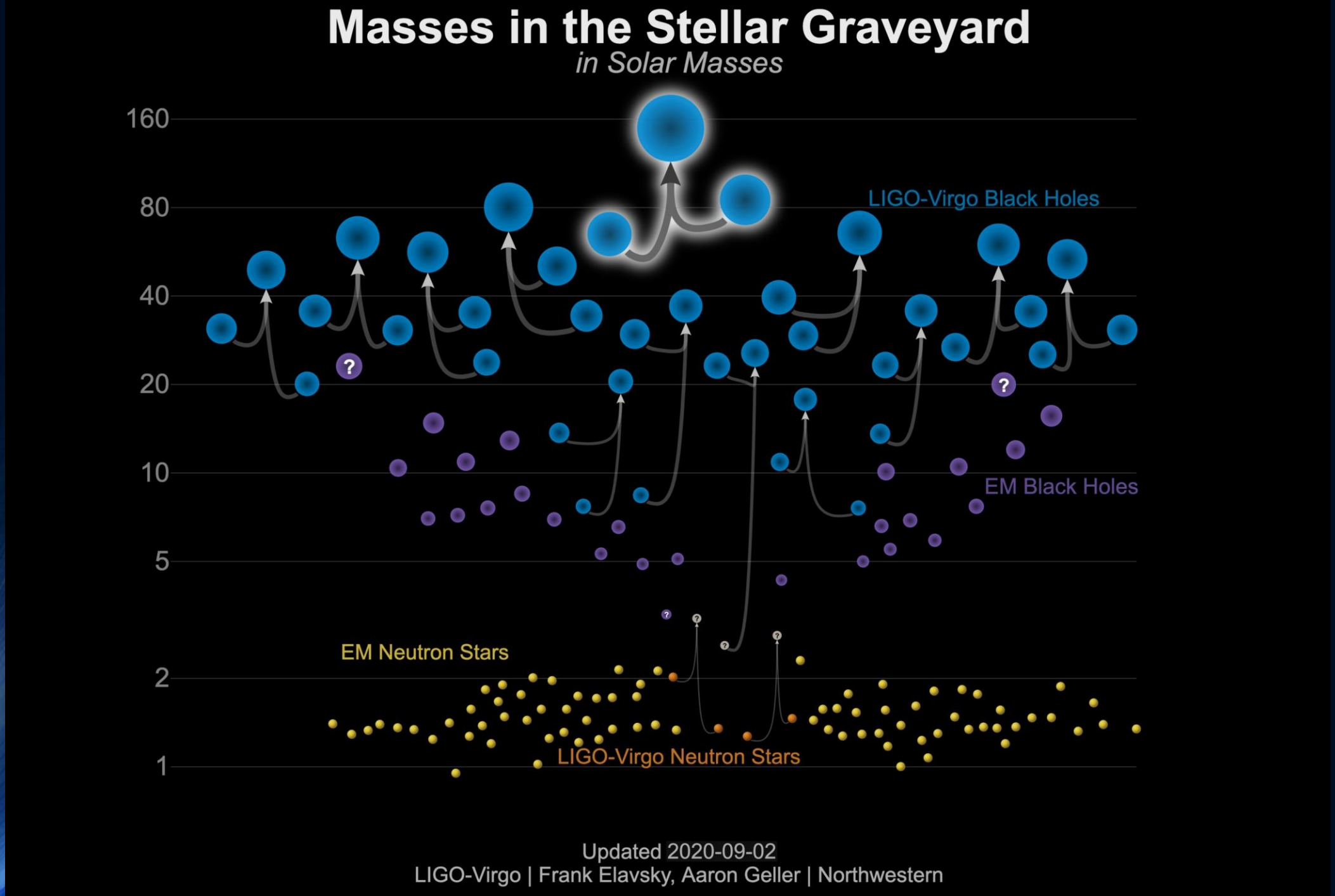
Masses in the Stellar Graveyard
in Solar Masses
160
80
40
20
10
5
2
1
LIGO-Virgo Black Holes
EM Black Holes
EM Neutron Stars
LIGO-Virgo Neutron Stars
?
Updated 2020-09-02
LIGO-Virgo | Frank Elavsky, Aaron Geller | Northwestern

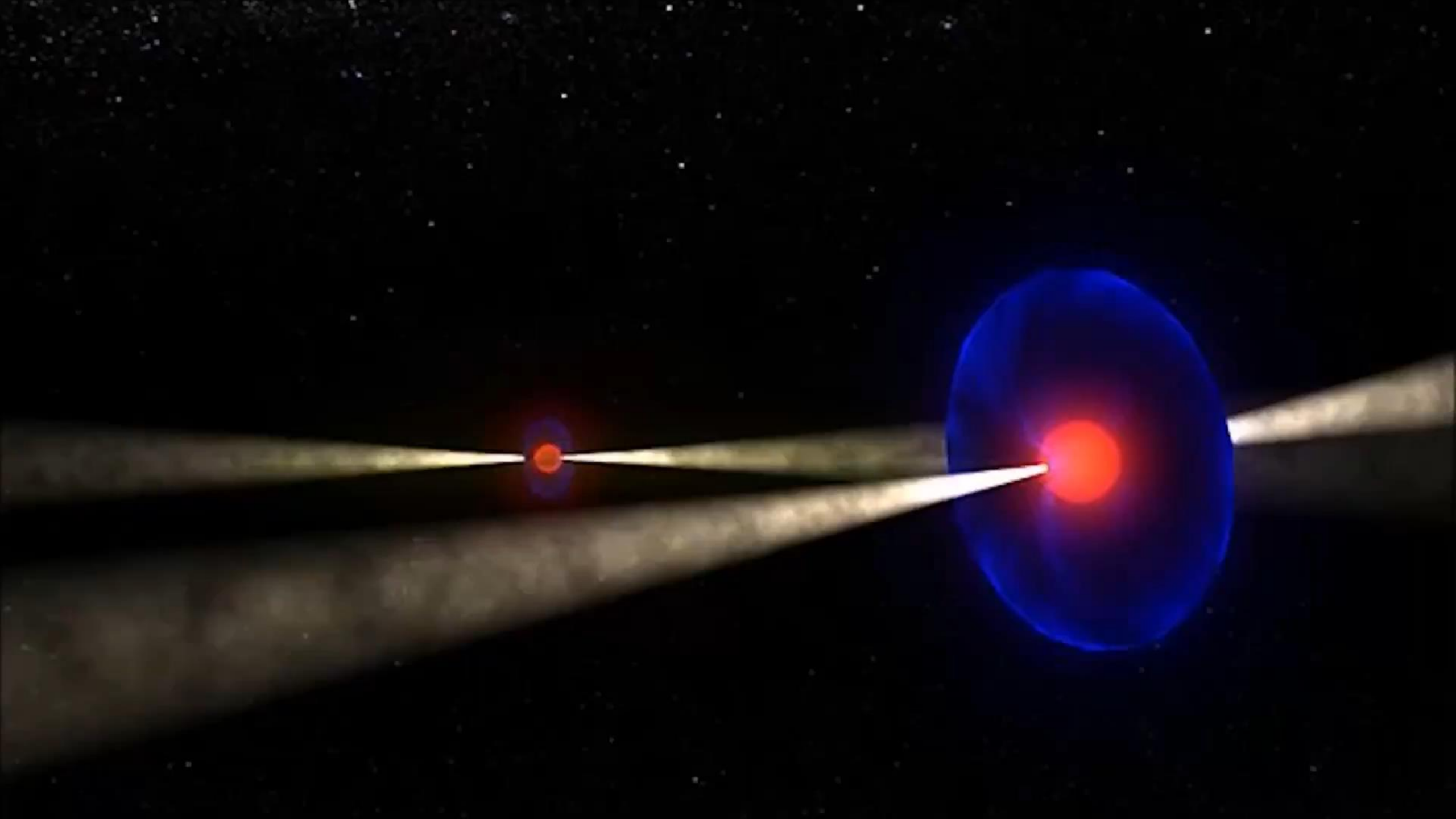

# arXiv:1912.09340v1

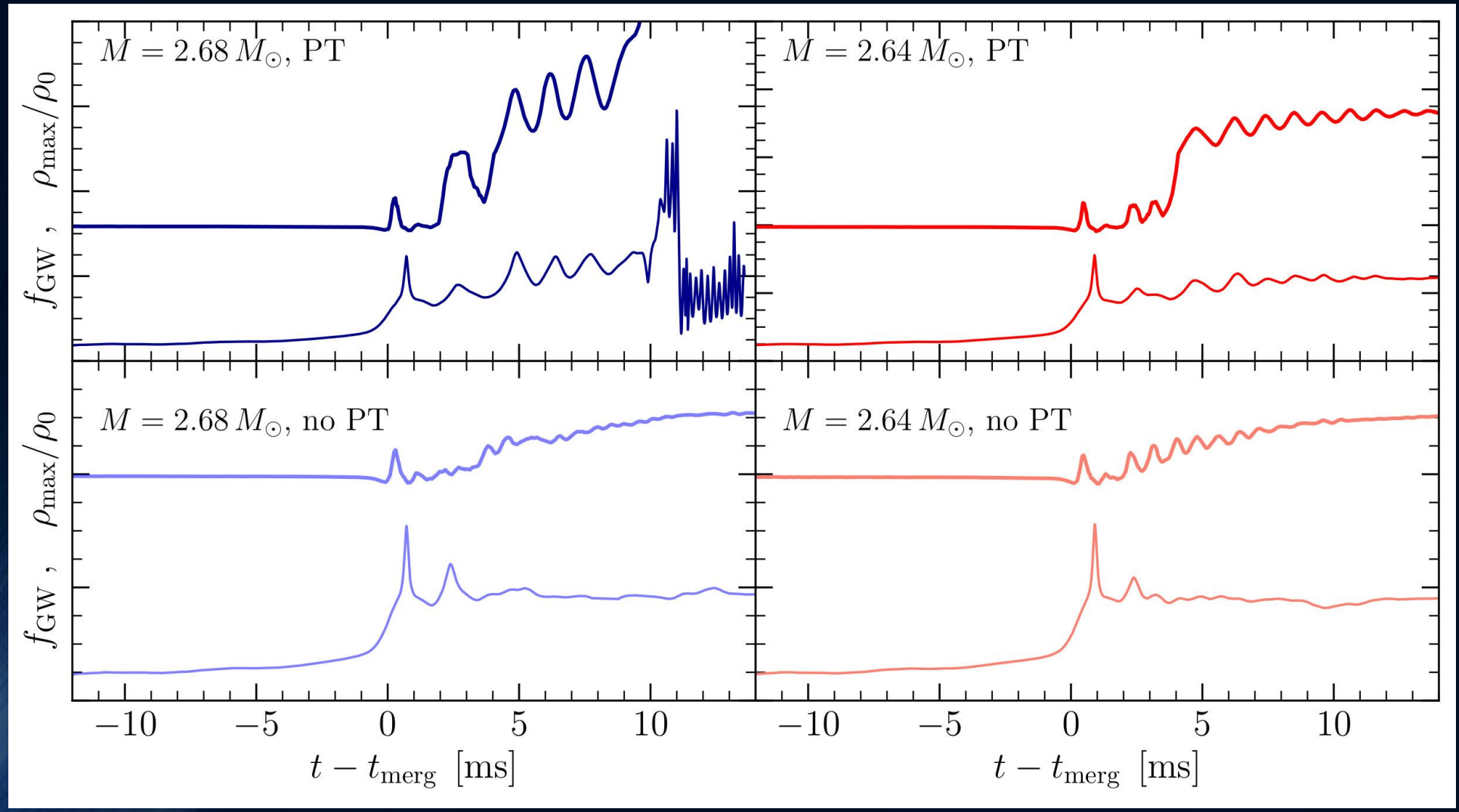


Evolution of the central rest-mass density (top)
and instantaneous gravitational wave frequency (bottom).

# Post-merger gravitational-wave signatures of phase transitions in binary compact star mergers

PRL 124, 171103 (2020)

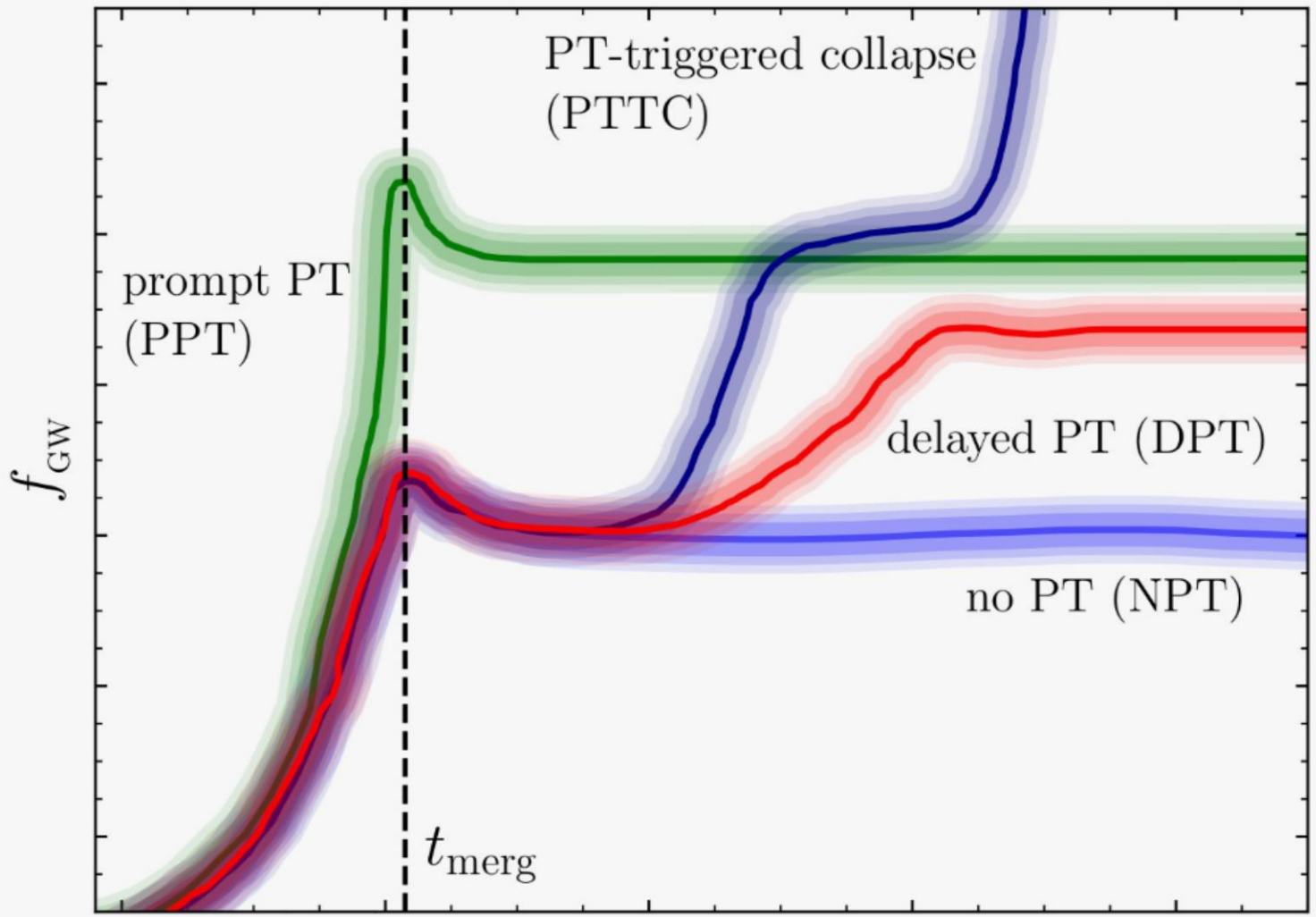


Schematic overview of the instantaneous gravitational wave frequency and how its evolution can be used to classify the different scenarios associated with a hadron-quark phase transition.

# How to detect the hadron-quark phase transition with gravitational waves

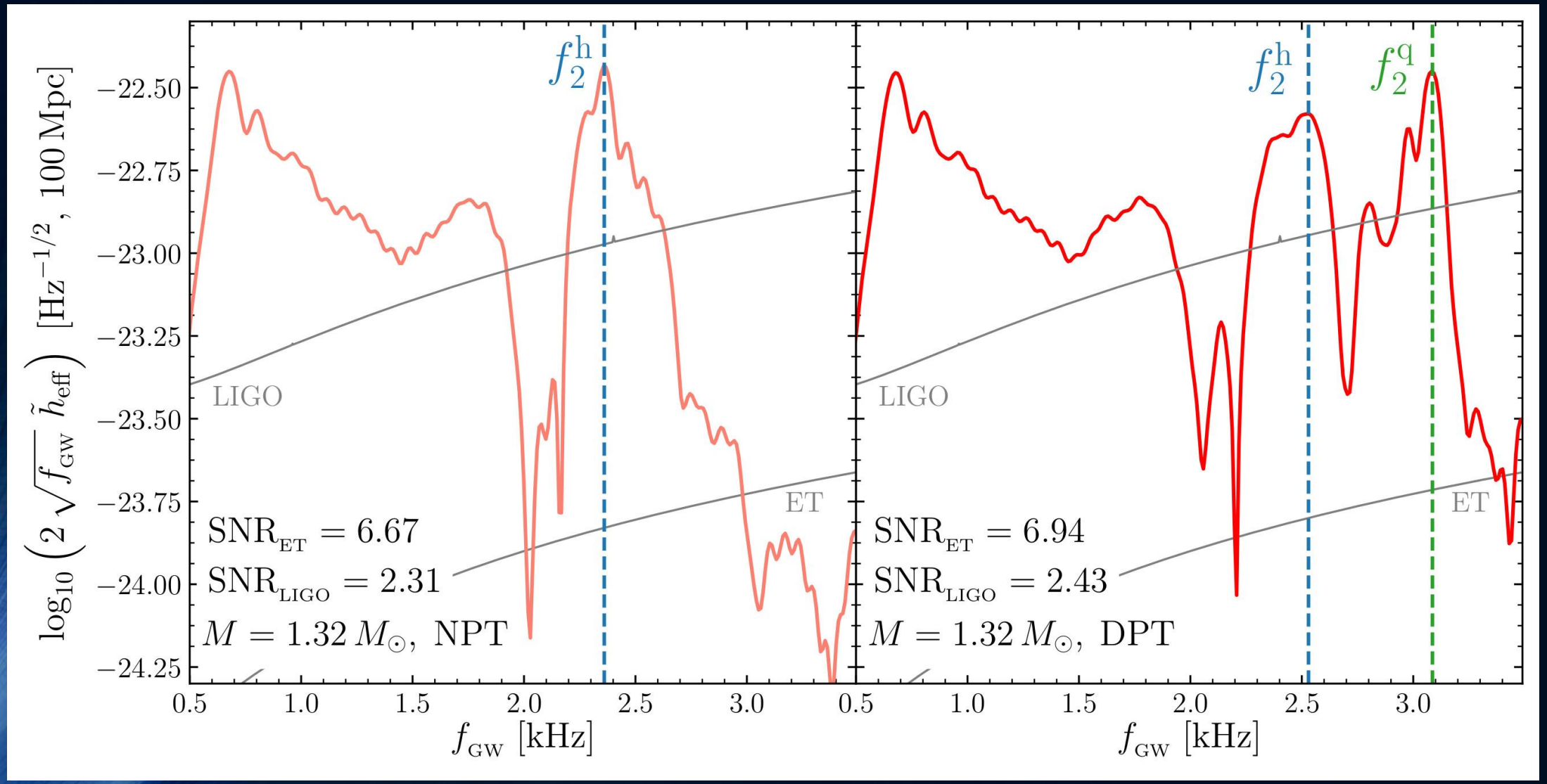


Total gravitational wave spectrum (left NPT, right DPT), PRL 124, 171103 (2020)

# GW170817: Constraining the maximum mass of Neutron Stars

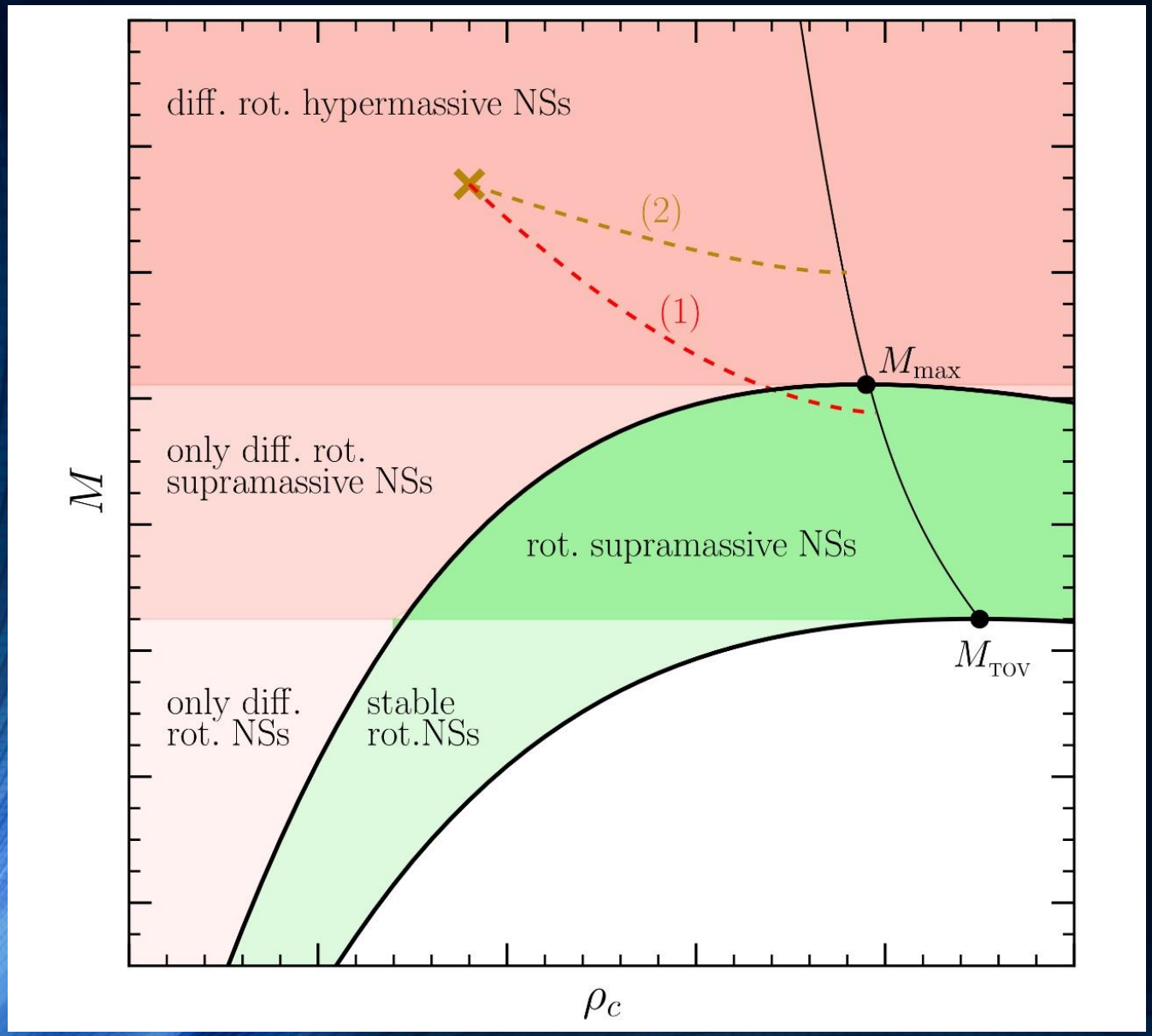


The highly differentially rotating hypermassive/supramassive neutron star will spin down and redistribute its angular momentum (e.g. due to viscosity effects, magnetic braking). After ~1 second it will cross the stability line as a uniformly rotating supramassive neutron star (close to $M_{max}$) and collapse to a black hole. Parts of the ejected matter will fall back into the black hole producing the gamma-ray burst.

L.Rezzolla, E.Most, L.Weih, "Using Gravitational Wave Observations and Quasi-Universal Relations to constrain the maximum Mass of Neutron Stars",The Astrophysical Journal Letters 852, L25 (2018):
$2.01 \pm 0.04 < M_{TOV} < 2.16 \pm 0.17$

See also: S.Lawrence et al. ,APJ808,186, 2015
Margalit & Metzger, The Astrophysical Journal Letters 850, L19 (2017): $M_{TOV} < 2.17$ (90%)
Zhou, Zhou, Li, PRD 97, 083015 (2018)
Ruiz, Shapiro, Tsokaros, PRD 97,021501 (2018)

# Evolution of the density in the post merger phase

ALF2-EOS: Mixed phase region starts at $3\rho_0$ (see red curve), initial NS mass: 1.35 $M_\odot$

Hanauske, et.al. PRD, 96(4), 043004 (2017)

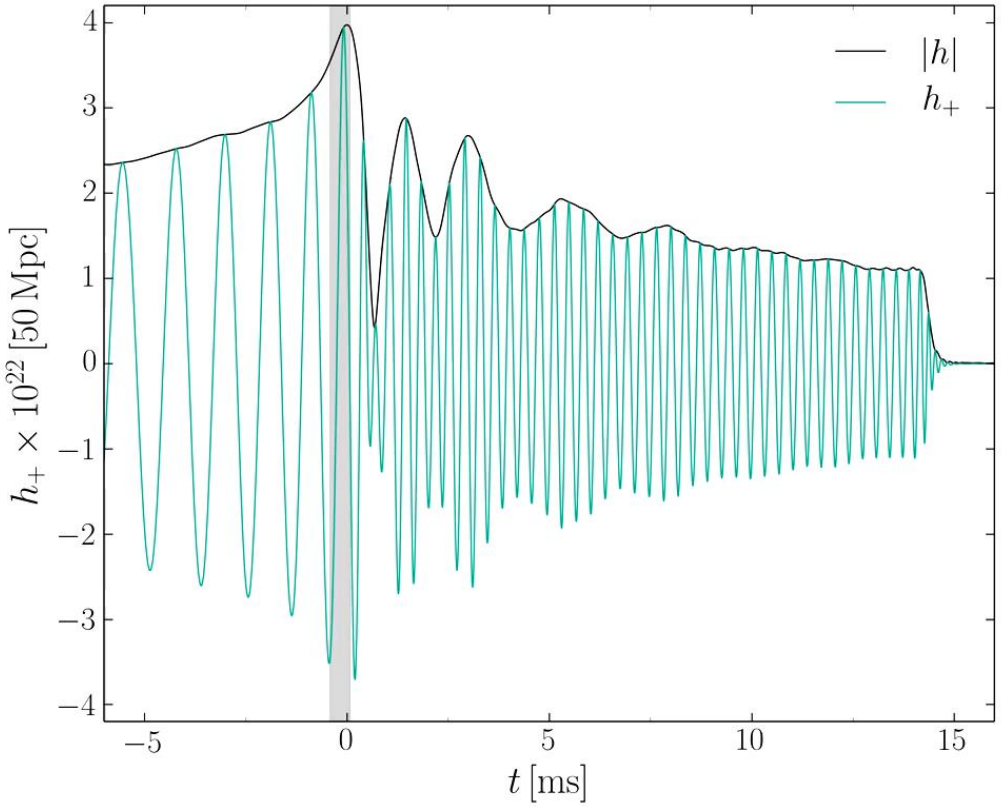


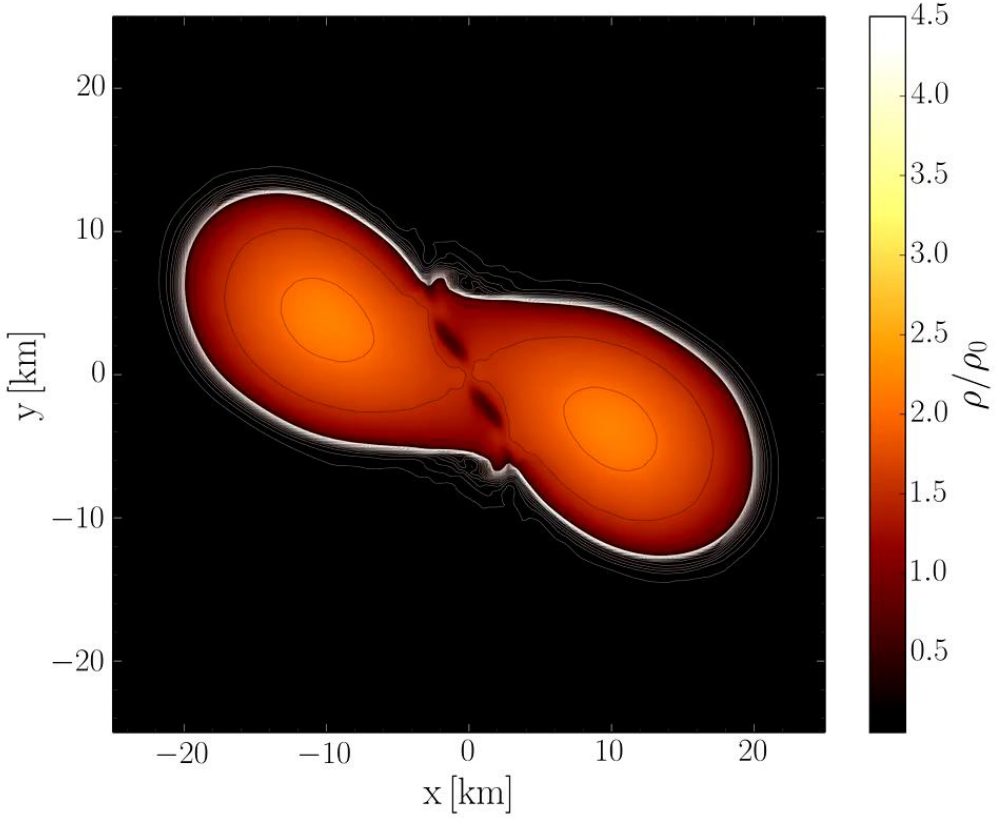


Gravitational wave amplitude
at a distance of 50 Mpc

Rest mass density distribution ρ(x,y)
in the equatorial plane

in units of the nuclear matter density $\rho_0$

# The Gibbs Construction

Hadronic and quark surface:

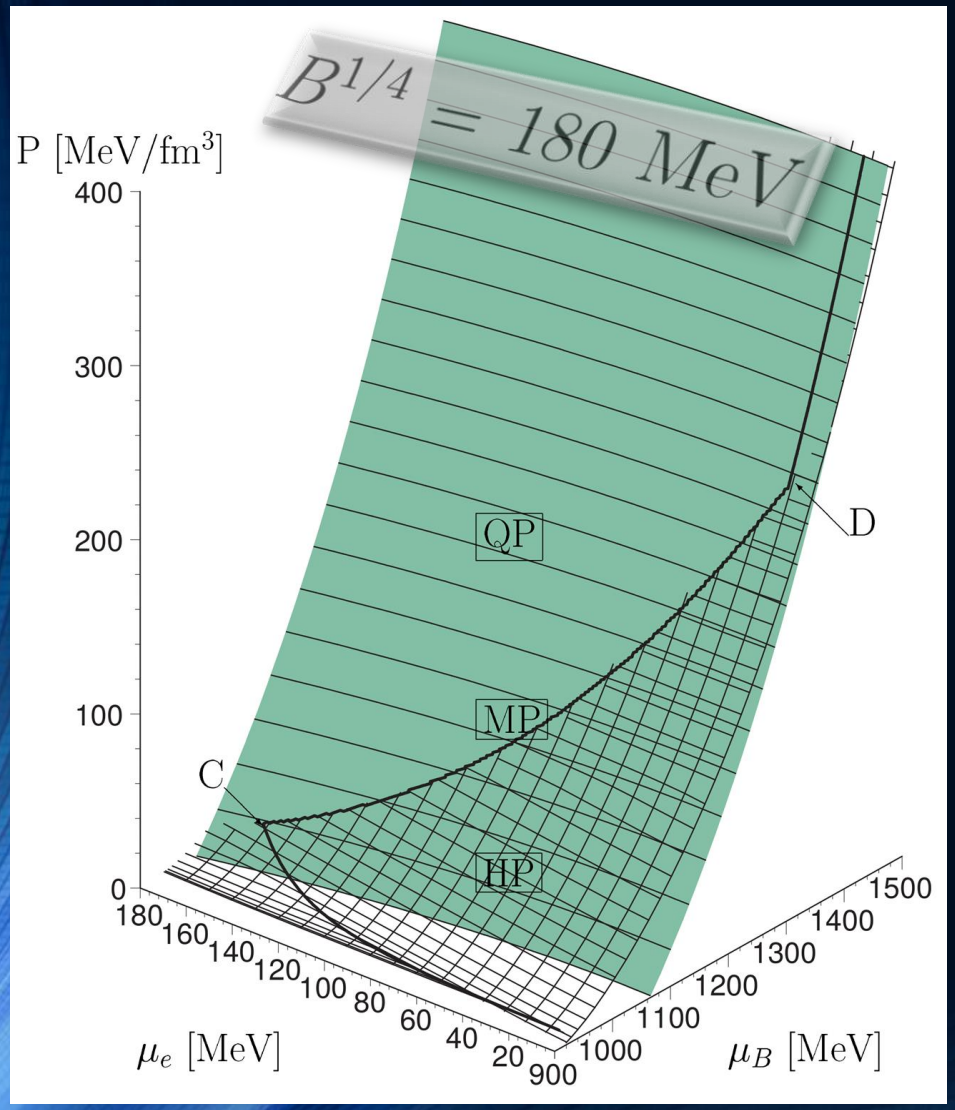


Charge neutrality condition is only globally realized

$$\rho_e := (1-\chi)\,\rho_e^H(\mu_B,\mu_e) + \chi\,\rho_e^Q(\mu_B,\mu_e) = 0\,.$$

The pressure in the mixed phase depends on two independent chemical potentials

$$\begin{aligned} P^H(\mu_B,\mu_e) &= P^Q(\mu_B,\mu_e)\,, \\ \mu_B = \mu_B^H &= \mu_B^Q\,, \\ \mu_e = \mu_e^H &= \mu_e^Q \end{aligned}$$

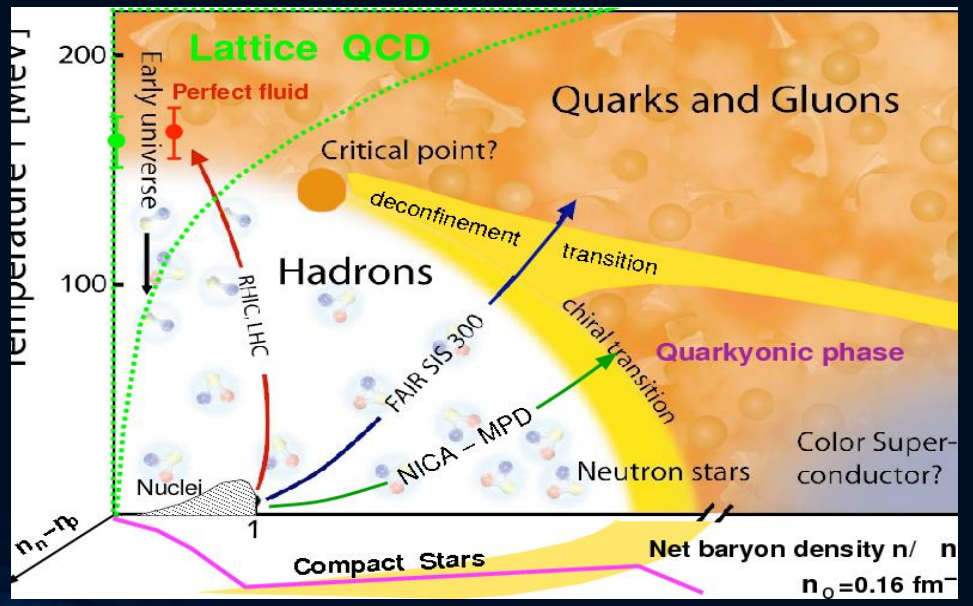

# The Gibbs Construction

Hadronic and quark surface:

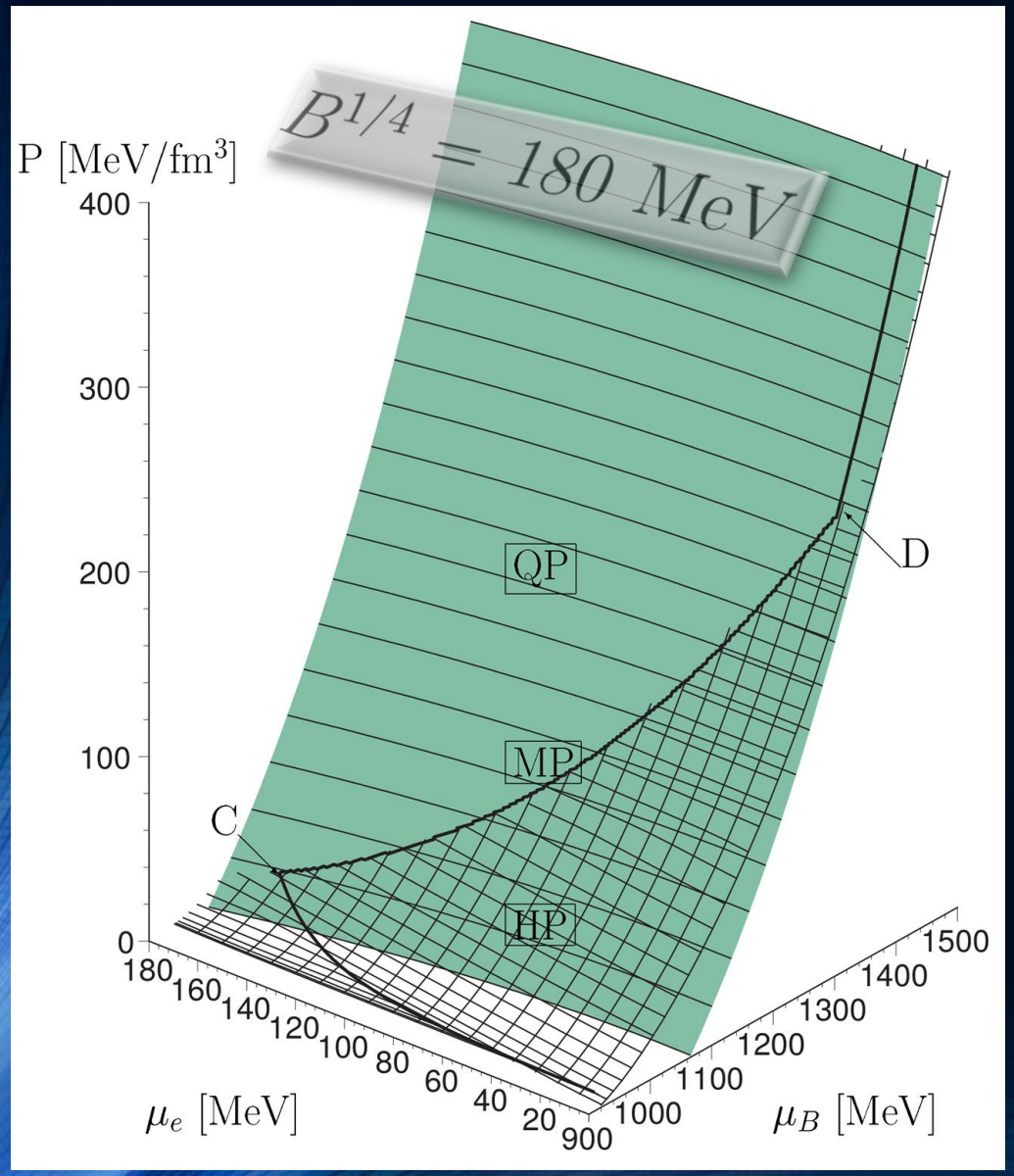


Charge neutrality condition is only globally realized

$$\rho_e := (1-\chi)\,\rho_e^H(\mu_B,\mu_e) + \chi\,\rho_e^Q(\mu_B,\mu_e) = 0\,.$$

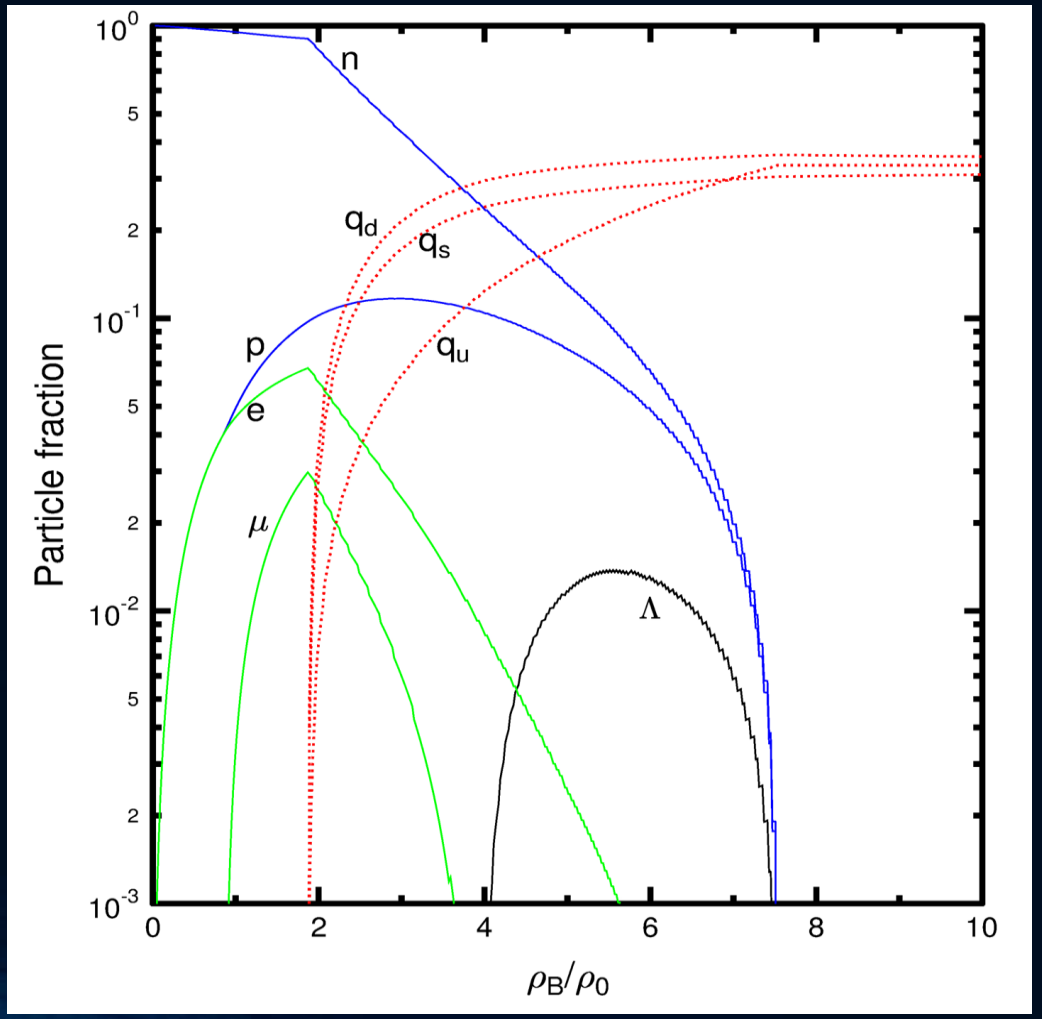

# The Gibbs Construction

Hadronic and quark surface:

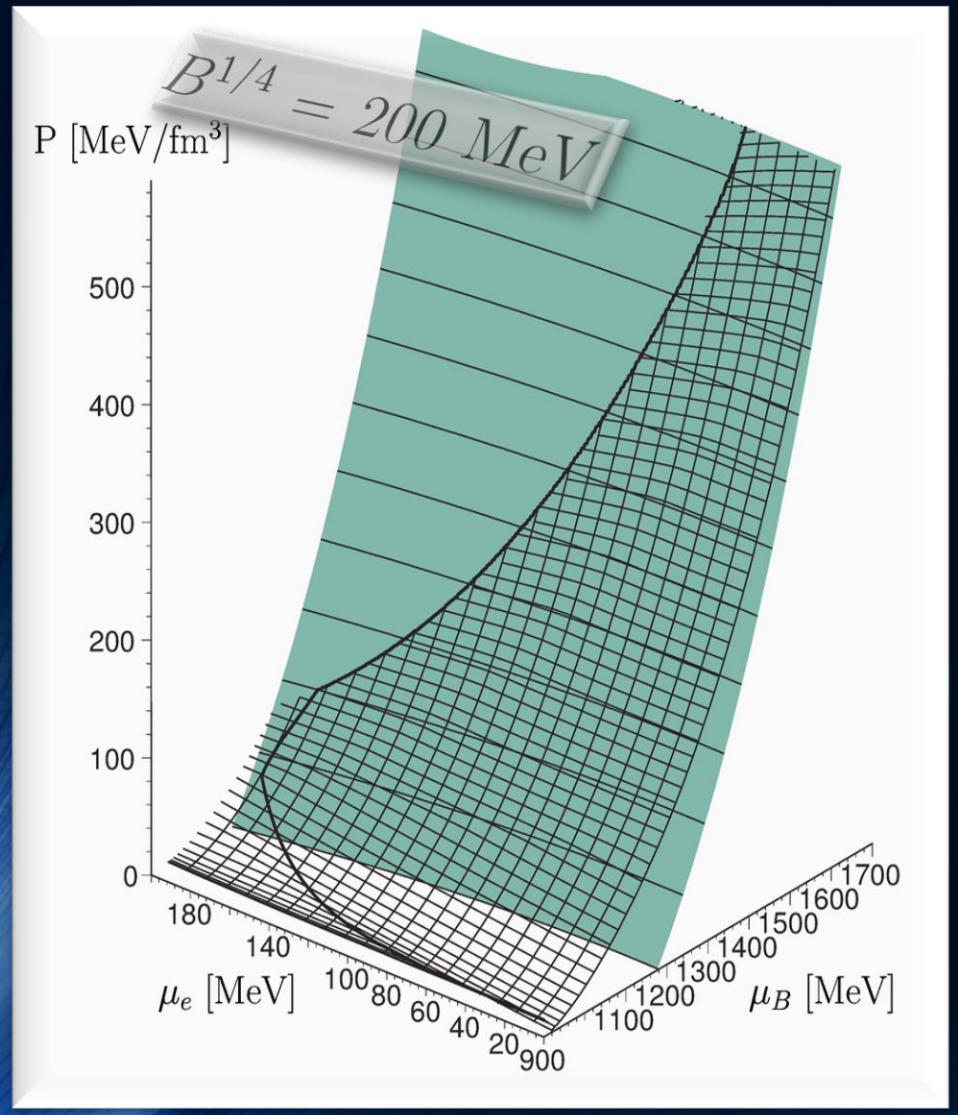


Particle composition:

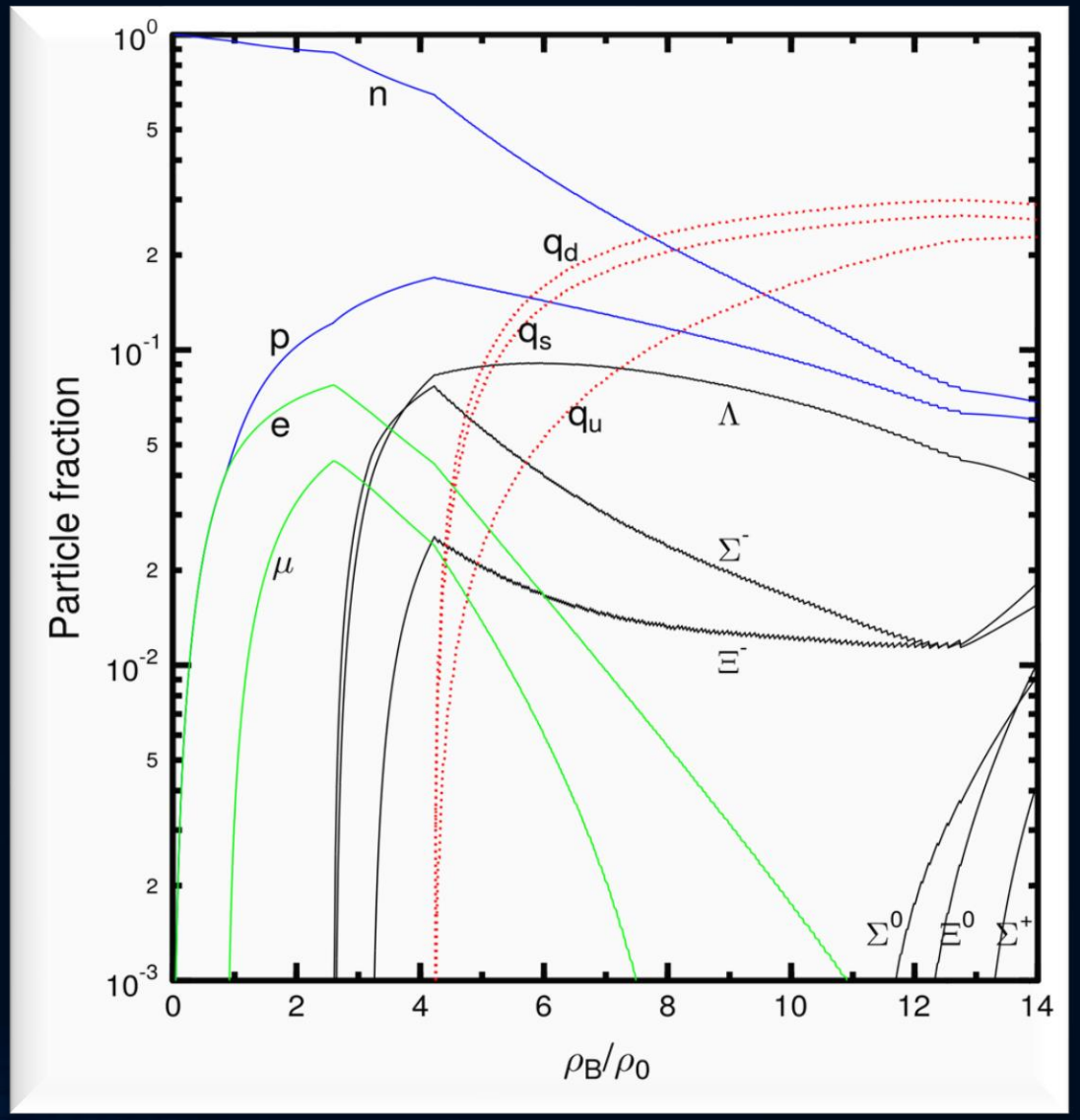


M. Hanauske, Dissertation, "Properties of Compact Stars within QCD-motivated Models"

# Merging Neutron Stars

- Lecture I: The math of neutron-star mergers
  - Introduction
  - A brief review of General Relativity
  - Numerical relativity of neutron-star mergers
    - The 3+1 decomposition of spacetime
    - ADM equations
    - BSSNOK/ccZ4 formulation
    - Initial data, gauge conditions, excising parts of spacetime and gravitational wave extraction
- Lecture II: The physics/astrophysics of neutron-star mergers
  - Introduction
  - GW170817 - the long-awaited event
  - Determining neutron-star properties and the equation of state using gravitational wave data
  - Hypermassive  neutron stars and the post-merger gravitational wave  emission
  - Detecting the hadron-quark phase transition with gravitational waves

# Initial data

Einstein equations represent an initial-value boundary problem (IVBP). Stated differently, once the solution is known/specified at any initial time, the hyperbolic nature of the equations completely determines the space of future solutions

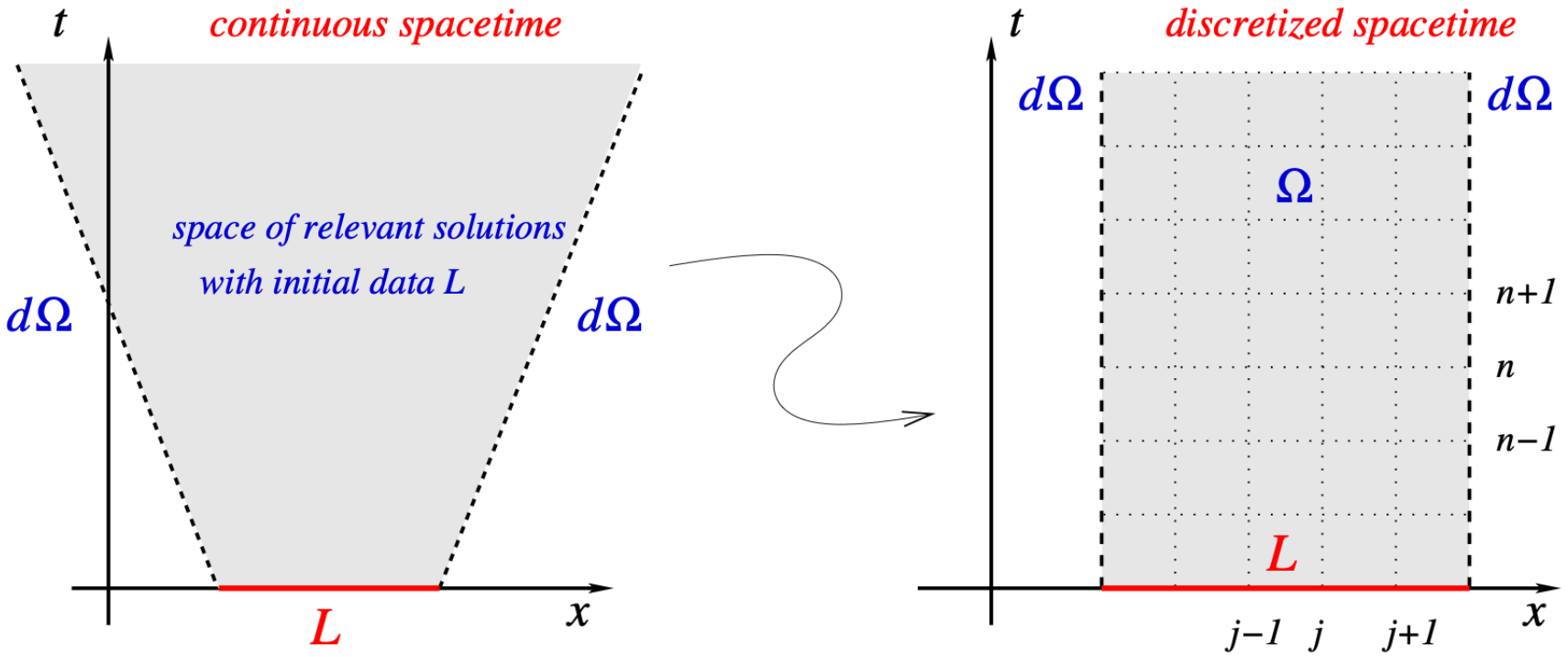

# Gauge conditions

Let us recap what we have already seen for the interpretation ofthe lapse, shift and spatial metric. Using the expression for the covariant 4-dim covariant metric, the line element is given

$$\mathrm{d}s^2 = g_{\mu\nu}\mathrm{d}x^\mu \mathrm{d}x^\mu = -(\alpha^2 - \beta^i\beta_i)\mathrm{d}t^2 + 2\beta_i \mathrm{d}x^i \mathrm{d}t + \gamma_{ij}\mathrm{d}x^i\mathrm{d}x^j$$

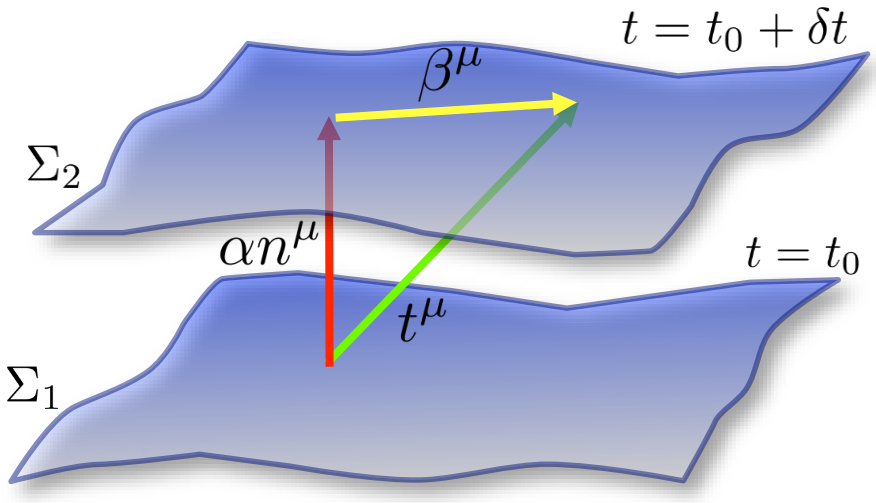


Hence:

the lapse measures proper time between two adjacent hypersurfaces

$$\mathrm{d}\tau^2 = -\alpha^2(t, x^j)\mathrm{d}t^2$$

the shift relates spatial coordinates between two adjacent hypersurfaces

$$x^i_{t_0+\delta t} = x^i_{t_0} - \beta^i(t, x^j)\mathrm{d}t$$

the spatial metric measures distances between points on every hypersurface

$$\mathrm{d}l^2 = \gamma_{ij}\mathrm{d}x^i\mathrm{d}x^j$$

We can now have a more intuitive interpretation of the lapse, shift and spatial metric. Using the expression for the covariant 4-dim covariant metric, the line element is given

$$\mathrm{d}s^2 = g_{\mu\nu}\mathrm{d}x^\mu \mathrm{d}x^\mu = -(\alpha^2 - \beta^i\beta_i)\mathrm{d}t^2 + 2\beta_i \mathrm{d}x^i \mathrm{d}t + \gamma_{ij}\mathrm{d}x^i\mathrm{d}x^j$$

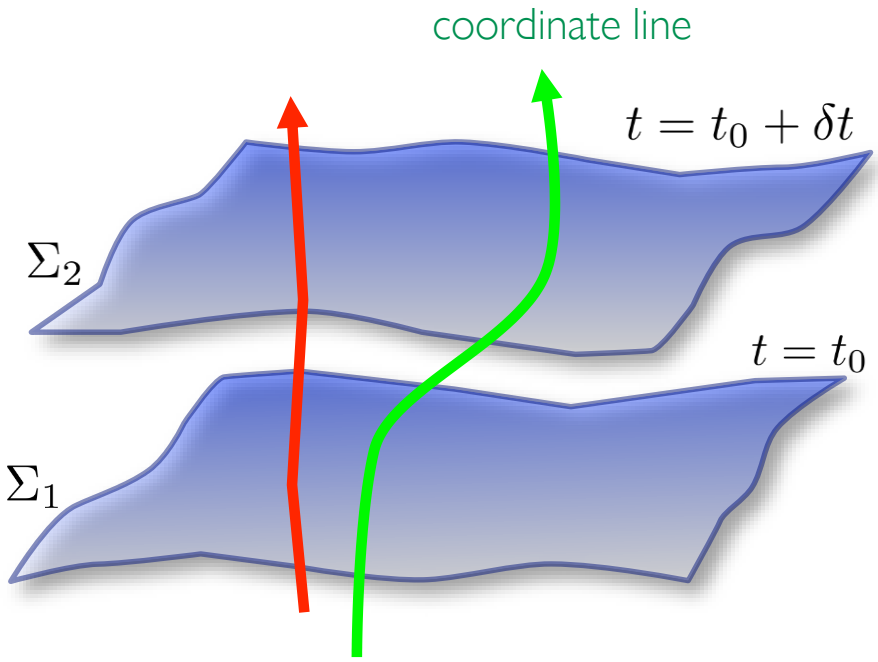


Hence:

the lapse measures proper time between two adjacent hypersurfaces

$$\mathrm{d}\tau^2 = -\alpha^2(t, x^j)\mathrm{d}t^2$$

the shift relates spatial coordinates between two adjacent hypersurfaces

$$x^i_{t_0+\delta t} = x^i_{t_0} - \beta^i(t, x^j)\mathrm{d}t$$

the spatial metric measures distances between points on every hypersurface

$$\mathrm{d}l^2 = \gamma_{ij}\mathrm{d}x^i\mathrm{d}x^j$$

NOTE: the lapse, and shift are not solutions of the Einstein equations but represent our “gauge freedom”, namely the freedom (arbitrariness) in which we choose to foliate the spacetime.

Any prescribed choice for the lapse is usually referred to as a ”slicing condition”, while any choice for the shift is usually referred to as ”spatial gauge condition”

While there are infinite possible choices, not all of them are equally useful to carry out numerical simulations. Indeed, there is a whole branch of numerical relativity that is dedicated to finding suitable gauge conditions.

Several possible routes are possible

i) make a guess (i.e. prescribe a functional form) for the lapse,
and shift and hope for the best: eg geodesic slicing $\alpha = 1\,,\ \beta^i = 0$

obviously not a good idea

# Choosing the right temporal gauge

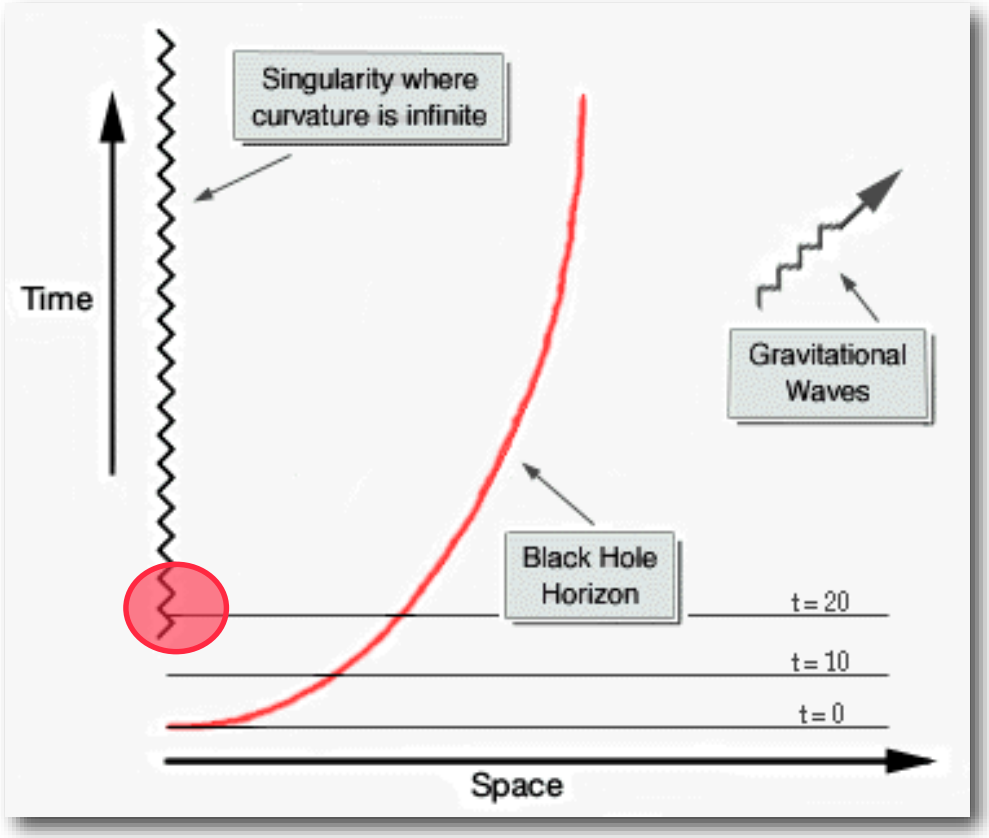


Suppose you want to follow the gravitational collapse to a bh and assume a simplistic gauge choice (geodesic slicing):

$$\alpha = 1, \quad \beta^i = 0$$

That would lead rapidly ($t \approx \pi M$) to a code crash No chance of measuring GWs which need to be collected on timescales $t \sim 10^3\, M$!

Several possible routes are possible

i) make a guess (i.e. prescribe a functional form) for the lapse, and shift and hope for the best: eg geodesic slicing $\alpha = 1\,,\ \beta^i = 0$

obviously not a good idea

ii) fix the lapse, and shift by requiring they satisfy some condition: eg maximal slicing for the lapse

$$\partial_t K = 0 \quad \Longrightarrow \quad D^i D_i \alpha = \alpha[K_{ij}K^{ij} + 4\pi(e+S)]$$

which has the desired "singularity-avoiding" properties. Similarly, the minimal distortion shift condition guarantees minimizes the changes in the conformally related metric

Good idea mathematically (the coordinates do exactly what they should). Unfortunately this leads to elliptic eqs which are computationally too expensive to solve at each time

iii) fix the lapse, and shift dynamically by requiring they satisfy comparatively simple evolution equations

This is the common solution. The advantage is the eqs for the lapse and shift are simple time evolution eqs.

A family of slicing conditions that works very well to obtain both a strongly hyperbolic evolution eqs. and for stable numerical evolutions is the Bona-Masso slicing

$$\partial_t \alpha - \beta^i \partial_i \alpha = -\alpha^2 f(\alpha)(K - K_0)$$

where $K_0 \equiv K(t=0)$ and $f(\alpha)$ is positive but otherwise arbitrary.

Indeed the condition $\partial_t \alpha \sim -\alpha^2 f(\alpha) K$ represents a family of slicing conditions such that:

$$
\begin{aligned}
f = 0\,, (\alpha = 1 \text{ initially})\,, &\quad : \text{geodesic slicing} \\
f = 1\,, &\quad : \text{harmonic slicing} \\
f = 2/\alpha\,, &\quad : \text{"}1 + \log\text{"slicing} \\
f \to \infty\,, &\quad : \text{maximal slicing}
\end{aligned}
$$

The "1+log" slicing condition also has excellent singularity avoiding properties since $\partial_t \alpha \sim -\alpha$ and hence the lapse remains very small in those regions where it has "collapsed" to small values

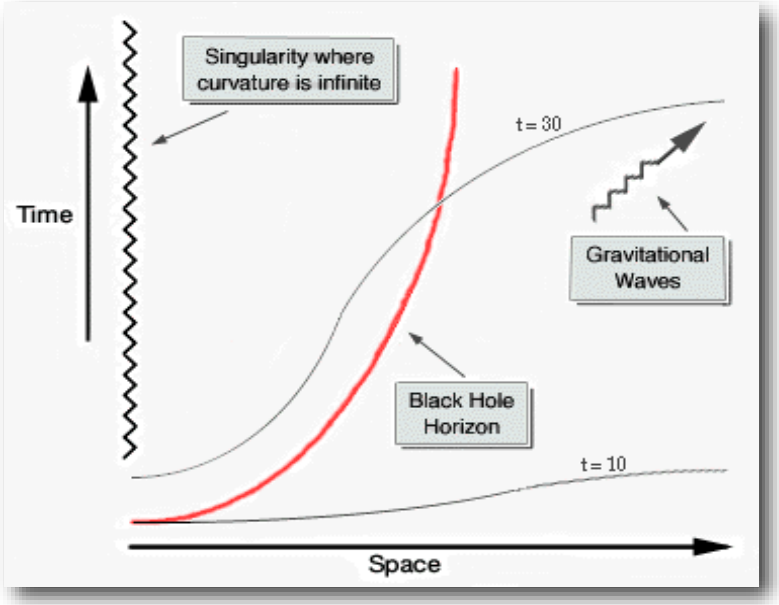

Similarly, a popular choice for the shift is the hyperbolic "Gamma-driver" condition

$$\begin{aligned}
\partial_t \beta^i - \beta^j \partial_j \beta^i &= \frac{3}{4} \alpha B^i \,, \\
\partial_t B^i - \beta^j \partial_j B^i &= \partial_t \tilde{\Gamma}^i - \beta^j \partial_j \tilde{\Gamma}^i - \eta B^i \,,
\end{aligned}$$

where $\eta$ acts as a restoring force to avoid large oscillations in the shift and the driver tends to keep the Gammas constant (reminiscent of minimal distortion)

Overall, the "1+log" slicing condition and the "Gamma-driver" shift condition are the most widely used both in vacuum and non-vacuum spacetimes

# excising parts of the spacetime with singularities…

apparent horizon found on a given $\Sigma_t$

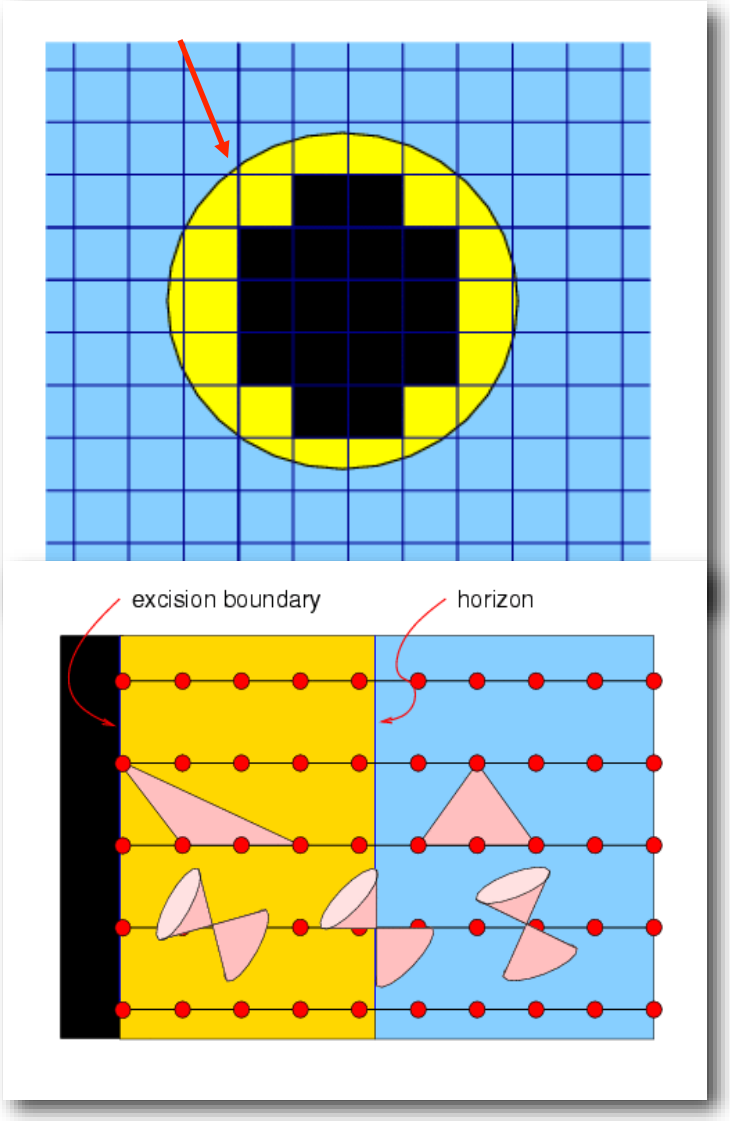


Images by D. Pollney

***In principle,*** the yellow region is causally disconnected from the blue one (ligth cones are "tilted in"); no boundary conditions would be needed at the apparent horizon.

***In practice,*** the actual excision region (***"legosphere"***: black region) carved well inside the horizon.

NOTE:

- the Einstein equations are highly nonlinear in the yellow region! All sorts of numerical problems...
- the (apparent) horizon must be found; this is an expensive operation…
- the excised region has to move on the grid…

# Extraction of gravitational waves

# Wave-extraction techniques

Computing the waveforms is the ultimate goal of most numerical relativity and there are several ways of extracting GWs from numerical relativity codes:

- asymptotic measurements
  - null slicing
  - conformal compactification
- non-asymptotic measurements (finite-size extraction worldtube)
  - Weyl scalars
  - perturbative matching to a Schwarzschild background

All have different degrees of success and this depends on the efficiency of the process which is very different for different sources

$$\frac{\Delta M}{M} \sim 10^{-2}\ (\text{binary bhs}) - 10^{-7}\ (\text{collapse to bh})$$

# Wave-extraction techniques

In both approaches, "***observers***" are placed on nested 2-spheres and calculate there either the Weyl scalars or decompose the metric into tensor spherical-harmonics to calculate the gauge-invariant perturbations of a Schwarzschild black hole

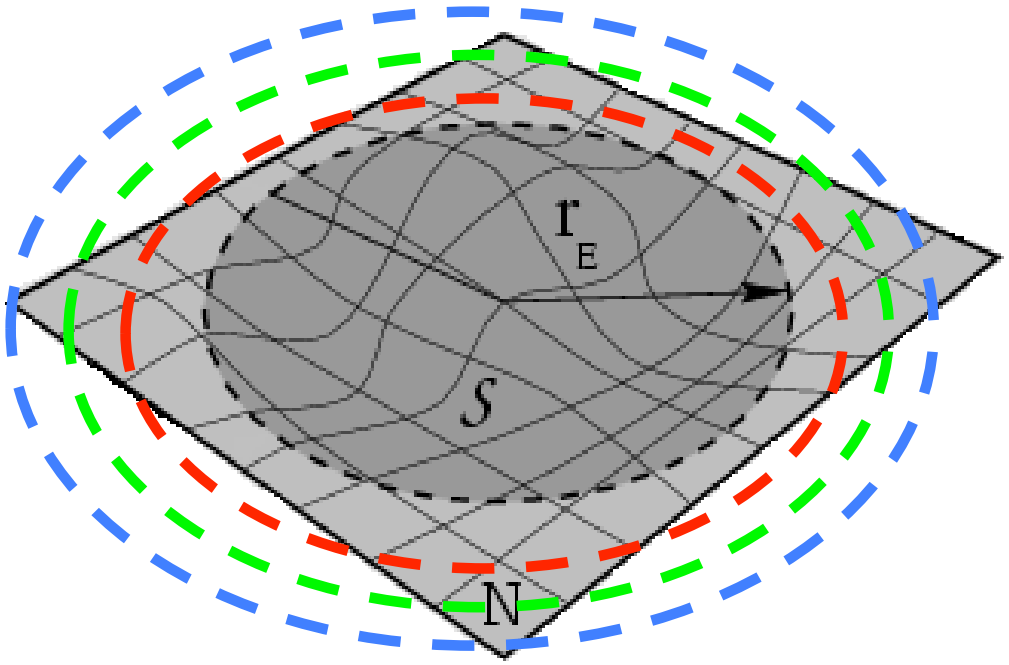


Once the waveforms are calculated, all the related quantities: energy, momentum and angular momentum radiated can be derived simply.

Lects. IV and V will show some examples

# Gauge-invariant pertubations

Similarly, at a sufficiently large distance from the source and assuming the spacetime resembles that of a Schwarzschild BH

$$h_+ - \mathrm{i}h_\times = \frac{1}{\sqrt{2}r}\sum_{l,m}\left(Q^+_{\ell m} - \mathrm{i}\int_{-\infty}^{t} Q^\times_{\ell m}(t')\mathrm{d}t'\right) Y^{-2}_{\ell m} + \mathcal{O}\left(\frac{1}{r^2}\right)$$

where $Q^\times_{\ell m}$, $Q^+_{\ell m}$ are the odd and even-parity *gauge-invariant* perturbations of a Schwarschild bh. The projection of the momenutm flux on the equatorial plane is, for instance,

$$\mathcal{F}_x^{\ell m} + \mathrm{i}\mathcal{F}_y^{\ell m} \equiv \frac{(-1)^m}{16\pi\ell(\ell+1)}\Bigg\{ -2\mathrm{i}\left[a_{\ell m}\dot{Q}^+_{\ell -m}Q^\times_{\ell\, m-1} + b_{\ell m}\dot{Q}^+_{\ell m}Q^\times_{\ell\, -(m+1)}\right]$$

$$+\sqrt{\frac{\ell^2(\ell-1)(\ell+3)}{(2\ell+1)(2\ell+3)}}\Big[c_{\ell m}\left(\dot{Q}^+_{\ell\, -m}\dot{Q}^+_{\ell+1\, m-1} + Q^\times_{\ell\, -m}\dot{Q}^\times_{\ell+1\, m-1}\right)$$

$$+d_{\ell m}\left(\dot{Q}^+_{\ell m}\dot{Q}^+_{\ell+1\, -(m+1)} + Q^\times_{\ell m}\dot{Q}^\times_{\ell+1\, -(m+1)}\right)\Big]\Bigg\}\,,$$

This quantity can be used, for instance, to calculate the recoil.

# Weyl scalars

The Newman-Penrose formalism provides a convenient representation for radiation-related quantities as spin-weighted scalars. In particular, the component of the Weyl tensor

$$\Psi_4 \equiv -C_{\alpha\beta\gamma\delta} n^\alpha \bar{m}^\beta n^\gamma \bar{m}^\delta,$$

can be associated with the gravitational-radiation content of the spacetime because it falls like ~*1/r*. Here $(\boldsymbol{l}, \boldsymbol{n}, \boldsymbol{m}, \bar{\boldsymbol{m}})$, is a null frame and in practice we define an orthonormal polar coordinate basis $(\boldsymbol{r}, \boldsymbol{\theta}, \boldsymbol{\phi})$, centred on the Cartesian grid origin and with poles along $\boldsymbol{e}_z$.

Using then the normal to the slice as $\boldsymbol{e}_0 = \hat{\boldsymbol{t}}$ the components of the frame are

$$\boldsymbol{l} = \frac{1}{\sqrt{2}}(\hat{\boldsymbol{t}} - \hat{\boldsymbol{r}}), \quad \boldsymbol{n} = \frac{1}{\sqrt{2}}(\hat{\boldsymbol{t}} + \hat{\boldsymbol{r}}), \quad \boldsymbol{m} = \frac{1}{\sqrt{2}}(\hat{\boldsymbol{\theta}} - \mathrm{i}\hat{\boldsymbol{\phi}})$$

# Weyl scalars

We then calculate $\Psi_4$ in terms of ADM related quantities as

$$\Psi_4 = C_{ij}\bar{m}^i\bar{m}^j,$$

where

$$C_{ij} \equiv R_{ij} - KK_{ij} + K_i{}^k K_{kj} - \mathrm{i}\epsilon_i{}^{kl}\nabla_l K_{jk}.$$

Then at a sufficiently large distance from the source the GWs in the two polarizations $h_\times, h_+$ can be written as

$$h_+ - \mathrm{i}h_\times = \lim_{r\to\infty}\int_0^t \mathrm{d}t' \int_0^{t'} \mathrm{d}t''\Psi_4$$

Then, eg, the projection of the momentum flux on the equatorial plane as

$$\mathcal{F}_i = \frac{\mathrm{d}P_i}{\mathrm{d}t} = \lim_{r\to\infty}\left\{\frac{r^2}{16\pi}\int d\Omega\, n_i \left|\int_{-\infty}^{t} dt\Psi_4\right|^2\right\}.$$

This quantity can be used, for instance, to calculate the recoil.

# Recap

☑ The lapse and the shift have simple physical definitions and relate events on two different hypersurfaces.

☑ Getting a good formulation of the Einstein eqs will work only in conjunction with good gauge conditions. "1+log" slicing "Gamma-driver" conditions work well in a number of conditions.

☑ Even with suitable formulations and gauge conditions, any astrophysical prediction needs the calculation of "realistic" initial data and hence the solution of elliptic equations.

☑ GWs can be extracted with great accuracy. Several methods using either the radiative part of the Riemann tensor or perturbations of the Schwarzschild spacetime.

# Recap (II)

☑ The ADM eqs are ill posed and not suitable for numerics.

☑ Alternative formulations (BSSNOK, CCZ4, Z4c) have been developed that are strongly hyperbolic and hence well-posed.

☑ Both formulations make use of the constraint equations and can use additional evolution equations to damp the violationsns

☑ The hyperbolic evolution eqs. to solve are: 6+6+(3+1+1) = 17.
We also "compute" 3+1=4 elliptic constraint eqs

$$\mathcal{H} \equiv {}^{(3)}R + K^2 - K_{ij}K^{ij} = 0 \,, \quad \text{(Hamiltonian constraint)}$$

$$\mathcal{M}^i \equiv D_j(K^{ij} - g^{ij}K) = 0 \,, \quad \text{(momentum constraints)}$$

NOTE: these eqs are not solved but only monitored to verify

$$||\mathcal{H}|| \simeq ||\mathcal{M}^i|| < \varepsilon \sim 10^{-4} - 10^{-2}$$

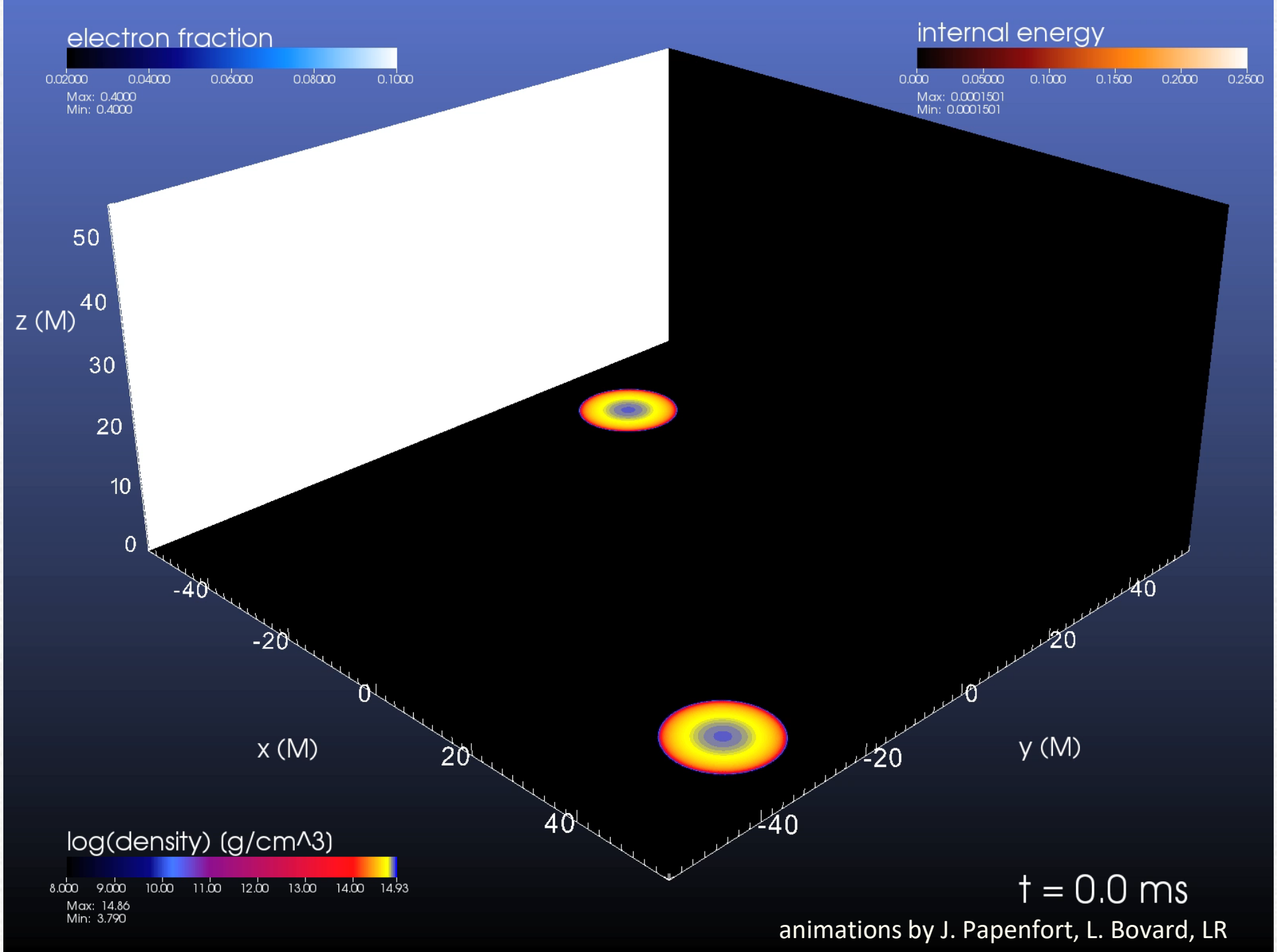
electron fraction
0.02000 0.04000 0.06000 0.08000 0.1000
Max: 0.4000
Min: 0.4000
internal energy
0.000 0.05000 0.1000 0.1500 0.2000 0.2500
Max: 0.0001501
Min: 0.0001501
z (M)
50
40
30
20
10
0
x (M)
-40
-20
0
20
40
y (M)
40
20
0
-20
-40
log(density) (g/cm^3)
8.000 9.000 10.00 11.00 12.00 13.00 14.00 14.93
Max: 14.86
Min: 3.790
t = 0.0 ms
animations by J. Papenfort, L. Bovard, LR

# Viscous effects?

Alford, Bovard, Hanauske, LR, Schwenzer (2018)

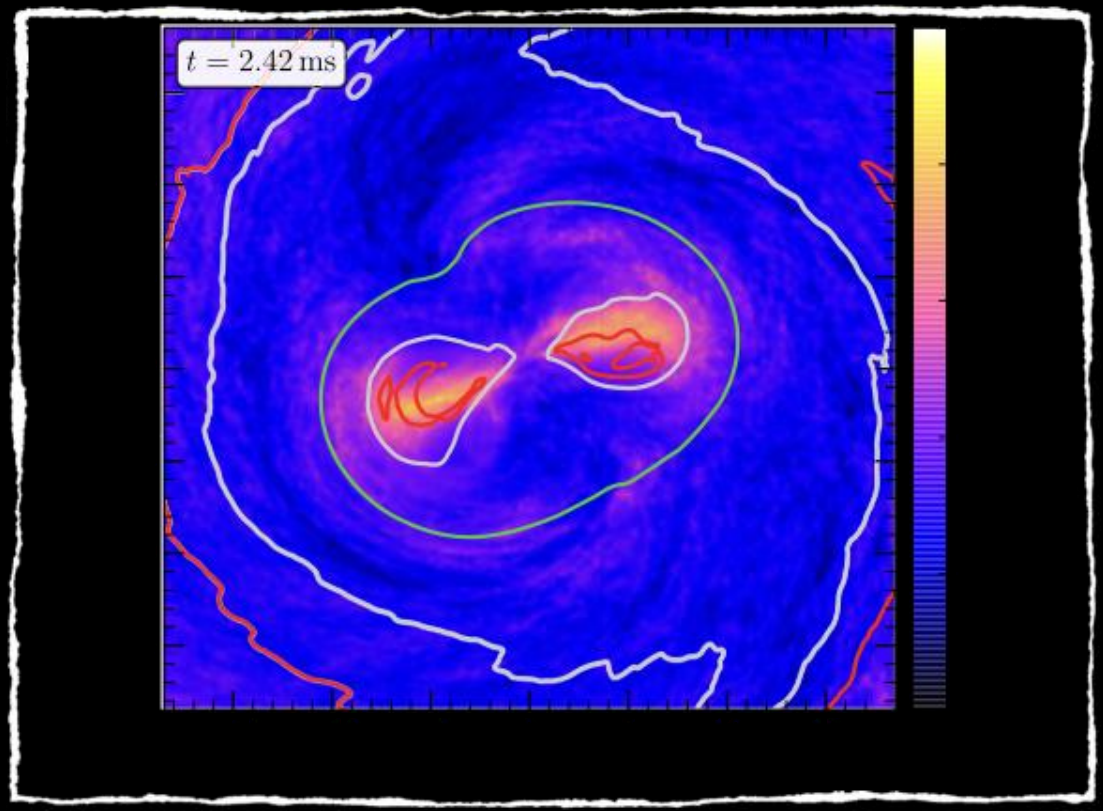

# Potential viscous contributions

Alford+(2018)

- Possible channels of micro/macroscopic viscosity are:
  1. nuclear-matter **shear** viscosity
  2. nuclear-matter **bulk** viscosity
  3. neutrino **shear** viscosity (Guilet+ 2016)
  4. "**MRI**-induced" **viscosity** (Radice2017, Shibata+2017a, b)
- Channels 3. and 4. act on timescales typical of MRI, which depends on B-field and very **uncertain** still.
- Impact of MRI on GWs depends on the value for viscous angular momentum transport.
- This is presently essentially unknown: $\tau \gtrsim 10 - 100\,\mathrm{ms}$ ?

# Viscous contributions: 1. shear viscosity

- Low-temperature, **electron-dominated** regime, i.e.

$$T \lesssim 10\,\mathrm{MeV}$$

$$\tau_\eta^{(e)} \approx 1.6\times10^8\,\mathrm{s}\left(\frac{z_{\rm typ}}{1\,\mathrm{km}}\right)^2\left(\frac{T}{1\,\mathrm{MeV}}\right)^{\frac{5}{3}}\left(\frac{n_0}{n_B}\right)^{\frac{5}{9}}\left(\frac{0.1}{x_p}\right)^{\frac{14}{9}},$$

- High-temperature, **neutrino-dominated** regime, i.e.

$$T \gtrsim 10\,\mathrm{MeV}$$

$$\tau_\eta^{(\nu)} \approx 54\,\mathrm{s}\left(\frac{0.1}{x_p}\right)\left(\frac{m_n^*}{0.8\,m_n}\right)^2\left(\frac{\mu_e}{2\,\mu_\nu}\right)^4\left(\frac{z_{\rm typ}}{1\,\mathrm{km}}\right)^2\left(\frac{T}{10\,\mathrm{MeV}}\right)^2,$$

Hence, shear viscosity not relevant unless neutrinos dominate and flow is turbulent with $z_{\rm typ} \sim 10 - 100\,\mathrm{m}$, not likely.

# Viscous contributions: 2. **bulk viscosity**

- Impact of bulk viscosity depends sensitively on process responsible for flavor re-equilibration.
- If **direct-Urca** dominates, bulk viscosity will be very **small**: never possible for softer EOSs, hard for stiff EOS at small T.
- If **modified-Urca** dominates, then bulk viscosity

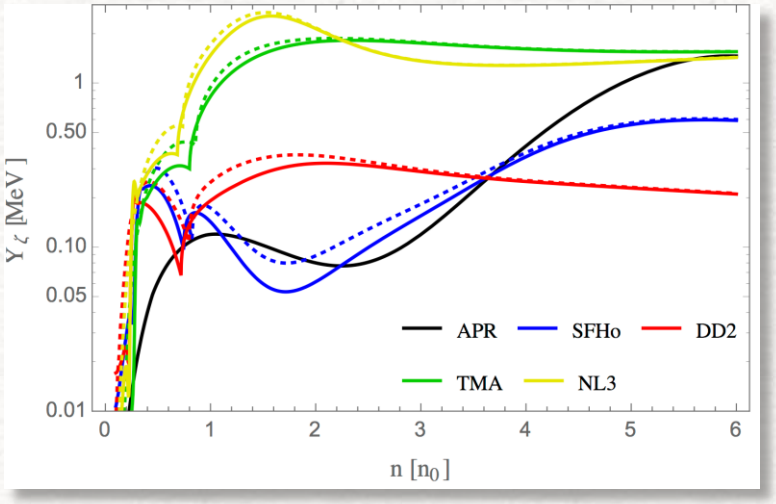


$\mathcal{E}_{\rm comp}$: en. density variation due comp.

$$\mathcal{E}_{\rm comp} \approx K\bar{n}(\Delta n/\bar{n})^2/18$$

$$\tau_\zeta \equiv \mathcal{E}_{\rm comp}/\left(d\mathcal{E}/dt\right)_{\rm bulk} \approx K\bar{n}\,t_{\rm exp}^2/(36\pi^2\,\bar{\zeta})$$

$$\approx 7\,{\rm ms}\left(\frac{t_{\rm exp}}{1\,{\rm ms}}\right)\left(\frac{K}{250\,{\rm MeV}}\right)\left(\frac{0.1\,{\rm MeV}}{Y_\zeta}\right)$$

$t_{\rm exp}$ ~bulk-dissipation timescale of internal energy key!

$K$ nuclear compressibility at $n_0$ $Y_\zeta$ bulk viscosity prefactor

# Viscous contributions

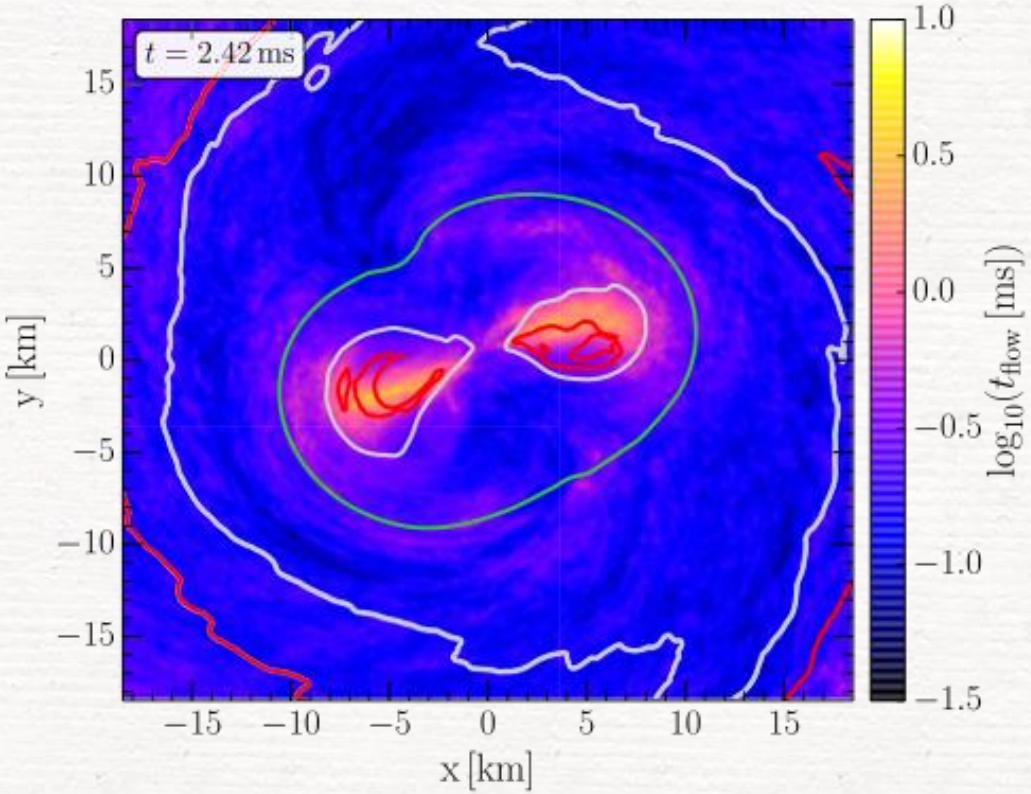


instantaneous bulk-dissipation timescale can be measured in simulations.

$$\langle t_{\mathrm{flow}} \rangle := \left\langle \frac{\rho}{D_t \rho} \right\rangle = \left\langle \frac{1}{\nabla \cdot \vec{v}} \right\rangle$$

right after merger

$$t_{\mathrm{flow}} \lesssim \tau_{\mathrm{dyn}} = \frac{R}{c_s}$$

Soon after merger ***bulk-dissipation timescale*** comparable with dynamical timescale in large portions of the object: **cannot be ignored**.

# Viscous contributions

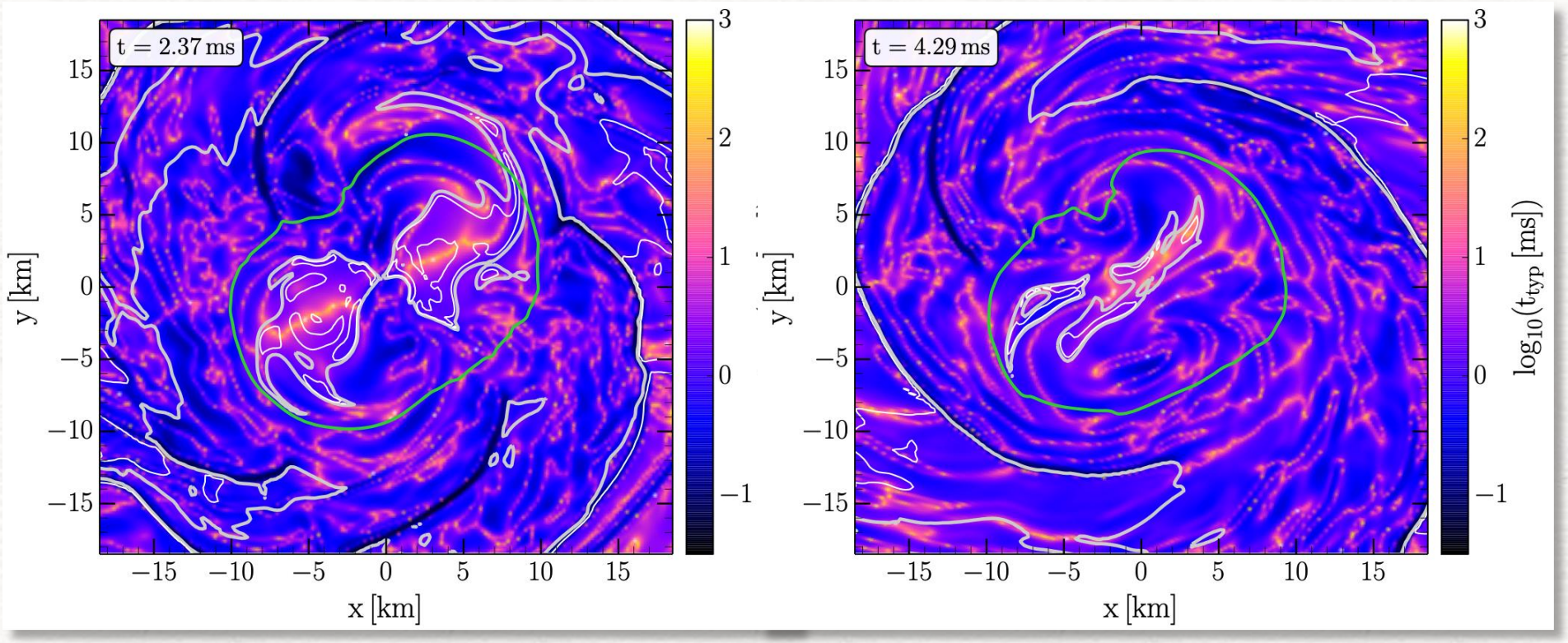


$$t_{\rm exp}^{\rm inst} \sim \frac{\rho}{D_t \rho} = \frac{1}{\nabla \cdot \vec{v}}$$

instantaneous bulk-dissipation timescale can be measured in simulations.

right after merger

$$t_{\rm exp} \lesssim \tau_{\rm dyn} = \frac{R}{c_s}$$

***bulk-dissipation timescale comparable with dynamical timescale***

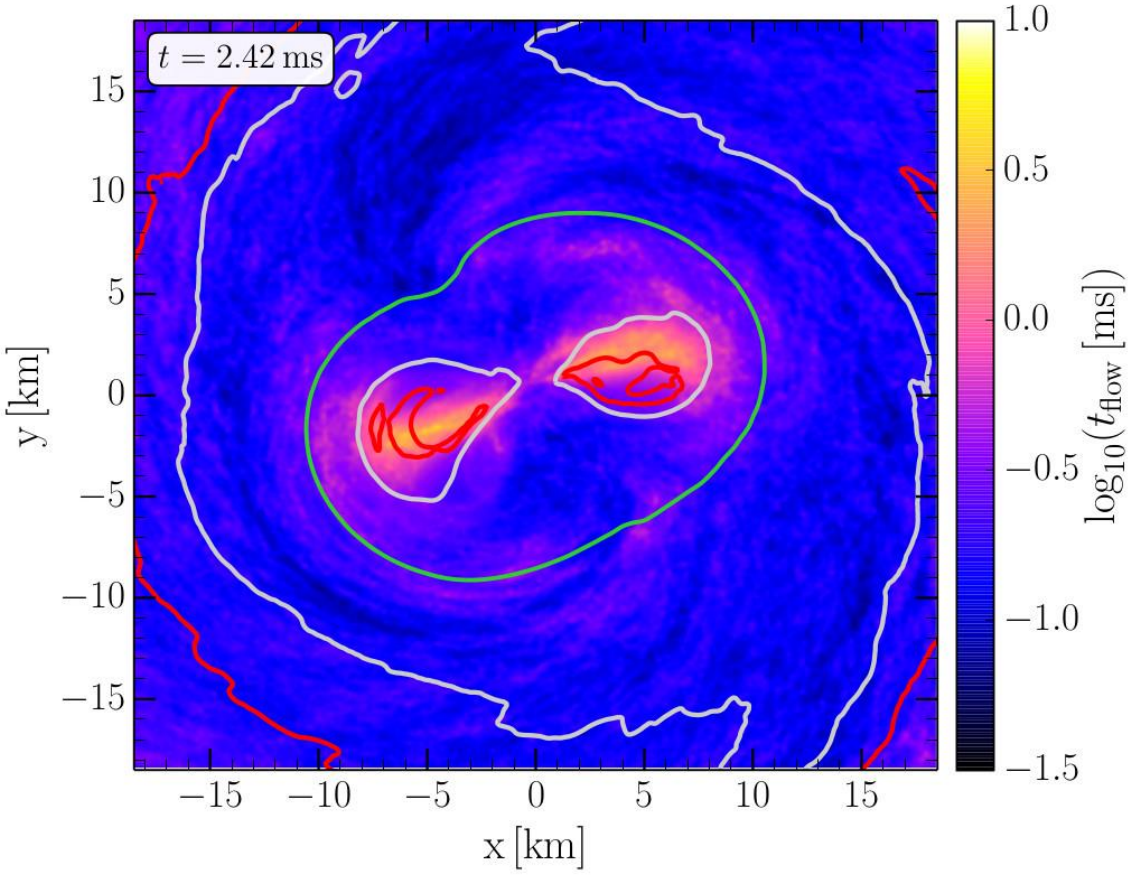


Figure 3: The flow timescale $t_{\rm flow}$ obtained from a numerical-relativity simulation of two 1.35 $M_\odot$ neutron stars [40]. The red (4 MeV) and gray (7 MeV) contours show the boundaries of the temperature range in which the bulk viscosity roughly takes its maximum value, while the green contour shows the inner region where the rest-mass density exceeds nuclear saturation density.

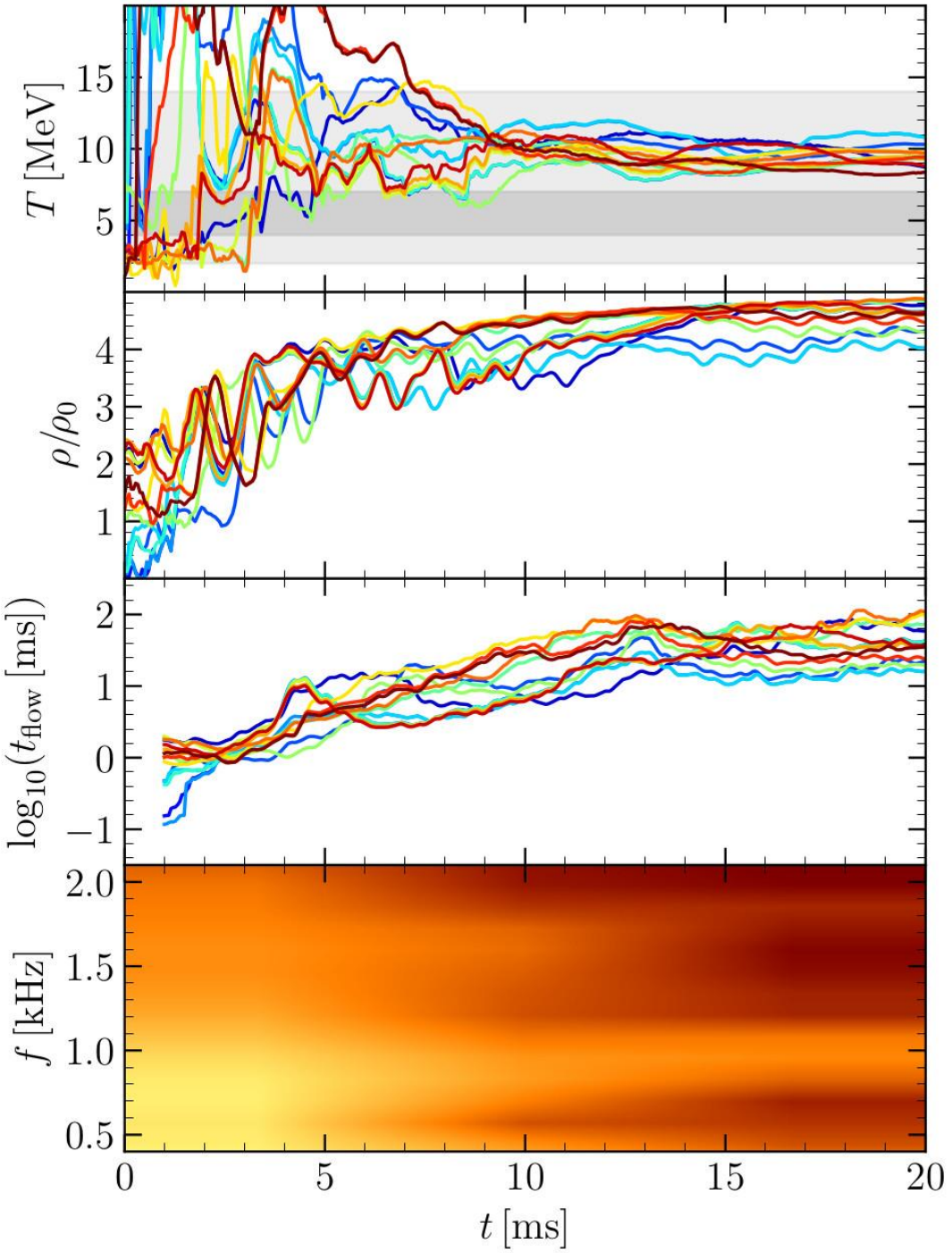


density region where the bulk viscosity is maximal (i.e., for

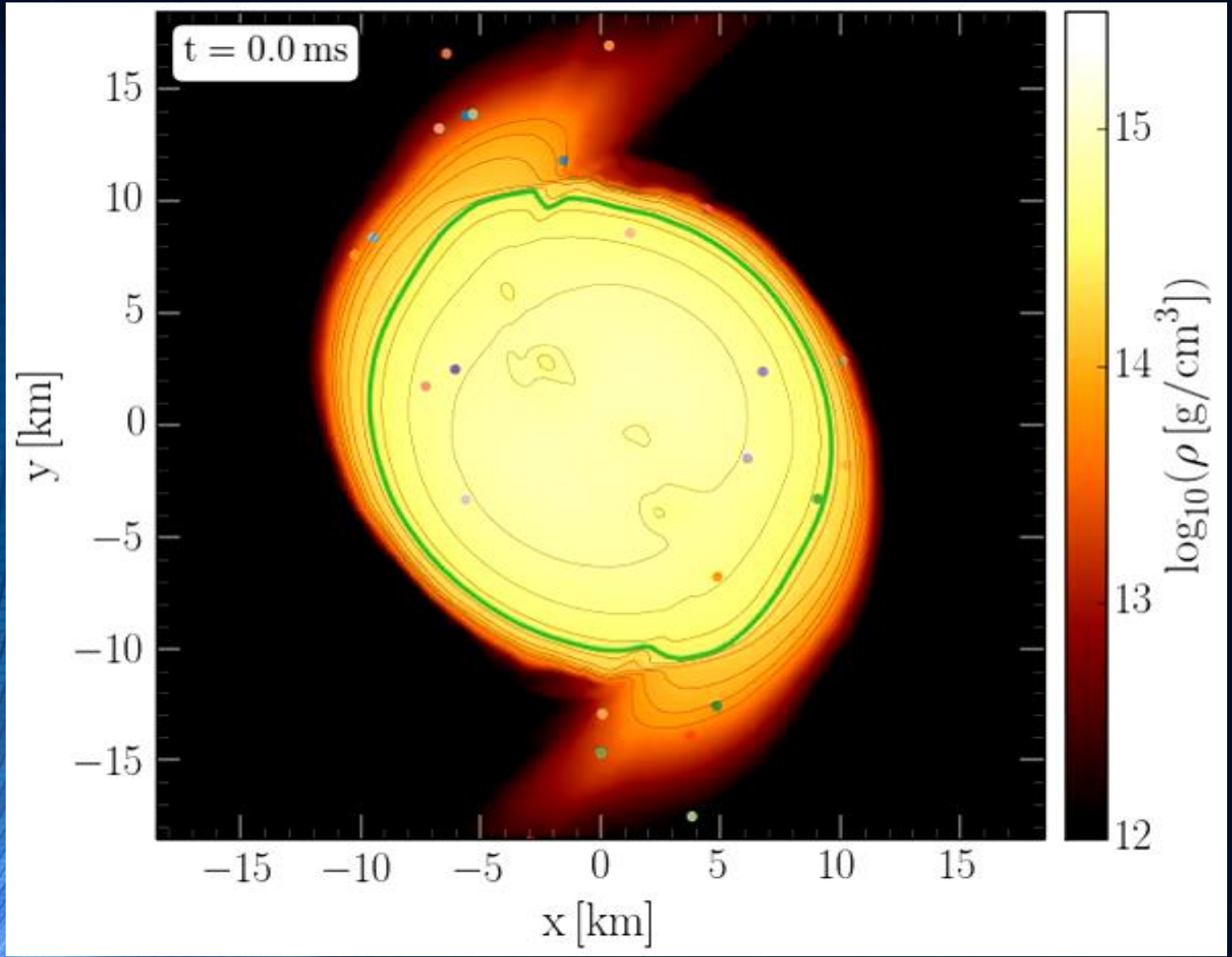
t = 0.0 ms
y [km]
x [km]
$\log_{10}(\rho\,[\mathrm{g/cm^3}])$

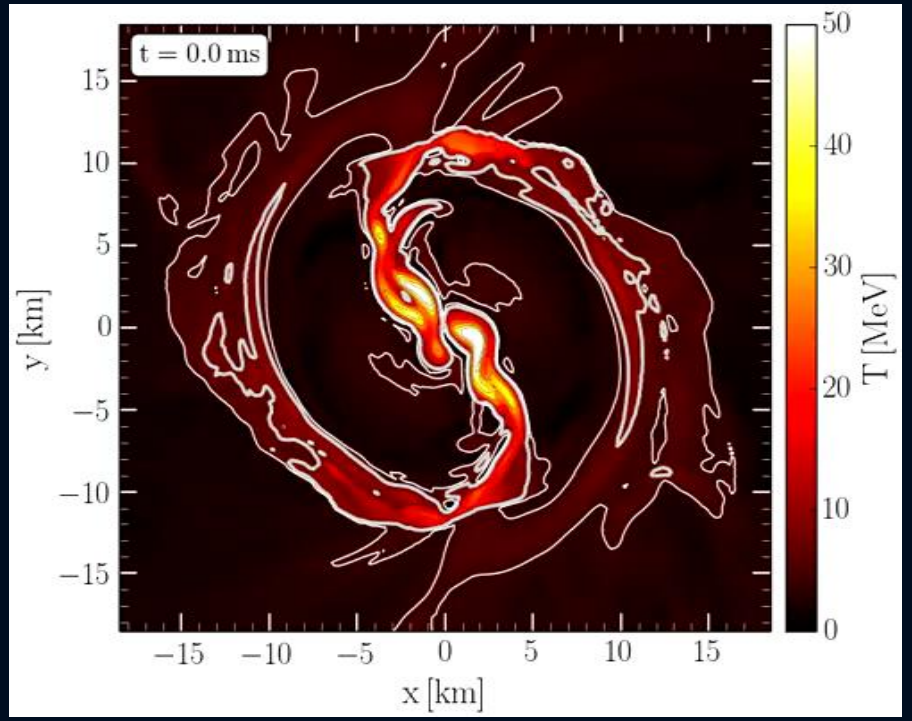
t = 0.0 ms
y [km]
x [km]
T [MeV]

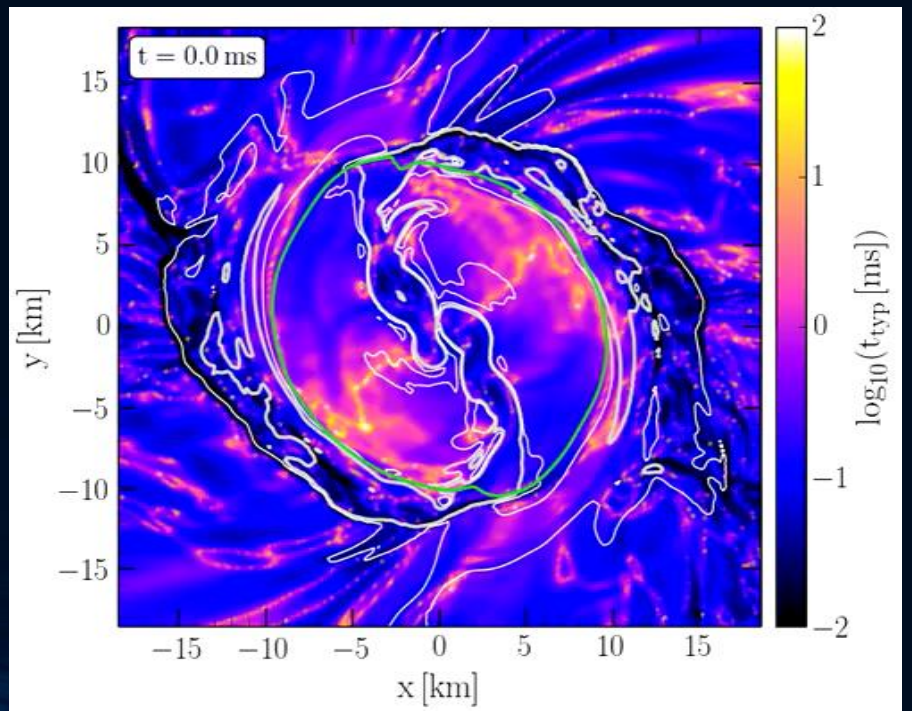
t = 0.0 ms
y [km]
x [km]
$\log_{10}(t_{typ}\,[\mathrm{ms}])$

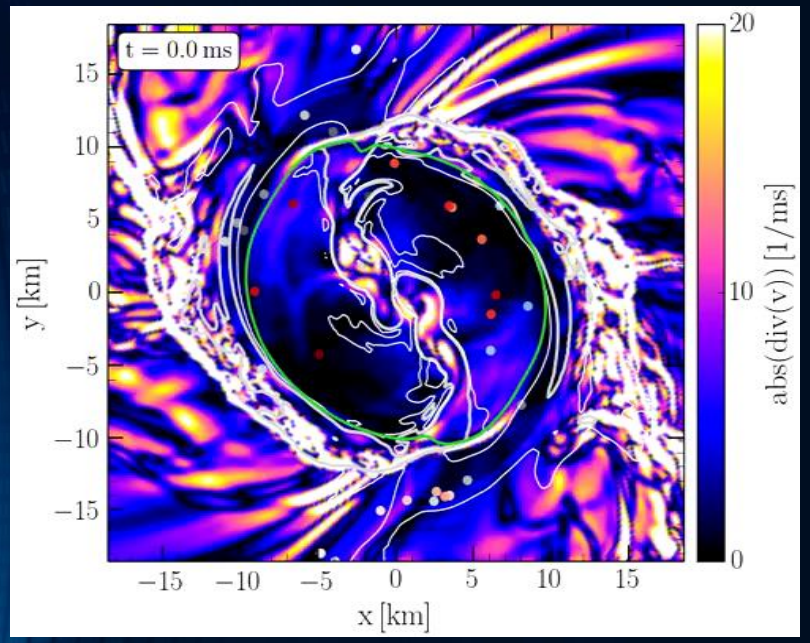
t = 0.0 ms
y [km]
x [km]
abs(div(v)) [1/ms]

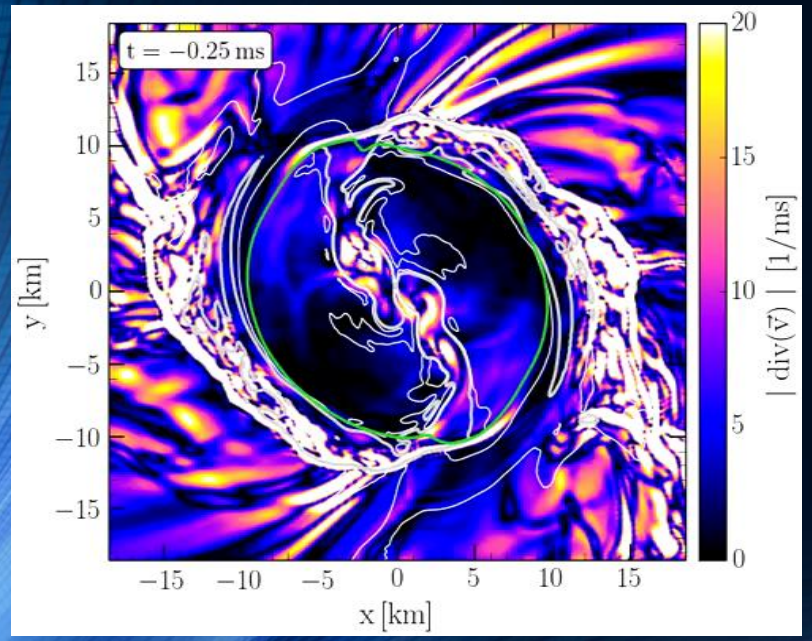
t = −0.25 ms
y [km]
x [km]
| div(v) | [1/ms]

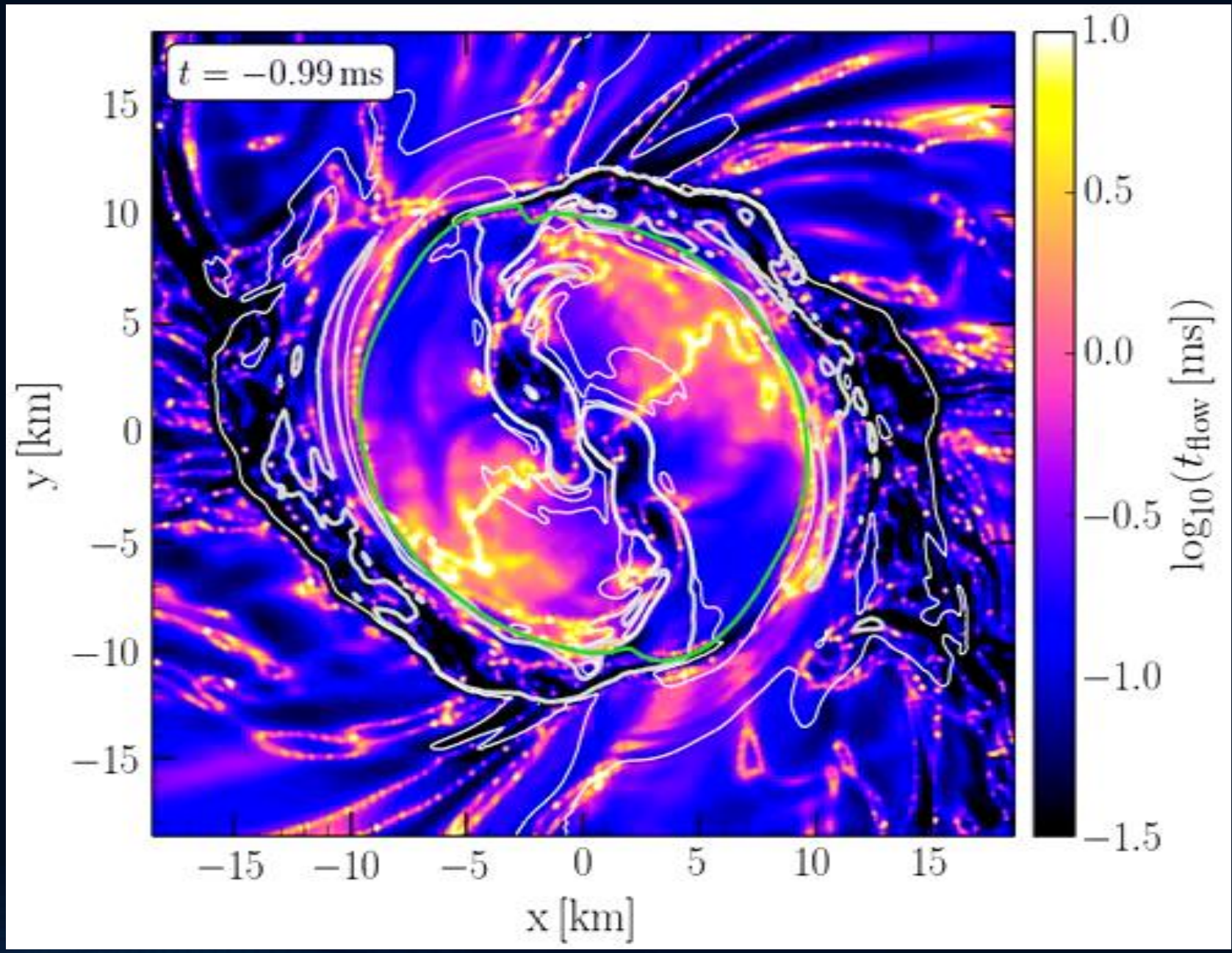
t = −0.99 ms
y [km]
x [km]
log10(tflow [ms])